

Carbon emissions and sustainability of launching 5G mobile networks in China

Tong Li¹, Li Yu², Yibo Ma¹, Tong Duan³, Wenzhen Huang¹, Yan Zhou², Depeng Jin¹, Yong Li^{*1}, and Tao Jiang^{*4}

¹Beijing National Research Center for Information Science and Technology (BNRist), Department of Electronic Engineering, Tsinghua University, Beijing, China

²China Mobile Research Institute, Beijing, China

³National Digital Switching System Engineering and Technological Research Center, Zhengzhou, China

⁴Research Center of 6G Mobile Communications, Huazhong University of Science and Technology, Wuhan, China.

*liyong07@tsinghua.edu.cn; taojiang@hust.edu.cn

ABSTRACT

Since 2021, China has deployed more than 2.1 million 5G base stations to increase the network capacity and provide ubiquitous digital connectivity for mobile terminals. However, the launch of 5G networks also exacerbates the misalignment between cellular traffic and energy consumption, which reduces carbon efficiency — the amount of network traffic that can be delivered for each unit of carbon emission. In this study, we develop a large-scale data-driven framework to estimate the carbon emissions induced by mobile networks. We show that the decline in carbon efficiency leads to a carbon efficiency trap, estimated to cause additional carbon emissions of 23.82 ± 1.07 megatons in China. To mitigate the misalignment and improve energy efficiency, we propose DeepEnergy, an energy-saving method leveraging collaborative deep reinforcement learning and graph neural networks. DeepEnergy models complex collaboration among cells, making it possible to effectively coordinate the working state of tens of thousands of cells, which could help over 71% of Chinese provinces avoid carbon efficiency traps. In addition, applying DeepEnergy is estimated to reduce 20.90 ± 0.98 megatons of carbon emissions at the national level in 2023. We further assess the effects of adopting renewable energy and discover that the mobile network could accomplish more than 50% of its net-zero goal by integrating DeepEnergy and solar energy systems. Our study provides insight into carbon emission mitigation in 5G network infrastructure launching in China and overworld, paving the way towards achieving sustainable development goals and future net-zero mobile networks.

Introduction

Connectivity has become a defining feature of the modern economy and society¹. 5G mobile networks play a big role by being recognized as providing high network capacity and ubiquitous digital connectivity for a massive number of terminals², including but not limited to smartphones, vehicles, and sensors. 5G connectivity will usher in a new era of the digital economy, unlocking a series of innovative services, including healthcare³, autonomous vehicles⁴, smart cities⁵, and intelligent manufacturing⁶. According to a report from the Global Mobile Suppliers Association (GSA)⁷, more than 70 countries had launched 5G networks by June 2022. Among countries with ambitious plans to deploy 5G, China has been the global leader in commercializing 5G networks. By the end of August 2022, China has set up more than 2.1 million 5G base stations⁸, which accounts for more than 60% of the total 5G base stations worldwide.

On the other side, the primary concern for launching 5G is the high energy consumption. Compared to previous generations of mobile networks, 5G networks have more antennas⁹ and larger bandwidths¹⁰, which dramatically increase the energy consumption of base stations. China Mobile’s measurement report¹¹ indicates that the energy consumption of a 5G base station is 4.3 KWh, which is four times that of a 4G base station of 1.1 KWh. One 5G base station is estimated to produce 30 tons of carbon emissions for one year of operation¹². Thus, 5G networks in China are estimated to produce over 60 megatons of carbon emissions annually at the national level. Such high energy consumption and carbon emissions would cause severe environmental problems. In order to avoid or mitigate the negative environmental impacts, we need to collect more detailed and concrete evidence from large-scale real-world data¹³ to reveal and quantify the greenhouse impacts caused by the launch of 5G networks, and further explore a sustainable development pathway for mobile networks in China.

In this study, we delve into the sustainability of 5G mobile networks in China, aiming to find an environmentally friendly method to launch and operate 5G mobile networks. To quantify carbon emissions induced by mobile networks, we propose a simulation-based model considering both the mobile communication system and the power generation system and monitoring their complicated interactions. Specifically, we first collect a large-scale real-world dataset from Nanchang, a provincial capital

in China, for modeling the energy consumption of mobile networks. The dataset includes energy consumption data (Dataset D1) of sampled base stations and traffic data (Dataset D2) of the entire network over several months. To the best of our knowledge, the dataset we collected is one of the largest in terms of data size and duration. Based on the energy consumption dataset, we build reliable energy consumption models of various types of base stations (Method M1), which estimate energy consumption with a high R-square of around 0.8 based on their traffic loads. By feeding traffic data of mobile networks into the energy consumption model, we obtain the estimated energy consumption. Next, we quantify the thermal coal consumption of power plants supporting functions of mobile networks by jointly modeling the energy consumption of mobile networks and power generation systems (Method M2).

Based on the energy consumption and carbon emission estimation model, we discover the energy and carbon efficiency traps caused by the launch of 5G. Energy efficiency^{2,11,14}, defined as the ratio of mobile network traffic to energy consumption, is a crucial metric in the operation of mobile networks. We calculate the energy efficiency of mobile networks in Nanchang using the energy consumption model and network traffic data (Datasets D2). Our results indicate that the launch of 5G will lead to high energy consumption and a sharp decline in the energy efficiency of the entire mobile networks, which include both 4G and 5G networks: the energy efficiency in Nanchang pre-5G is 2.02 TByte/MWh, and is estimated to drop to 1.42 TByte/MWh after the launch of 5G (Supplementary Figure 1). The lower energy efficiency makes the mobile system consume extra energy to support the same amount of network traffic, forming an energy efficiency trap. According to our estimation model (Method M2), China is expected to consume an extra 35.02 ± 0.33 Terawatt-hour (TWh) of energy, equivalent to an additional 23.82 ± 1.07 megatons of carbon emissions. The additional carbon emissions are approximately equivalent to 80% of the annual carbon emissions of the power sector in France¹⁵. Therefore, if our societies do not take effective actions to cut down on the additional carbon emissions caused by the launch of 5G, the negative environmental impact could be catastrophic and irreversible. By exploring the link between energy efficiency and the launch of 5G, we identify that the decrease in energy efficiency is primarily due to the exacerbated misalignment between cellular traffic and energy consumption. Specifically, the misalignment occurs when a network's energy consumption is not directly proportional to its traffic load in spatial and temporal domains (see Supplementary Note 1 for details).

To mitigate the misalignment and improve energy efficiency, we propose DeepEnergy, an energy-saving method leveraging collaborative deep reinforcement learning and graph neural networks to adaptively control the working state of base stations based on their dynamic traffic loads (Method M3). When a base station's traffic load is relatively low, DeepEnergy will proactively switch the base station into a low-power operation mode to mitigate the misalignment between traffic loads and energy consumption. By implementing DeepEnergy on Nanchang's mobile networks, the misalignment factors¹ are estimated to reduce from 0.56 to 0.28 on average. As a result, the energy efficiency and carbon efficiency will reach 2.83 TByte/MWh and 4.16 TByte/tCO₂, respectively, nearly twice as much as the case without employing DeepEnergy. It is estimated that DeepEnergy would successfully help over 71% of Chinese provinces to avoid energy efficiency traps and additional carbon emissions. In addition, applying DeepEnergy would reduce 20.90 ± 0.98 megatons of carbon emissions at the national level in China in 2023. By further integrating DeepEnergy and solar energy systems, the mobile network is estimated to accomplish over 50% of its net-zero target. Our study paves the way for achieving sustainable development goals and future net-zero mobile networks by providing insight into carbon emission mitigation in 5G network infrastructure operations.

Results

Launching 5G Leads to Carbon Efficiency Trap

We quantify and estimate the carbon emissions of mobile network operations in Nanchang from 2020 to 2023 (Method M2.1). As illustrated in Figure 1 (a), the launch of 5G results in an increase in daily network capacities from 12 PByte (12,264 4G base stations) to 22 PByte (12,264 4G base stations and 2,159 5G base stations). The operation of newly launched 5G base stations has led to a sharp increase in energy consumption and a decline in energy efficiency (Supplementary Figure1). Correspondingly, there has been a dramatic increase in daily carbon emissions of 178 tons after launching 5G (Figure 1 (b)). Carbon efficiency, the amount of network traffic that can be delivered for one unit of carbon emissions, decreases from 2.98 TByte/tCO₂ to 2.08 TByte/tCO₂ (Figure 1 (c)). After launching the 5G network, there is a large and rapid increase in carbon emissions. Nevertheless, the traffic load does not grow in the same trend, exacerbating the misalignment between cellular network traffic and energy consumption, which is the critical reason for lowering the carbon efficiency of the mobile network. Although the carbon efficiency does increase over time as mobile users consume more network traffic, Nanchang is estimated to take more than six months to return to its pre-5G level of carbon efficiency. This decrease in carbon efficiency and subsequent recovery process is referred to as the carbon efficiency trap, as depicted by the grey shadow area in Figure 1 (c). In the carbon efficiency trap, the mobile network will produce additional carbon emissions to carry the same network traffic due to the reduction in

¹A metric to measure the severity of misalignment between traffic loads and energy consumption, which is in the interval [0, 1]. The misalignment is more severe as the factor increases. (See Supplementary Note 1 for details)

carbon efficiency. In Nanchang, for example, the efficiency trap is estimated to cause additional 13.11 ± 0.74 Kilotons of carbon dioxide.

The energy consumption of a mobile network depends on the number of base stations (Supplementary Figure 2). We next generalize the simulation results from Nanchang to all provinces in China using the Monte Carlo method by considering the number of 4G and 5G base stations in each province (Method M2.2). The uncertainty in carbon emissions caused by mobile networks in each province is approximate -6% and +6% at the 95% confidence level (see Supplementary Tables 7 and 16 for details). According to the estimation results, the eastern provincial regions have a higher number of 5G base stations and generate more additional carbon emissions (Figures 1 (d) and 1 (e)). Guangdong, Jiangsu, and Zhejiang are the top three contributors, each accounting for 0.13, 0.11, and 0.08 of the national carbon emissions. In contrast, the western provincial regions, such as Qinghai and Tibet, have fewer 5G base stations and produce fewer additional carbon emissions. In addition, compared to the less developed western areas, the wealthier eastern provincial regions have higher additional carbon emissions per unit area (Figure 1 (f)). Tibet has the lowest additional carbon emissions per unit area of $0.0155 \text{ tCO}_2/\text{km}^2$, whereas Shanghai's additional carbon emissions per unit area are roughly 10,811 times higher ($167.58 \text{ tCO}_2/\text{km}^2$). Notably, the amount of carbon dioxide each square kilometer of the forest is capable of absorbing approximately 500 tons per year¹⁶. In other words, the additional carbon emissions caused by the launch of 5G in Shanghai would require a forest, which is the same size as Shanghai city, to take at least four months to absorb. Therefore, based on the intensity and density of additional carbon emissions, China, especially the eastern provincial regions, may face severe environmental issues which would cause irreversible damage during the launch of 5G. We urgently need to dig into the root causes and find a solution to sustainably launch and operate 5G networks.

Cellular Traffic and Energy Consumption Show Huge Spatio-temporal Misalignment

To uncover the causes of the carbon efficiency trap, we investigate the spatio-temporal misalignment between cellular traffic and energy consumption, which refers to the fact that the energy consumption of a mobile network is not directly proportional to the traffic load. Taking the network traffic data of Nanchang as an example, Figure 2 (a) shows how the energy consumed by the mobile network varies with the aggregated traffic load. Even with light traffic of 2.5 TBytes, i.e., 1% of the network capacity, the energy consumption is relatively high at 25.6 MWh, roughly 42% of the maximum energy consumption. A mobile network reaches its maximum energy consumption, denoted by E_{Max} , when the carried traffic reaches its available capacity C . In contrast, the desired energy consumption¹⁷, which is proportional to the traffic load (the green dashed line in Figure 2 (a)), is much less, at only about 0.6 MWh for light traffic of 2.5 TBytes. To measure the misalignment between traffic load L and energy consumption E , we define a metric called the misalignment factor, denoted by $M = \tilde{E} - \tilde{L}$, where $\tilde{E} = E/E_{Max}$ represents the normalized energy consumption and $\tilde{L} = L/C$ represents the normalized traffic load. The misalignment factor is in the interval $[0, 1]$ to measure the discrepancy between normalized energy consumption and traffic load (see Supplementary Note 1 for details). It is more severe as the factor increases. When $M = 0$, the energy consumption is directly proportional to the traffic load, and there is no misalignment.

The misalignment factor between traffic load and energy consumption changes over time and space. As illustrated in Figure 2 (b), the misalignment factor shows an apparent daily pattern, with higher values at night and lower values during the day. Specifically, the misalignment factor of 5G networks (0.68) is much higher than that of 4G networks (0.49), increasing the misalignment factor of the entire mobile network to 0.56 on average. Regarding spatial distribution, the misalignment factors of 5G networks are higher in the city center where the 5G base stations are more concentrated (Figure 2 (d)). The misalignment factors of 4G networks are generally uniformly distributed with low values (Figure 2 (c)). Thanks to years of optimization of 4G base station deployments, the energy consumption of 4G base stations has been having a similar spatial distribution with the traffic loads (Supplementary Figure 3). In contrast, due to the insufficient traffic profiles of 5G applications, the deployment of 5G base stations is not yet optimized, which leads to extremely high misalignment factors, often exceeding 0.8, in most regions.

Given a mobile network's traffic load L , the energy efficiency, denoted by $\eta^{Energy}(L)$, can be expressed as $\eta^{Energy}(L) = \eta_{Desired}^{Energy} / (1 + M/\tilde{L})$, where $\eta_{Desired}^{Energy} = C/E_{Max}$ denotes the desired energy efficiency of that mobile network (see Supplementary Note 1 for details). Thus, the energy efficiency is affected by three key factors: \tilde{L} , $\eta_{Desired}^{Energy}$, and M . Specifically, $\eta_{Desired}^{Energy}$ depends on the technologies used in the mobile network. Thanks to the advanced technologies of 5G, such as massive MIMO and subframe silence^{18, 18}, the desired energy efficiency of 5G is 6.29 TByte/MWh, which is twice that of 4G (3.01 TByte/MWh). However, the rise in the misalignment factor reduces energy efficiency. As illustrated in Figure 2 (f)-(h), regions with large misalignment factors exhibit low energy efficiency and vice versa. The average energy efficiency of the city center falls from 2.98 TByte/MWh (4G networks) to 1.94 TByte/MWh (covering both 4G and 5G networks), corresponding to the increase in the misalignment factor. In summary, launching 5G networks increases the misalignment between traffic load and energy consumption, and lowering the energy efficiency of the entire mobile networks.

Figures 2 (i) and (j) depict one-week patterns of 4G and 5G networks for traffic loads, energy consumption in the real world, and the desired energy consumption without misalignment, respectively. The traffic loads of both 4G and 5G exhibit a diurnal

rhythm. Whereas, the network energy consumption remains almost constant throughout the day. Such findings are consistent with Figure 2 (a). Also, there is a vast gap between the current energy consumption with huge misalignment and the desired energy consumption without misalignment (colored areas in Figure 2 (i)), indicating a remarkable potential to reduce energy consumption and increase energy efficiency by addressing the spatio-temporal misalignment between cellular traffic and energy consumption in mobile networks.

Energy-Saving Methods Mitigate Efficiency Trap and Misalignment

The main factor behind the misalignment between traffic and energy is that the energy consumption of cooling devices and fixed radio transmission overhead at the base station are unaffected by traffic load (see Supplementary Note 2 for details). One solution to mitigate the misalignment is to switch the base station into low-power operation mode by proactively turning off some components, such as the power amplifier and cooling devices, when the traffic load is relatively low. This low-power operation mode of the base station is known as the sleep mode¹⁹. Notably, a base station in sleep mode cannot provide service. Therefore, other active compensation base stations nearby must handle mobile users who were previously served by the base station in sleep mode (see Supplementary Note 4 for details).

We propose an artificial intelligence (AI) empowered energy-saving method, DeepEnergy, which is based on collaborative deep reinforcement learning to control the working state of cells² adaptively (Method M3). Specifically, DeepEnergy models each cell as an intelligent agent that self-decides its working state based on traffic loads. DeepEnergy aims to learn an action-value network for cells, which would help quantify how much energy could be saved from each cell's working state decision. Since the mobile network is enormous and cells may interact with each other, DeepEnergy adopts a collaborative grid-based learning strategy to learn the action-value network. DeepEnergy divides the region into small grids based on the compensation relationships of cells. The cells in each grid are equivalent in service capability, and thus can act as collaborative compensation cells for each other. Moreover, DeepEnergy models the attribution relationships between cells and base stations. As a result, DeepEnergy considers both intra-grid and intra-base station collaboration among cells, making it possible to effectively coordinate the working state of tens of thousands of cells.

We compare DeepEnergy with two classical energy-saving methods: threshold-based method²⁰ and greedy method¹⁷ (see Supplementary Note 4 for details). Overall, DeepEnergy outperforms others on the entire mobile network, consisting of 4G and 5G, reducing the misalignment factors from 0.56 to 0.28 on average (Figure 3 (e)). The threshold-based method performs the worst because there is no inter-cell collaboration, and cells independently decide whether to enter sleep mode based on a predefined traffic load threshold. As a result, the threshold-based method can only barely work at night when base station traffic is typically low (Figures 3 (a)). Alternatively, the greedy method considers intra-grid collaboration and has a comparable performance with DeepEnergy (Figure 3 (c)). Regarding the spatial distribution, DeepEnergy performs noticeably better in the city center with a misalignment factor of 0.22, which is much lower than that of the greedy method (0.53) and of the threshold-based method (0.41) (Figures 3 (b), (d), and (f)). This is because the city center's base station density is comparatively high. DeepEnergy considers both intra-grid and intra-base station collaborations of cells, making it more effective in dealing with regions with dense base station deployments and complex interactions between cells. Considering that the average density of 5G base stations is expected to be three times higher than that of 4G in the future¹¹, DeepEnergy has greater potential for energy savings in future mobile networks with super base station densities.

Accredit to the reduction in misalignment factors, DeepEnergy significantly improves the energy efficiency and carbon efficiency of mobile networks, reaching 2.83 TByte/MWh and 4.16 TByte/tCO₂, almost doubled in comparison to the case without energy-saving (Figure 3 (g)). We next generalize the results from Nanchang to all provinces in China (Method M2.2). Our results show that energy-saving methods can reduce the additional carbon emissions caused by launching 5G in China from 23.82 ± 1.07 megatons to 11.34 ± 0.46 megatons (threshold), to 4.24 ± 0.17 megatons (greedy), and to 0.18 ± 0.01 megatons (DeepEnergy). Specifically, DeepEnergy can help more than 71% of provinces in China successfully avoid the energy efficiency trap without producing additional carbon emissions (Figure 3 (h)). In addition, applying DeepEnergy would continue to reduce carbon emissions every year, which is estimated to reduce 25.12 out of 50.52 megatons (2021), 24.65 out of 51.03 megatons (2022), and 20.90 out of 55.42 megatons (2023) at the national level (see Supplementary Tables 9-11 and 16 for details).

Renewable Energy Helps Achieve Net-zero Mobile Networks

Due to diurnal rhythms, DeepEnergy performs better at night than in the daytime (Figure 4 (a)). Also, with the increase in traffic, the carbon reduction ratio will decrease significantly during the day, dropping below 0.3 when the traffic load reaches 90% of network capacity. Thus, DeepEnergy will have limitations in terms of energy-saving during the daytime. Fortunately, the photovoltaic (PV) power system can operate during the day and provide renewable energy to the mobile network, further reducing carbon emissions in the daytime (Figure 4 (b)). By deploying PV panels on base stations²¹, DeepEnergy and the PV power system can work together to reduce carbon emissions both day and night.

²A cell refers to a carrier on a sector of a base station. A base station generally has multiple cells.

We next assess the carbon efficiency of the mobile network in Nanchang when we jointly operate DeepEnergy and the PV system through our proposed simulation-based system. Specifically, we locate PV panels at each base station and use PVWatts^{22,23} to estimate the potential electric generation of the PV system (Method M4). Figure 4 (c) depicts the carbon efficiency of PV systems with various sizes of PV panels for DeepEnergy and the case without energy-saving. The carbon efficiency of PV system using DeepEnergy is much higher than the case without energy-saving. The overall carbon efficiency increases as cellular traffic boosts. The gap in carbon efficiency between DeepEnergy and the case without energy-saving widens from 1.50 TByte/tCO₂ to 3.12 TByte/tCO₂ when the traffic load reaches 90% of network capacity. Therefore, combining DeepEnergy and the PV system can significantly improve the carbon efficiency of a mobile network.

The establishment of PV systems must take into account the economic investment²⁴. We next estimate the costs of construction and maintenance of PV systems and reveal how system performance changes with various economic investments. As illustrated in Figure 4 (d), as investment increases, the mobile network becomes closer to the goal of net-zero. The mobile network is estimated to achieve over 50% of its net-zero targets with DeepEnergy and a PV system when the annual investment contributed to the PV system is 13.85 million CNY. However, as the size of the PV system increases, the energy curtailment will become severe^{25,26}, lowering the cost efficiency due to marginal utility. We find that applying solar energy alone to reduce carbon emissions is not enough to achieve cost-effectiveness, with levelized cost of carbon abatement (LCCA) of 308.18 CNY/tCO₂. The LCCA can be reduced to about one ninth when we integrate DeepEnergy, which is 34.29 CNY/tCO₂. As a result, DeepEnergy can help solar energy become an affordable path toward net-zero mobile networks in terms of cost efficiency.

Discussion and Implications

Our study reveals that the launch of 5G will lower the energy efficiency of the entire mobile network due to the high misalignment between traffic loads and energy consumption. The decline in energy efficiency will result in significant additional energy consumption and additional carbon emissions, causing irreparable harm to the environment. Therefore, we are facing urgent needs for an environmentally friendly launch and operation strategy and must alter how we currently launch and operate 5G mobile networks. In this paper, we propose an energy-saving method, DeepEnergy, to proactively control base stations' working states based on their dynamic traffic loads. DeepEnergy can mitigate the misalignment between traffic and energy in mobile networks, remarkably improving energy efficiency. As a result, in addition to assisting cities in avoiding energy efficiency traps, DeepEnergy continues to reduce energy consumption over time. For instance, it is estimated that from January 2021 to January 2023, the energy efficiency gain of Nanchang introduced by DeepEnergy will rise from 1.41 TByte/MWh to 3.73 TByte/MWh, and DeepEnergy will reduce 30.74 TWh of energy consumption in 2023. Furthermore, by integrating DeepEnergy and solar energy, the mobile network is estimated to accomplish over 50% of its net-zero target. Consequently, DeepEnergy can assist in the launch of 5G and make the mobile network infrastructure update process more environmentally friendly. However, there are several potential obstacles that might be encountered when implementing DeepEnergy. Firstly, DeepEnergy is a machine learning model requiring significant data to train and optimize. The availability and quality of the data could be a potential limitation. Secondly, implementing DeepEnergy at scale would require computational resources and technical expertise, which could be hard to achieve for some organizations. Finally, operators may emphasize encouraging the usage of 5G networks and be reluctant to set 5G base stations to sleep, which may cause the operators to forgo DeepEnergy for commercial reasons.

As an initial attempt, our study still has some limitations. Our analysis is conducted based on real-world datasets collected from China Mobile. The carbon emissions of mobile networks are underestimated because China Mobile only accounts for a portion of the market share (over 58%). We generalize the simulation results from Nanchang to all the provinces in China, which would cause uncertainty. Renewable energy resources in different provinces in China are expected to be uneven. Many regions in western China have abundant indigenous renewable energy resources. The uncertainty resulting from differences in the distribution of energy resources will affect the path toward net-zero goals. In China, the deployment of new 5G base stations is still ongoing. Our study only examined the first wave of 5G base station launches, which may lead to an underestimation of carbon emissions.

Sustainable development goals (SDGs) are urgent call for actions for all industries. Our study quantifies the environmental impacts of launching 5G mobile networks and proposes a practical approach to achieve the SDGs in mobile networks by integrating energy-saving methods and solar energy systems. Our study offers a firm foundation for further research into the environmental deployment and operation of 5G networks. Additionally, as newer AI architectures and more powerful reinforcement learning models continue emerging, our study opens the door for developing more sophisticated systems for carbon emission reduction in mobile networks. The cost of deploying AI algorithms on base stations is much lower than the investment in renewable energy equipment, making it more affordable for developing countries to launch 5G environmentally friendly. Consequently, AI technologies not only help achieve the SDGs in mobile networks accredit to their superior performance, but also mitigate digital inequality among developed and developing countries because of low deployment costs.

Datasets

In this paper, we simulate the carbon emissions from mobile networks in Nanchang and then extrapolate the results to all provinces in China. The following data are collected to assess the investigation: energy consumption data of base stations, network traffic data in Nanchang, and the number of base stations and mobile users in each province.

D1. Energy Consumption Data of Base Stations

Energy consumption data are essential for building the energy consumption model of base stations. We collected the data from 300 4G base stations and 266 5G base stations in real-world mobile networks over one week in May 2022. The energy consumption records of base stations are collected every half hour. Each record includes the base station ID, timestamp, physical resource block (PRB) usage ratio, traffic volume, the number of users served, transmit power, baseband unit (BBU) power, and remote radio unit (RRU)³ power (see Supplementary Table 1 for details). The energy consumption dataset covers four types of 5G base stations and three types of 4G base stations, each with a different maximum transmit power setting (see Supplementary Note 2 for details).

D2. Network Traffic Data in Nanchang

Network traffic load is a crucial factor that determines the energy consumption of mobile networks. The network traffic data was also collected from China Mobile. We carried out a city-level measurement in Nanchang and collected fine-grained records on the network traffic of all 4G and 5G base stations for one week in May 2022. The network traffic data covers 12,264 4G base stations and 2,159 5G base stations. Each network traffic record is collected every half hour and contains the base station ID, timestamp, PRB usage ratio, traffic volume, and the number of users served (see Supplementary Table 1 for details). The fine-grained dataset is to reveal the mobile network’s daily energy consumption patterns. We also conducted a long-term monthly measurement in Nanchang and collected its monthly network traffic for 4G and 5G networks over 17 months, from January 2021 to May 2022 (see Supplementary Table 2 for details). The monthly dataset is used to examine the long-term trends in energy consumption and carbon emissions.

D3. Number of Base Stations and Mobile Users in Each Province

We gathered the number of 4G and 5G base stations in each province in China to generalize the results from Nanchang to all provinces because the quantity of energy consumption and carbon emissions of mobile networks are directly related to the number of base stations (Supplementary Figure 2). Also, we gathered the number of mobile users in each province to estimate its network traffic since the average traffic per user across regions is comparable. The Ministry of Industry and Information Technology of the People’s Republic of China²⁷ releases monthly data on the number of base stations and mobile users in each province (see Supplementary Tables 3 and 4 for details).

Methods

In this paper, we first build a reliable data-driven energy consumption model of base stations, which estimates energy consumption based on base stations’ traffic loads. Next, we develop a carbon emission estimation model consisting of two parts: carbon emission estimation in Nanchang and carbon emission estimation across provinces. The estimation model considers both the mobile communication system and the power generation system and monitors the complicated interactions between these two systems. We next propose an energy-saving method called DeepEnergy, which uses a collaborative multi-agent deep reinforcement learning method that learns to optimize the working states of cells dynamically. Lastly, we analyze solar energy systems to discover the net-zero path of the mobile network.

M1. Energy Consumption Model of Base Stations

Base stations are fundamental elements of mobile networks and are their principal energy consumers¹¹. A base station generally consists of a communication subsystem and a supporting subsystem (see Supplementary Figure 7 for details). The Remote Radio Unit (RRU) and Baseband Unit (BBU), major components of the communication subsystem, are responsible for transceiving radio signals and processing baseband signals, respectively. A base station may have several RRUs and BBUs. The cooling and other auxiliary devices are part of the supporting subsystem. The cooling equipment, like air conditioning, is used to keep the base station at a proper operating temperature. The total power consumption P_{BS} of a base station can be calculated as follows,

$$P_{BS} = P_{Tx} + P_{cooling}, \quad (1)$$

where P_{Tx} denotes the power consumption of the communication subsystem and $P_{cooling}$ denotes the power consumed by cooling equipment to maintain an appropriate operating temperature. In this paper, we only model the cooling devices for the supporting subsystem because they account for over 90% of the supporting system’s power consumption²⁸.

³In 5G networks, this part is called the active antenna processing unit (AAU). In this paper, we uniformly refer to the RRU for both 4G and 5G.

The power consumption of the communication subsystem P_{Tx} is dominated by two components,

$$P_{Tx} = P_{BBU} + P_{RRU}, \quad (2)$$

where P_{RRU} varies according to the amount of base station traffic. When the traffic load is heavy, RRU has to consume more power to support more active physical resource blocks (PRBs)⁴. On the other hand, baseband processing is handled by BBUs. P_{BBU} is proportional to the number of BBUs equipped at base stations. No matter how many PRBs are active, their power consumption remains constant and does not change in response to base station traffic. By analyzing real-world data, we find that the BBU power of a base station is related to the number of cells it has (Supplementary Figure8) because a base station with more cells generally has more BBUs. There are three types of base stations (BSes) in terms of their number of cells and network types: 4G BS with three cells, 5G BS with three cells, and 5G BS with six cells. Since the BBU power of a particular BS type is mainly distributed in a small interval ($\pm 8.88\%$), we use the average value to approximate it (Supplementary Table 20). Specifically, for a 4G BS with three cells, its BBU power is simulated as 89.3771 W. For a 5G BS with three cells, its BBU power is simulated as 305.0409 W. For a 5G BS with six cells, its BBU power is simulated as 499.6484 W.

According to the energy consumption data of base stations, P_{RRU} varies from 200W to 1200W and shows a linear relation with transmit power P_{Trans} (Supplementary Figures 9 and 11).

$$P_{RRU} = \alpha \cdot P_{Trans} + \gamma, \quad (3)$$

where α and γ denote slope and offset, respectively. In practice, α depends on the power amplifier efficiency of base stations, and γ depends on fixed circuit power²⁹. The linear regression model can approximate the P_{RRU} of various base stations well, with an R-squared of over 0.75 for 5G base stations (Supplementary Figure 10) and over 0.93 for 4G base stations (Supplementary Figure 11). Different base station types have specific coefficients in the linear regression model, as depicted in Supplementary Tables 21 and 22. The offset γ of 5G base stations is typically 2 to 7 times greater than that of 4G base stations, reflecting the extremely high fixed circuit power of 5G base stations.

The transmit power P_{Trans} ranges from 0W to 300W. We find that transmit power varies with the PRB usage ratio, and a linear regression model can approximate this relationship (Supplementary Figures 12 and 14).

$$P_{Trans} = \beta \cdot r_{PRB} + \sigma, \quad (4)$$

where r_{PRB} denotes the PRB usage ratio, β and σ denote slope and offset, respectively. As depicted in Supplementary Tables 21 and 22, base stations of different types also have different coefficients. The linear regression model can model transmit power with an R-squared of over 0.96 for 5G base stations and 1 for 4G base stations. Also, since 5G base stations adopt more advanced physical technologies, e.g., subframe shutdown³⁰, the offset σ in (4) equals 0. By substituting (4) into (3), we obtain the relationship between RRU power (P_{RRU}) and PRB usage ratio (r_{PRB}). Given a base station's traffic load L , r_{PRB} can be approximated as L/C , where C denotes the base station's capacity.

Alternatively, when a base station is in sleep mode, its RRU power becomes independent of its traffic load and principally distributed into a small interval (Supplementary Figure 15). Therefore, we use the average value to approximate the RRU power in sleep mode for different base station types (Supplementary Table 23). The RRU power in the sleep mode of 5G base stations ranges from 69.43W to 90.56W, which is significantly lower than that of 4G base stations, which range from 119.03W to 133.90W. Thanks to the advanced physical energy-saving technology utilized by 5G³¹.

The power consumption of the cooling devices is simulated using EnergyPlus³², a widely used program developed by Lawrence Berkeley National Laboratory (LBNL). EnergyPlus can simulate the power consumption of the cooling system every half hour, given the outdoor air temperature, the indoor proper operating temperature, the power generated by the communication subsystem, and the room size of a base station. Specifically, the outdoor air temperature data can be found in the World Meteorological Organization's weather dataset⁵. The communication subsystem is modeled as an electrical heat source, and its power consumption is estimated according to (2). According to the "Technical Standard for Mobile Communication Infrastructure of Construction" recognized by the Chinese government, we set the room size of a base station as $20m^2$ and $20^\circ C$ as the indoor proper operating temperature.

M2. Carbon Emission Estimation Model

We develop a carbon emission estimation model consisting of two parts: carbon emission estimation in Nanchang and carbon emission estimation across provinces. The first part quantifies the thermal coal consumption of power plants in Nanchang by jointly modeling the mobile network and the power generation system and monitoring the complicated interactions between these two systems. The second part aims to expand the results of Nanchang to all of China's provinces.

⁴A physical resource block is the smallest unit of resources allocated to a mobile user for carrying network traffic.

⁵<https://worldweather.wmo.int/en/home.html>

M2.1. Carbon Emission Estimation in Nanchang

Electricity Dispatch Model. Electricity dispatching, which selects available generating units in a region to meet the power loads, is typically used to schedule the amount of power generated by each plant. In this paper, a day-ahead unit commitment model is formulated to quantify the thermal coal consumption of power plants, which is expressed as a linear programming optimization problem:

$$\min_X \sum_{i \in \Phi} \sum_{t \in T} [c_i^{power} x_i^{power}(t) + c_i^{up} x_i^{up}(t) + c_i^{down} x_i^{down}(t)], \quad (5)$$

subject to:

$$\sum_{i \in \Phi} x_i^{power}(t) + P_{outside}(t) = P_{load}(t)/(1 - r_{loss}), \forall t \in T, \quad (6)$$

$$P_i^{min} x_i^{on/off}(t) \leq x_i^{power}(t) \leq P_i^{max} x_i^{on/off}(t), \forall i \in \Phi, \forall t \in T, \quad (7)$$

$$\sum_{i \in \Phi} P_i^{max} x_i^{on/off}(t) \geq P_{res}(t), \forall t \in T, \quad (8)$$

$$\sum_{\tau=t}^{t+T_i^{up}-1} x_i^{on/off}(\tau) \geq T_i^{up} x_i^{up}(t), \forall i \in \Phi, \forall t \in T, \quad (9)$$

$$\sum_{\tau=t}^{t+T_i^{down}-1} [1 - x_i^{on/off}(\tau)] \geq T_i^{down} x_i^{down}(t), \forall i \in \Phi, \forall t \in T, \quad (10)$$

$$x_i^{up}(t) + x_i^{down}(t) \leq 1, \forall i \in \Phi, \forall t \in T, \quad (11)$$

$$x_i^{up}(t) - x_i^{down}(t) = x_i^{on/off}(t) - x_i^{on/off}(t-1), \forall i \in \Phi, \forall t \in T, \quad (12)$$

$$x_i^{power}(t) \geq 0, \forall i \in \Phi, \forall t \in T, \quad (13)$$

$$x_i^{up}(t), x_i^{down}(t), x_i^{on/off}(t) \in \{0, 1\}, \forall i \in \Phi, \forall t \in T, \quad (14)$$

where Φ is the set of coal-fired power units and $T = \{1, 2, \dots, 48\}$ represents the time slots among a day's 48 half-hours. $X = \{x_i^{power}(t), x_i^{up}(t), x_i^{down}(t), x_i^{on/off}(t)\}$ are decision variables. $x_i^{power}(t)$ indicates the scheduled power generation of coal-fired power unit i at time slot t . $x_i^{up}(t)$ and $x_i^{down}(t)$ denote the startup and shutdown operations of the coal-fired power unit i at time slot t . $x_i^{on/off}(t)$ denotes the on/off states of the coal-fired unit i at time slot t . The objective (5) is to minimize the total economic cost, including the power generation cost $c_i^{power} x_i^{power}(t)$, the startup cost $c_i^{up} x_i^{up}(t)$ and shutdown cost $c_i^{down} x_i^{down}(t)$. (6) represents the equilibrium between power generation and consumption. $P_{outside}(t)$ denotes the input power from outside regions. $P_{load}(t)$ denotes the local power load at time slot t . r_{loss} denotes the average loss rate of power transmission. (7) specifies the upper and lower bounds of power generation. (8) regulates that the total capacity of working units must exceed the spinning reserve requirement $P_{res}(t)$. (9) and (10) indicate that each unit must maintain a working state for a minimum of half an hour. T_i^{up} and T_i^{down} denote the minimum on and off half-hours of power unit $i \in \Phi$. (11) and (12) show the connections between startup/shutdown operations and each power unit's on/off state. In (14), $x_i^{up}(t) = 1$ indicates a startup operation. $x_i^{down}(t) = 1$ indicates a shutdown operation. $x_i^{on/off}(t) = 1$ indicates that the power unit i is on.

In Nanchang, the source of electricity has two parts. One is from the local power plants distributed in Nanchang ($x_i^{power}, i \in \Phi$), and the other is from the input power from outside regions ($P_{outside}$). The local power plants in Nanchang are controllable in the electricity dispatch model, which support the energy consumption of mobile networks. According to the government report³³, Nanchang has three local power plants: the Nanchang plant, the Xinchang plant, and the Hongping plant.

The annual development report of China's power industry³⁴ shows that the thermal coal consumption rate for generation with different capacities is,

$$c_i^{coal} = \begin{cases} 0.3007 \text{ t/MWh}, & P_i^{max} > 300 \text{ MW} \\ 0.3357 \text{ t/MWh}, & P_i^{max} \leq 300 \text{ MW} \end{cases} \quad (15)$$

By optimizing (5), the optimal scheduling strategies for coal-fired power units can be obtained. Let $x_i^{power*}(t)$ denote the optimal solution. The total thermal coal consumption within one day, denoted by Q^{Coal} , can be calculated as follows:

$$Q^{Coal} = \sum_{i \in \Phi} \sum_{t \in T} \frac{1}{2} c_i^{coal} x_i^{power*}(t). \quad (16)$$

The coefficient $1/2$ refers to half an hour because the time slot in our case is in half an hour.

Carbon Emission Estimation for Mobile Networks. To examine the carbon emissions from mobile networks, the total power load $P_{load}(t)$ is divided into two parts:

$$P_{load}(t) = P_{orig}(t) + P_{BS}(t), \forall t \in T, \quad (17)$$

where $P_{orig}(t)$ is the residential and industrial power load excluding base station power load and $P_{BS}(t)$ is the power dispatched to base stations to meet their operational needs. The difference in carbon emissions with and without $P_{BS}(t)$ is used to characterize the carbon emission caused by mobile networks. Specifically, we first solve (5) with $P_{load}(t) = P_{orig}(t) + P_{BS}(t)$ and obtain the optimal solution of power generation $x_i^{power*(1)}(t)$. We next get the optimal solution of power generation $x_i^{power*(2)}(t)$ with $P_{load}(t) = P_{orig}(t)$. In terms of (16), the thermal coal consumption of mobile networks within one day, denoted by Q_{Mobile}^{Coal} , is computed as follows,

$$Q_{Mobile}^{Coal} = \sum_{i \in \Phi} \sum_{t \in T} \frac{1}{2} c_i^{coal} [x_i^{power*(1)}(t) - x_i^{power*(2)}(t)], \quad (18)$$

We consider China's thermal coal, which consists of anthracite, bituminous, lignite, etc. Liu et al.³⁵ pointed out that China's thermal coal has its unique low heating values ($h^{coal} = 20.95$ GJ/T) comparing with the global average heating value (29.3 GJ/T) provided by the United Nations. The net carbon content per energy is $\alpha^{coal} = 26.59$ tC/TJ, and the oxidation rate of thermal coal is set as $O^{coal} = 99\%$. Thus, the emission factor of China's thermal coal, denoted by e^{coal} , is calculated as follows,

$$e^{coal} = O^{coal} \cdot h^{coal} \cdot \alpha^{coal} \cdot 3.67 = 2.02 \text{ tCO}_2/\text{t}. \quad (19)$$

The carbon emissions from mobile networks, denoted by $Q_{Mobile}^{CO_2}$, is computed as follows:

$$Q_{Mobile}^{CO_2} = e^{coal} Q_{Mobile}^{Coal}. \quad (20)$$

In practice, the $P_{orig}(t)$ of Nanchang is approximated through the yearly and daily typical power load curves of Jiangxi province (see Supplementary Note 3 for details). Also, we assumed that solar panels are installed on base stations, which can supply a portion of the base stations' power load. Therefore, the power dispatched to a single base station is expressed as,

$$P_{BS,j}(t) = \begin{cases} \hat{P}_{BS,j}(t) - PV_{BS,j}(t), & \text{if } \hat{P}_{BS,j}(t) > PV_{BS,j}(t) \\ 0, & \text{otherwise} \end{cases}, \quad (21)$$

where $\hat{P}_{BS,j}(t)$ denotes the power load of base station j at time slot $t \in T$, $PV_{BS,j}(t)$ denotes the power generated by the solar panel installed on base station j , and $P_{BS,j}(t)$ denotes the power dispatched to base station j from power plants. Therefore, the power dispatched to base stations $P_{BS}(t)$ can be expressed as,

$$P_{BS}(t) = \sum_j P_{BS,j}(t). \quad (22)$$

M2.2. Carbon Emission Estimation Across Provinces

In this paper, we generalize the simulation results from Nanchang to all of China's provinces. We first estimate each province's network capacity and traffic through the number of base stations and mobile users. By assuming traffic and energy misalignment factors are comparable across different cities, we then estimate the energy efficiency for each province. We further estimate the energy consumption of mobile networks by dividing network traffic by energy efficiency. Lastly, we convert energy consumption to carbon emissions using the grid emission factors derived from Nanchang.

We apply the Monte Carlo method to estimate the capacity of mobile networks in each province. We repeatedly and randomly sample base stations from the Nanchang set according to the number of 4G base stations and 5G base stations in each province. The Monte Carlo simulations are performed 1,000 times for each province. By adding each sampled base station's capacity and maximum energy consumption, we can obtain the total network capacity C_p and maximum energy consumption $E_{Max,p}$ of mobile networks in province p .

We next estimate the network traffic of each province. We assumed that, for a given month, the average traffic per user across regions is comparable. Thus, we determine the average traffic per user in Nanchang.

$$\bar{L} = (L_{4G} + L_{5G})/N_{user}, \quad (23)$$

where \bar{L} denotes the average traffic per user, L_{4G} and L_{5G} refer to the traffic load of 4G and 5G networks in Nanchang, and N_{user} denotes the number of mobile users in Nanchang (Supplementary Table 2). We next estimate provincial network traffic based on the number of mobile users in each province (Supplementary Table 4),

$$L_p = \bar{L} \cdot N_{p,user}, \quad (24)$$

where L_p and $N_{p,user}$ denote the traffic load and the number of mobile users in province p , respectively.

Given the misalignment factor M_p of province p , the energy efficiency of the mobile network in province p , when the network traffic load is L_p , can be expressed as,

$$\eta_p^{Energy}(L_p) = \frac{C_p/E_{Max,p}}{(1 + M_p/\bar{L}_p)}, \quad (25)$$

where $\bar{L}_p = L_p/C_p$ denotes the normalized traffic load. We estimate the misalignment factor M_p of province p based on its normalized network traffic load and the energy-saving method it uses (see Supplementary Note 5 for details). The energy consumption of the mobile network in province p , denoted by E_p , can be estimated as,

$$E_p = E_{Max,p}(M_p + \bar{L}_p). \quad (26)$$

According to Nanchang's results, the average grid emission factor is $\gamma^{CO_2} = 0.68$ tCO₂/MWh, which has no significant difference before and after launching the 5G network (Supplementary Figure5). Thus, the carbon emissions of mobile networks in province p , denoted by $Q_{Mobile,p}^{CO_2}$, is computed as follows:

$$Q_{Mobile,p}^{CO_2} = E_p \cdot \gamma^{CO_2}. \quad (27)$$

M3. Energy-Saving Method in Mobile Networks

DeepEnergy divides all cells into multiple grids and then trains reinforcement learning (RL) agents to decide whether each cell should enter sleep mode at each time step (see Supplementary Note 4 for details). A cell refers to a carrier on a sector of a base station. Typically, a base station supports multiple sectors. Thus, a base station has multiple cells. The RL agents need to control the status of cells based on the current state of the mobile network to reduce the total amount of energy consumption. This includes the energy consumed by RRUs in cells and the energy consumed by BBUs and cooling devices in base stations. We model cell control as a multi-agent cooperation problem: each cell c_n is managed by an agent $agent_n$, and these agents cooperate to minimize energy consumption.

The observation of each agent $agent_n$ includes the feature vectors of other cells in the same base station or the same grid. The feature vector of cell c_n consists of time t , the traffic loads of the grid g_m that the cell c_n belongs to in the last four time steps, $(L_{t-4}^m, L_{t-3}^m, L_{t-2}^m, L_{t-1}^m)$, and the device parameters of the cells in $\mathcal{N}_m^g \cup \mathcal{N}_k^b$. \mathcal{N}_m^g denotes the set of cells in the grid g_m and \mathcal{N}_k^b denotes the set of cells of the base station BS_k that the cell c_n belongs to.

To encourage agents to work together, we set the reward for agent c_n to $r_n = -\sum_{n' \in \mathcal{N}_m^g} P_{n'}^{RRU} - P_k^{BBU} - P_k^{cooling}$ (see Supplementary Note 4 for details). The first term indicates the energy of RRUs in cells that belong to the same grid as cell c_n , so it could encourage the agent to cooperate with agents from these cells $\{c_{n'}\}_{n' \in \mathcal{N}_m^g}$. The second term indicates the energy of

BBUs and cooling devices in the base station that cell c_n belongs to, which may encourage the agent to cooperate with the agents from the same base station.

We consider training a policy network to output the action based on the current state to solve this multi-agent collaboration problem. However, the large number of agents will be a major challenge. On the one hand, the large-scale agents lead to massive state space. When an agent makes the decision, it should efficiently integrate the state of other associated agents. For this problem, we construct two graphs based on the intra-grid and intra-BS relationships and then use the graph neural network to integrate the information of the associated nodes (i.e., agents) in the graphs. On the other hand, large-scale agents also lead to complex interactions between agents, making the expected rewards of different actions difficult to estimate. Thus, we introduce the idea of Mean-Field MARL (MF-MARL³⁶) to integrate the effects of other agents' decisions on the target agent and design two masks to decrease the difficulty of action value estimation. The first mask denotes whether the grid's traffic demand could be met if the agent sets the respective cell to sleep. The second mask denotes whether all other cells under the same base station could sleep if the cell is set to sleep mode.

These masks are derived from the actions of other agents and can only be used as training input. Therefore, each agent has two action-value networks, $q^2(\mathbf{o}_n, a, \mathbf{m}_n; \theta_q^2)$ for training and $q^1(\mathbf{o}_n, a; \theta_q^1)$ for inference, where \mathbf{o} denotes the observation, a denotes the action, \mathbf{m} denotes masks, and θ denotes the parameters of action-value networks. In the execution stage, the action-value network without masks as input, $q^1(\mathbf{o}_n, a; \theta_q^1)$, predicts the rewards associated with different actions, setting the cell to sleep or not, based on the observation. Using ϵ -greedy method, the agent determines the status of the cell by sampling the action based on predicted rewards. After the statuses of all cells determined by the agents are executed, the rewards for all agents are calculated. All agents' observations, actions, and rewards are appended to the replay buffer. In the training stage, the action-value network with masks as input, $q^2(\mathbf{o}_n, a, \mathbf{m}_n; \theta_q^2)$, is trained with the replay buffer to predict the rewards of different actions based on the observation and masks. The network q^2 is optimized through the following loss function:

$$L_2 = \frac{1}{2} [q^2(\mathbf{o}_n, a, \mathbf{m}_n; \theta_q^2) - r_n]^2, \quad (28)$$

where the masks \mathbf{m}_n is obtained based on the actions recorded in replay buffer. The action-value network, $q^1(\mathbf{o}_n, a; \theta_q^1)$, is then optimized by imitating the second one, $q^2(\mathbf{o}_n, a, \mathbf{m}_n; \theta_q^2)$,

$$L_1 = \frac{1}{2} \sum_a [q^1(\mathbf{o}_n, a; \theta_q^1) - q^2(\mathbf{o}_n, a, \mathbf{m}_n; \theta_q^2)]^2, \quad (29)$$

where the mask \mathbf{m}_n are calculated based on the re-sampled actions, which is sampled as the process in the execution stage. The re-sampling process is equivalent to the sampling process for the distribution of the mask vector. Thus, the first network q^1 would learn to predict the rewards of various actions under the sampled distribution of the mask vector. The framework of DeepEnergy is shown in Supplementary Figure 19. The algorithm is shown in Supplementary Algorithm 1. Notably, after determining the working state of cells, we still need to re-distribute intra-grid network traffic among cells. The cells in each grid are equivalent in terms of service capability and thus intra-grid network traffic can be flexibly transferred between cells within the grid. Specifically, given the working state of cells, we will then re-distribute the intra-grid traffic of each active cell proportionally according to its capacity; namely, the cell with a higher capacity will carry more traffic.

M4. Solar Photovoltaic Modeling and Simulation

We use PVWatts^{22,23}, a photovoltaic system simulator developed by NREL (The National Renewable Energy Laboratory), to simulate the potential electric generation of a PV system. We locate PV panels using the coordinates of base stations and use the typical meteorological year data for simulation. Defaults set all other parameters as PVWatts provides the most up-to-date standards for PV installations (see Supplementary Table 5 for details).

The cost structure of a PV system is divided into the initial investment cost, the operation cost, and maintenance cost³⁷. The initial investment cost includes PV modules, supporting structures, inverters, wiring, junction boxes, engineering costs (design, transportation, and installation), and insurance. The annual operating costs are equivalent to 1% of system investment. The maintenance cost includes inverter replacement in the tenth year³⁸. We assume that the lifetime of the PV system is 20 years. The specific costs are listed in Supplementary Table 17, which are compiled from the China Photovoltaic Industry Association (China PV industry development roadmap; http://www.chinapv.org.cn/road_map.html). The cost data is real-world data collected from the photovoltaic industry of China by the China Photovoltaic Industry Association, and under the guidance of Ministry of Industry and Information Technology.

Data Availability

The number of base stations and mobile users in each province are listed in Supplementary Tables 3 and 4. The network traffic data and the number of mobile users in Nanchang are listed in Supplementary Table 2. Source data are provided with this paper.

Code Availability

The code used in this study can be downloaded from https://github.com/Tong89/Sustainability_5G.

References

1. Manyika, J. & Roxburgh, C. The great transformer: The impact of the internet on economic growth and prosperity. *McKinsey Glob. Inst.* **1** (2011).
2. Dang, S., Amin, O., Shihada, B. & Alouini, M.-S. What should 6G be? *Nat. Electron.* **3**, 20–29 (2020).
3. Mwangama, J., Malila, B., Douglas, T. & Rangaka, M. What can 5G do for healthcare in africa? *Nat. Electron.* **3**, 7–9 (2020).
4. Gohar, A. & Nencioni, G. The role of 5G technologies in a smart city: The case for intelligent transportation system. *Sustainability* **13**, 5188 (2021).
5. Dai, C., Liu, X., Lai, J., Li, P. & Chao, H.-C. Human behavior deep recognition architecture for smart city applications in the 5G environment. *IEEE Netw.* **33**, 206–211 (2019).
6. Taleb, T., Afolabi, I. & Baga, M. Orchestrating 5G network slices to support industrial internet and to shape next-generation smart factories. *IEEE Netw.* **33**, 146–154 (2019).
7. Global mobile suppliers association. 5G-market snapshot june 2022. <https://gsacom.com/paper/5G-market-snapshot-june-2022/> (2022).
8. Tomás, J. P. China ends august with 2.1 million 5G base stations: Report. <https://www.rcrwireless.com/20220923/5G/china-ends-august-2-million-5G-base-stations-report> (2022).
9. Al-Bawri, S. S., Islam, M. T., Islam, M. S., Singh, M. J. & Alsaif, H. Massive metamaterial system-loaded mimo antenna array for 5G base stations. *Sci. Reports* **12**, 1–16 (2022).
10. Hecht, J. *et al.* The bandwidth bottleneck. *Nature* **536**, 139–142 (2016).
11. I, C.-L., Han, S. & Bian, S. Energy-efficient 5G for a greener future. *Nat. Electron.* **3**, 182–184 (2020).
12. Ding, Y. *et al.* Carbon emissions and mitigation potentials of 5G base station in china. *Resour. Conserv. Recycl.* **182**, 106339 (2022).
13. Ilieva, R. T. & McPhearson, T. Social-media data for urban sustainability. *Nat. Sustain.* **1**, 553–565 (2018).
14. Yang, C., Li, J., Ni, Q., Anpalagan, A. & Guizani, M. Interference-aware energy efficiency maximization in 5G ultra-dense networks. *IEEE Transactions on Commun.* **65**, 728–739 (2016).
15. Tiseo, I. Power Sector Emissions in France from 2000 to 2021. <https://www.statista.com/statistics/1290541/power-sector-carbon-emissions-france/> (2022).
16. Birdsey, R. A. *Carbon storage and accumulation in United States forest ecosystems*, vol. 59 (US Department of Agriculture, Forest Service, 1992).
17. Peng, C., Lee, S.-B., Lu, S., Luo, H. & Li, H. Traffic-driven power saving in operational 3G cellular networks. In *Proceedings of the 17th annual international conference on Mobile computing and networking*, 121–132 (2011).
18. Rostami, S., Heiska, K., Puchko, O., Leppanen, K. & Valkama, M. Pre-grant signaling for energy-efficient 5g and beyond mobile devices: Method and analysis. *IEEE Transactions on Green Commun. Netw.* **3**, 418–432 (2019).
19. Wu, J., Zhang, Y., Zukerman, M. & Yung, E. K.-N. Energy-efficient base-stations sleep-mode techniques in green cellular networks: A survey. *IEEE communications surveys & tutorials* **17**, 803–826 (2015).
20. Yu, G., Chen, Q. & Yin, R. Dual-threshold sleep mode control scheme for small cells. *IET communications* **8**, 2008–2016 (2014).
21. Chamola, V. & Sikdar, B. Solar powered cellular base stations: current scenario, issues and proposed solutions. *IEEE Commun. magazine* **54**, 108–114 (2016).
22. Freeman, J. M. *et al.* System advisor model (sam) general description (version 2017.9. 5). Tech. Rep., National Renewable Energy Lab.(NREL), Golden, CO (United States) (2018).
23. Waldman, J., Sharma, S., Afshari, S. & Fekete, B. Solar-power replacement as a solution for hydropower foregone in us dam removals. *Nat. Sustain.* **2**, 872–878 (2019).

24. Peng, W. *et al.* Managing china's coal power plants to address multiple environmental objectives. *Nat. Sustain.* **1**, 693–701 (2018).
25. Wang, J. *et al.* Exploring the trade-offs between electric heating policy and carbon mitigation in china. *Nat. Commun.* **11**, 1–11, DOI: [10.1038/s41467-020-19854-y](https://doi.org/10.1038/s41467-020-19854-y) (2020).
26. Bogdanov, D. *et al.* Radical transformation pathway towards sustainable electricity via evolutionary steps. *Nat. communications* **10**, 1–16 (2019).
27. People's Republic of China's Ministry of Industry and Information Technology. Statistics in communication industry. <https://www.miit.gov.cn/gxsj/tjfx/txy/index.html> (2022).
28. Arnold, O., Richter, F., Fettweis, G. & Blume, O. Power consumption modeling of different base station types in heterogeneous cellular networks. In *2010 Future Network & Mobile Summit*, 1–8 (IEEE, 2010).
29. I, C.-L. *et al.* Toward green and soft: a 5G perspective. *IEEE Commun. Mag.* **52**, 66–73, DOI: [10.1109/MCOM.2014.6736745](https://doi.org/10.1109/MCOM.2014.6736745) (2014).
30. Huang, Y., Xu, X., Li, N., Ding, H. & Tang, X. Prospect of 5G intelligent networks. *IEEE Wirel. Commun.* **27**, 4–5, DOI: [10.1109/MWC.2020.9170260](https://doi.org/10.1109/MWC.2020.9170260) (2020).
31. Lopez-Perez, D. *et al.* A survey on 5G radio access network energy efficiency: Massive mimo, lean carrier design, sleep modes, and machine learning. *IEEE Commun. Surv. & Tutorials* **24**, 653–697, DOI: [10.1109/COMST.2022.3142532](https://doi.org/10.1109/COMST.2022.3142532) (2022).
32. Crawley, D. B. *et al.* Energyplus: creating a new-generation building energy simulation program. *Energy buildings* **33**, 319–331 (2001).
33. Government, N. M. P. Notice of the office of the people's government of nanchang city on forwarding the 2021 plan of the municipal development and reform commission and state grid nanchang power supply company for orderly power consumption of nanchang power grid. Tech. Rep., Gazette of Nanchang Municipal People's Government (2021). http://www.nc.gov.cn/nc_xxgk/jsp/zfgb/ncgb_content.jsp?mid=a731211fe1094abfaea8ab348bd5ba8b.
34. Council, C. E. *Annual Development Report of China's Power Industry (2021)* (China Building Materials Press, 2021), first edn.
35. Liu, Z. *et al.* Reduced carbon emission estimates from fossil fuel combustion and cement production in china. *Nature* **524**, 335–338 (2015).
36. Yang, Y. *et al.* Mean field multi-agent reinforcement learning. In *International conference on machine learning*, 5571–5580 (PMLR, 2018).
37. Yan, J., Yang, Y., Elia Campana, P. & He, J. City-level analysis of subsidy-free solar photovoltaic electricity price, profits and grid parity in china. *Nat. Energy* **4**, 709–717, DOI: [10.1038/s41560-019-0441-z](https://doi.org/10.1038/s41560-019-0441-z) (2019).
38. Kaabeche, A., Belhamel, M. & Ibtouen, R. Techno-economic valuation and optimization of integrated photovoltaic/wind energy conversion system. *Sol. energy* **85**, 2407–2420 (2011).

Author Contributions Statement

Tong Li, Depeng Jin, Yong Li and Tao Jiang conceived and designed the study. Li Yu and Yan Zhou collected and provided the data. Tong Li, Yibo Ma, Tong Duan, and Wenzhen Huang carried out the simulations and analyses. All authors contributed to the discussions on the method and the writing of this article.

Competing Interests

The authors declare no competing interests.

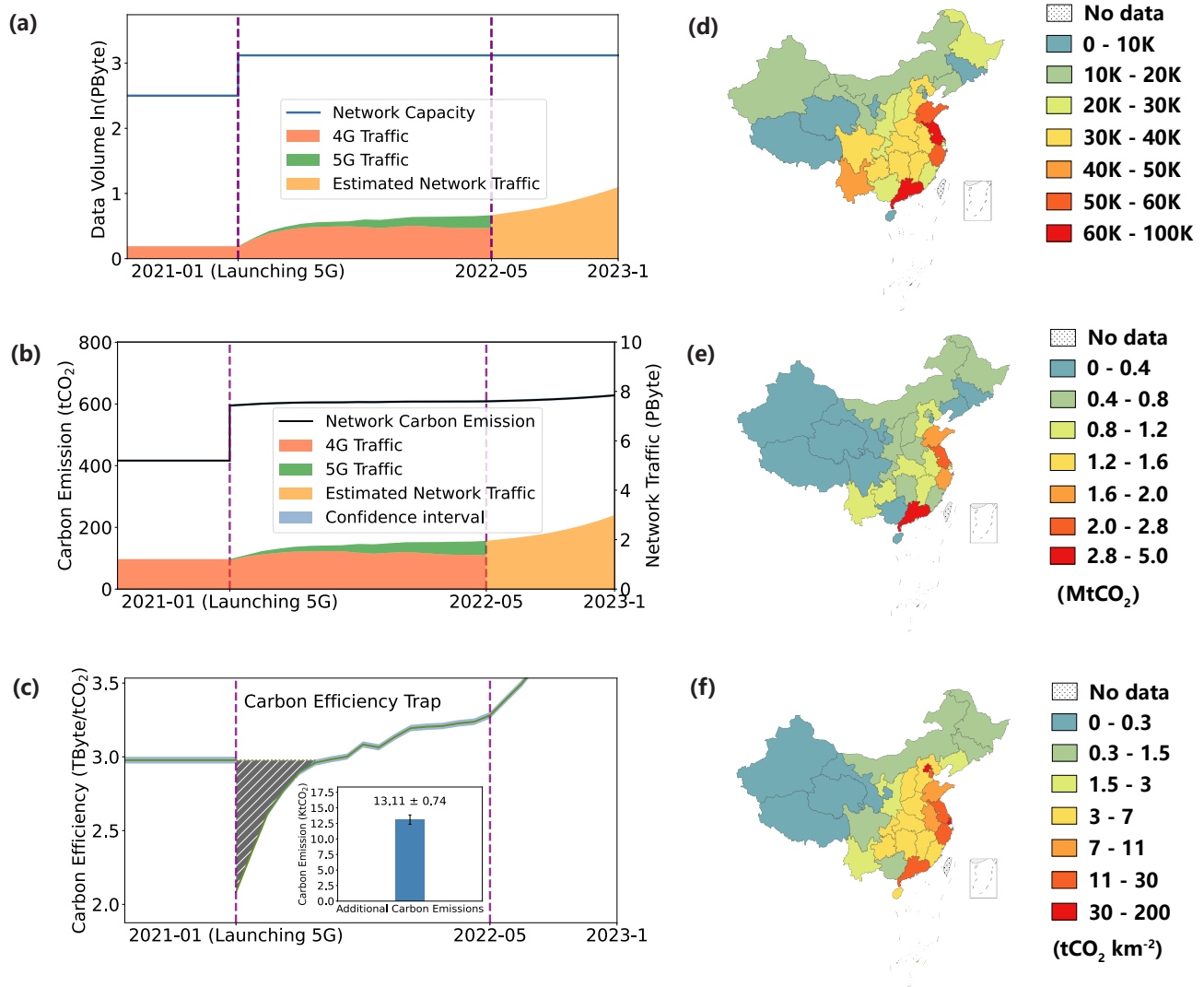


Figure 1. Analysis of the carbon efficiency after the launch of 5G networks. (a). Launching 5G leads to a substantial increase in daily network capacities in Nanchang. (b) The operation of newly launched 5G base stations has led to a sharp increase in carbon emissions in Nanchang. (c) Launching 5G leads to the appearance of a carbon efficiency trap and causes additional carbon emission of 13.11 ± 0.74 KtCO₂ in Nanchang. (d). The number of 5G base stations across different provinces in China. (e). The number of additional carbon emissions across different provinces in China. (f). The number of additional carbon emissions per unit space across different provinces in China.

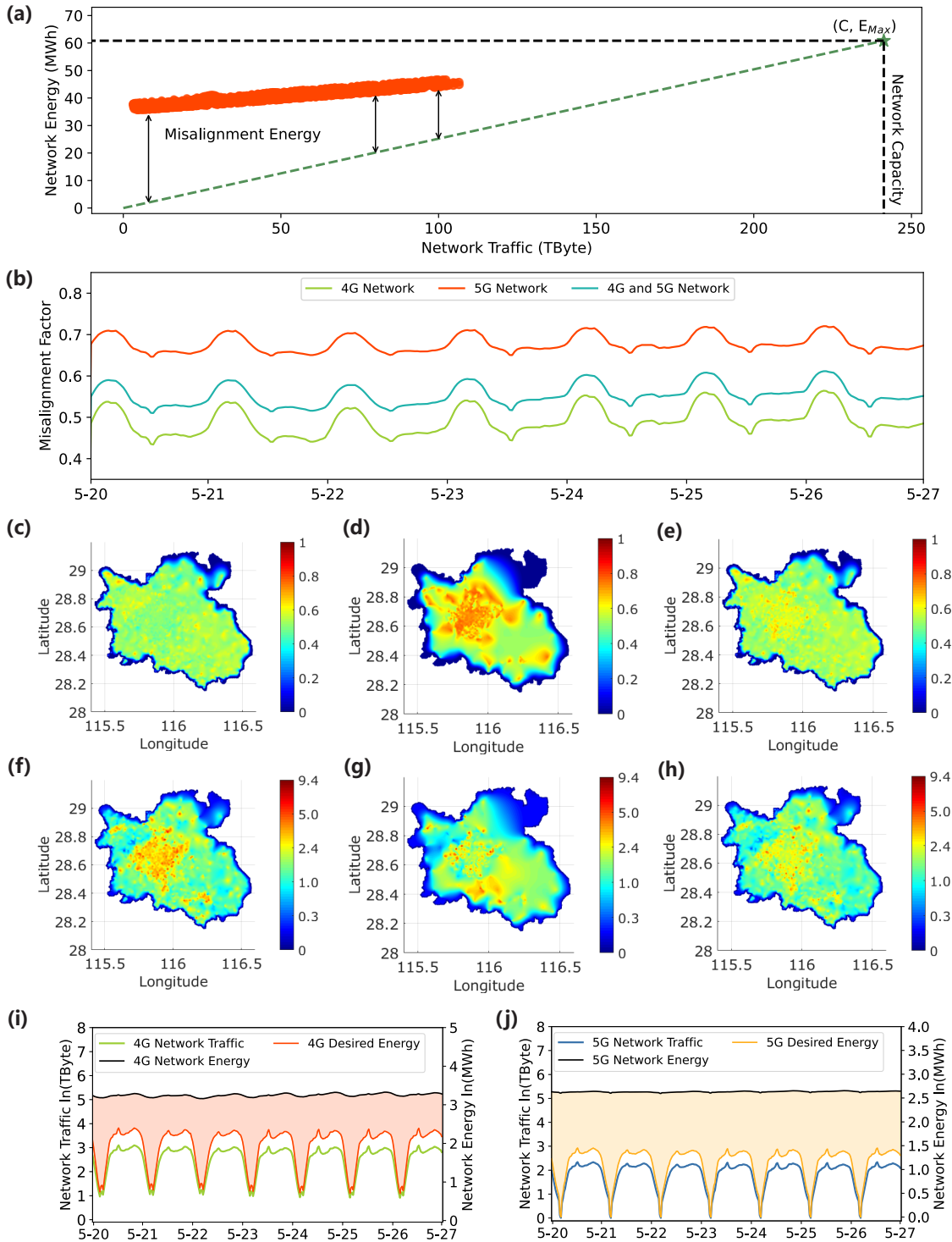


Figure 2. Cellular traffic and energy consumption show huge spatio-temporal misalignment. (a). The energy-traffic curve for mobile networks is based on the network performance data collected in Nanchang. Network energy is not proportional to its carried traffic load, showing the misalignment between traffic and energy. (b). One-week misalignment factor pattern of mobile networks. The launch of 5G networks causes the mobile network's misalignment factor to rise. (c). Spatial distribution of misalignment factors of 4G networks. (d). Spatial distribution of misalignment factors of 5G networks. (e). Spatial distribution of misalignment factors of the entire mobile networks. (f). Spatial distribution of energy efficiency of 4G networks. (g). Spatial distribution of energy efficiency of 5G networks. (h). Spatial distribution of energy efficiency of the entire mobile networks. Regions with large misalignment factors exhibit low energy efficiency and vice versa. (i). one-week traffic and energy pattern of the 4G network. (j). one-week traffic and energy pattern of the 5G network. Addressing the spatio-temporal misalignment between cellular traffic and energy consumption in mobile networks could significantly reduce energy consumption.

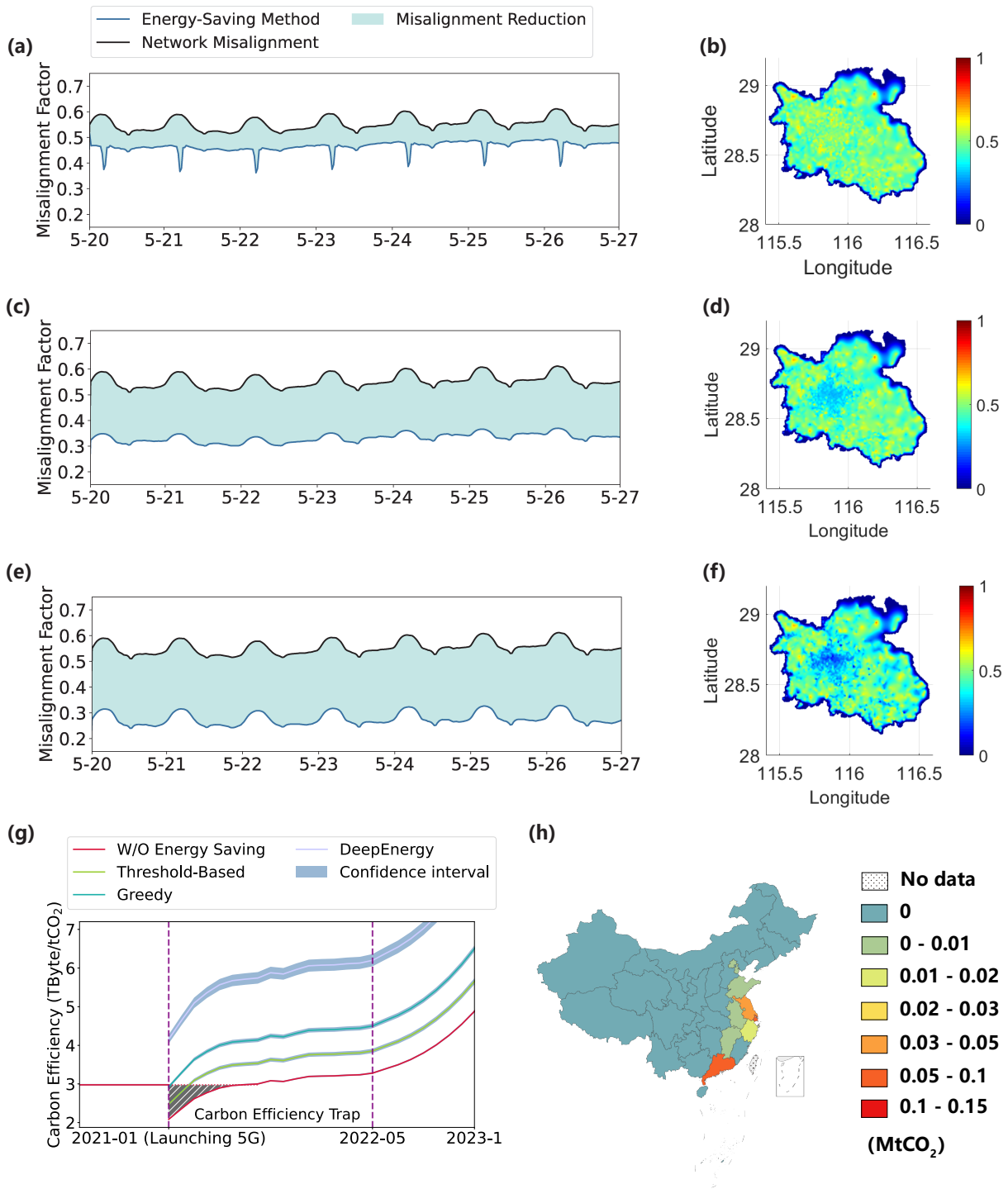


Figure 3. Performance analysis of energy-saving methods. (a). Temporal distribution of misalignment factors of the entire mobile networks in Nanchang using the threshold-based energy-saving method. (b). Spatial distribution of misalignment factor of the entire mobile networks in Nanchang using the threshold-based energy-saving method. (c). Temporal distribution of misalignment factors of the entire mobile networks in Nanchang using the greedy energy-saving method. (d). Spatial distribution of misalignment factors of the entire mobile networks in Nanchang using the greedy energy-saving method. (e). Temporal distribution of misalignment factors of the entire mobile networks in Nanchang using DeepEnergy. (f). Spatial distribution of misalignment factors of the entire mobile networks in Nanchang using DeepEnergy. (g). The energy-saving methods have effectively improved carbon efficiency, and the DeepEnergy method can effectively avoid the carbon efficiency trap caused by launching the 5G network. (h). The number of additional carbon emissions across different provinces in China after using DeepEnergy. Seventeen provinces have zero additional carbon emissions, and other provinces have seen significant reductions in additional carbon emissions.

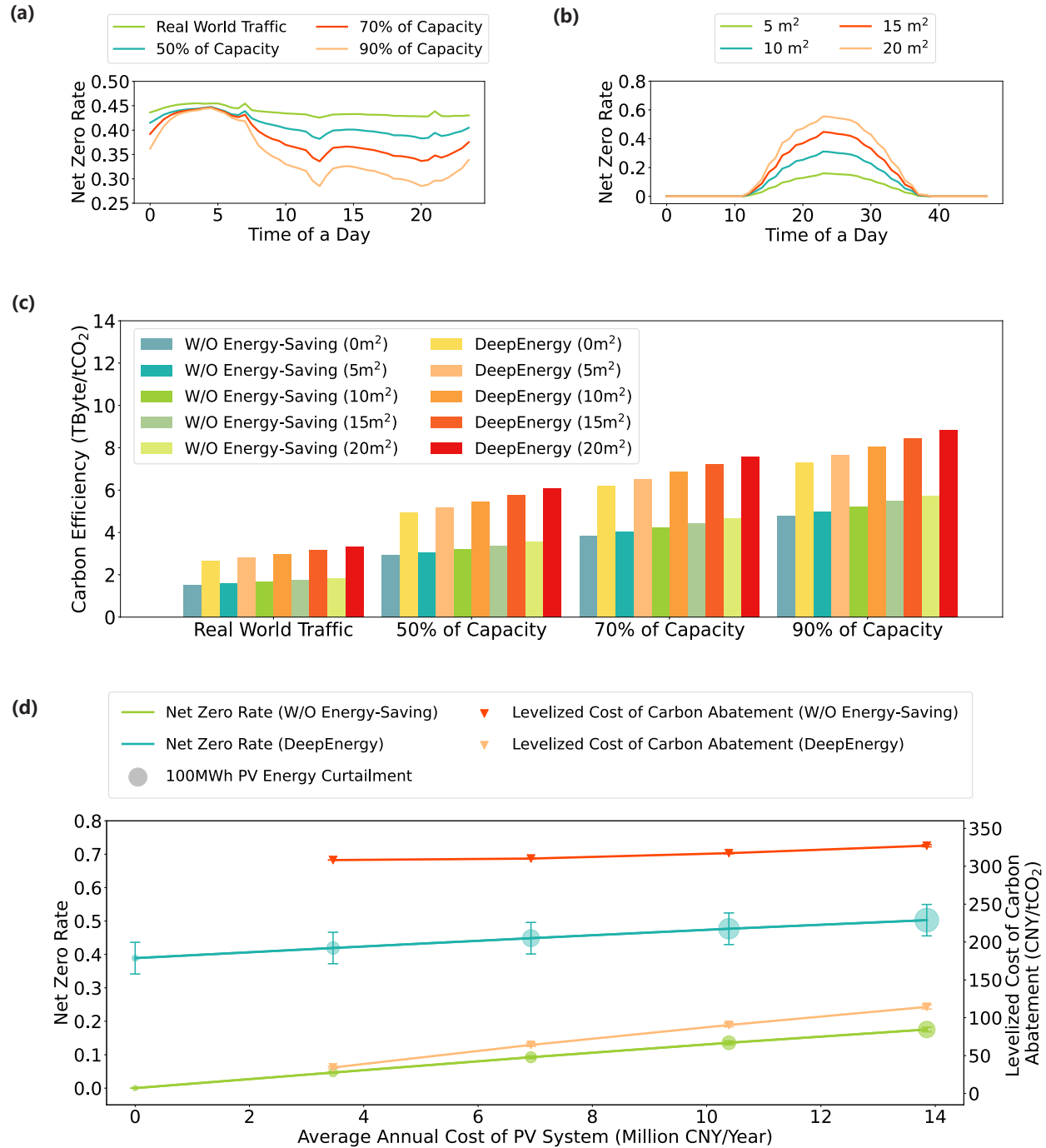


Figure 4. Renewable energy helps achieve net-zero mobile networks. (a). Net-zero rate using DeepEnergy in a day under different traffic loads. 50%, 70%, 90% of capacity refer to future counterfactual cases of change in traffic volume. For example, 50% of capacity means that the maximum traffic volume of each cell in a day reaches 50% or above of its capacity. The performance of DeepEnergy at night is superior to that of the daytime due to diurnal rhythms. (b). Net-zero rate of a PV system in a day under different panel sizes. PV power generation systems can operate in the daytime and deliver clean energy to the mobile network. (c). The carbon efficiency of the DeepEnergy versus the without (W/O) energy-saving scenario for various PV systems. Combining DeepEnergy and the PV system can significantly improve the carbon efficiency of a mobile network. (d). Net-zero rates and levelized cost of carbon abatement under different economic investments in the PV system. The radius of each bubble represents the energy curtailment for the solar energy system.

Supplementary Information for Carbon Emissions and Sustainability of Launching 5G Mobile Networks in China

SUPPLEMENTARY NOTE 1. MISALIGNMENT MEASUREMENT OF INFORMATION FLOW AND ENERGY FLOW

Network energy is not directly proportional to carried traffic load in mobile networks. An example presented in Fig. S6 is based on network traffic data collected from Nanchang, showing the total energy consumed versus the total traffic load. Even with almost no traffic, the total energy consumption is still relatively high at approximately 25.6 MWh. In contrast, the green dashed line in the figure depicts the desired energy consumption, which is proportional to traffic volume. The green star point in the figure denotes the (C, E_{Max}) point, where C represents network capacity, which is the maximum amount of traffic the mobile network can support. E_{Max} represents the maximum energy consumed when the carried traffic reaches the available capacity C . Given (L, E) , where L represents the traffic load, and E denotes the corresponding energy consumption in the real-world network, we then define the misalignment of energy between the real and desired cases as follows,

$$M^{Energy} = E - \frac{E_{Max}}{C} \cdot L, \quad (S1)$$

where M^{Energy} denotes the misalignment of energy and $\frac{E_{Max}}{C} \cdot L$ represents the desired energy consumption under a traffic load of L . We then have,

$$M^{Energy} \propto \tilde{E} - \tilde{L}, \quad (S2)$$

where $\tilde{E} = E/E_{Max}$ represents the normalized energy consumption and $\tilde{L} = L/C$ represents the normalized traffic load. We then define $M = \tilde{E} - \tilde{L}$ as the **misalignment factor** between traffic load and energy consumption, which lies within the interval $[0, 1]$. The main factor causing this misalignment is that each base station's cooling power and fixed radio transmission overhead are unaffected by traffic load.

The relationship between energy efficiency and misalignment factor is then illustrated. In our case, energy efficiency is defined as the amount of network traffic that can be delivered per unit of energy consumption.

$$\eta^{Energy}(L) = L/E, \quad (S3)$$

where $\eta^{Energy}(L)$ denotes the energy efficiency under a traffic load of L . We then have,

$$\eta^{Energy}(L) = \frac{L}{E_{Max} \cdot M + \frac{E_{Max}}{C} \cdot L}. \quad (S4)$$

By denoting C/E_{Max} as $\eta_{Desired}^{Energy}$, which represents the desired energy efficiency (the green dashed line in Fig. S6), we can derive the following expression,

$$\eta^{Energy}(L) = \frac{\eta_{Desired}^{Energy}}{1 + M/\tilde{L}}. \quad (S5)$$

Due to the misalignment between traffic load and energy consumption, the mobile network cannot achieve the desired energy efficiency. By reducing the misalignment factor, we can increase energy efficiency and mitigate both the energy and carbon efficiency traps.

SUPPLEMENTARY NOTE 2. ENERGY CONSUMPTION MODEL OF BASE STATIONS

Base stations are fundamental components and consume the largest part of energy in mobile networks [1]. Figure S7 depicts a typical mobile network base station. A base station comprises a communication subsystem and a support subsystem. The Remote Radio Unit (RRU) and Base Band Unit (BBU), major components of the communication subsystem, are responsible for transceiving radio signals and processing baseband signals, respectively. A base station (BS) may have multiple RRUs and BBUs. The cooling and other auxiliary devices are part of the supporting subsystem. The cooling equipment, such as air conditioning, is used to maintain the proper operating temperature of the base station.

According to a base station's components, the overall power consumption P_{BS} of a base station can be given by,

$$P_{BS} = P_{tx} + P_{cooling}, \quad (S6)$$

where P_{tx} denotes the power consumption of the communication subsystem, and $P_{cooling}$ accounts for the power consumed by cooling equipment to maintain an appropriate operating temperature.

Modeling Power Consumption of Communication Subsystem

The communication subsystem power consumption of a single base station is dominated by two components: RRU and BBU.

$$P_{tx} = P_{BBU} + P_{RRU}, \quad (S7)$$

where P_{BBU} and P_{RRU} represent the power consumed by BBUs and RRUs. Specifically, P_{RRU} varies according to the base station traffic amount. When the traffic load is heavy, RRU has to consume more power to support more active physical resource blocks (PRBs)¹. Thus, P_{RRU} increases proportionately to traffic volume, i.e., the number of resource blocks utilized. In contrast, BBUs are responsible for baseband processing. No matter how many RBs are active, their power consumption remains relatively constant and is not affected by traffic load. By analyzing real-world data, we find that the BBU power of a base station is related to the number of cells it has. Generally, base stations with more cells have more BBUs. Fig. S8 shows the BBU power distribution for different types of BSes with different cell numbers. In real-world networks, there are three types of BSes in terms of their number of cells and network types: 4G BS with three cells, 5G BS with three cells, and 5G BS with six cells. Table S20 illustrates the average and standard deviation of the BBU power of various base stations. Since the BBU power of a particular BS type is mainly distributed in a small interval ($\pm 8.88\%$), we use the average value to approximate it. Specifically, for a 4G BS with three cells, its BBU power is simulated as 89.3771 W. For a 5G BS with three cells, its BBU power is simulated as 305.0409 W. For a 5G BS with six cells, its BBU power is simulated as 499.6484 W.

We next model the power consumption of RRUs P_{RRU} . Using measurement data on real-world mobile networks, we find that linear models can approximate a variety of base stations reasonably well; this model has been widely used in the literature [2–4]. Figure S9(a) and Figure S11(a) illustrate the scatter plots of RRU power P_{RRU} and transmit power P_{trans} in 4G and 5G networks, respectively. P_{RRU} varies from 200W to 1200W. The relationship between RRU power and transmit power is strong and linear (Figure S10 and Figures S11(b) S11(c) S11(d)).

$$P_{RRU} = \alpha \cdot P_{trans} + \gamma, \quad (S8)$$

where α and γ denote slope and offset, respectively. Notably, base stations of different settings², e.g., maximum transmit power, have specific coefficients in the linear regression model, as depicted in Table S21(a) and Table S22(a).

We then discover that transmit power varies with the physical resource block (PRB) usage ratio. The PRB usage ratio is the proportion of the base station's total available PRBs currently in use, reflecting the traffic load of a base station. Figure S12 and Figure S14(a) display scatter plots of transmit power and PRB usage ratio based on measurements from real-world mobile networks. P_{trans} ranges between 0W and 300W. Given the same PRB ratio, the transmit power of 5G base stations is typically greater than that of 4G base stations because 5G base stations are equipped with more antennas³. Scatter plots clearly show that a linear model can approximate the transmit power with respect to the PRB usage ratio,

$$P_{trans} = \beta \cdot r_{PRB} + \sigma, \quad (S9)$$

¹A physical resource block (PRB) is the smallest unit of resources allocated to a mobile user for accessing cellular networks.

²As for 5G base stations, different base station types have specific settings for maximum transmit power (Figure S9(b)).

³5G base stations are typically equipped with 32 or 64 antennas, whereas 4G base stations only have 4 or 8 antennas

where r_{PRB} is the PRB usage ratio, β and σ denote slope and offset, respectively. As depicted in Table S21(b) and S22(b), base stations of different settings also have different coefficients. Notably, compared to 4G base stations, 5G base stations utilize an advanced technology known as subframe silence [5], in which transmit hardware is turned off when the subframe has no data to send. Consequently, the offset σ of 5G base stations equals 0. In other words, there is no transmit power when there is no traffic load.

RRU Power under Sleep Mode. In order to conserve energy, it is common for mobile networks to switch base stations into low-power operational modes when the traffic load is extremely low by turning off some RRU components, such as the power amplifier. These low-power modes are referred to as sleep modes. When a base station is in sleep mode, its RRU power becomes independent of traffic load. We then plot the cumulative distribution function (CDF) of RRU power in sleep mode based on real-world measurement data. Fig. S15 shows that the RRU power of 5G base stations in sleep mode is typically lower than that of 4G base stations, owing to the advanced physical Energy-saving technology utilized by 5G mobile networks [6]. In our case, we then approximate the RRU power in sleep mode based on the mean value of the various base station types. Table S23 illustrates the mean and standard deviation of RRU power in sleep mode for various base station types.

Modeling Power Consumption of Supporting Subsystem

In this paper, we only model the power consumption of cooling devices, as they account for the vast majority of the total power consumption of the supporting system. In practice, the power consumption of the cooling devices can be simulated using EnergyPlus [7], a program developed by Lawrence Berkeley National Laboratory (LBNL). EnergyPlus can simulate how the power consumption of the cooling system fluctuates every half-hour by receiving as inputs the outdoor air temperature, the indoor proper operating temperature, the power generated by the communication subsystem, and the room area of the base station. Specifically, information on outdoor air temperature can be found in the World Meteorological Organization's weather dataset⁴. The communication subsystem is modeled as an electrical heat source. According to the 'Technical Standard for Mobile Communication Infrastructure of Construction' recognized by the Chinese government, we established a base station room with a $20m^2$ area and a $20^\circ C$ proper operating temperature. The EnergyPlus parameter settings are displayed in Table S24.

⁴<https://worldweather.wmo.int/en/home.html>

SUPPLEMENTARY NOTE 3. ESTIMATION OF RESIDENTIAL AND INDUSTRIAL POWER LOAD IN NANCHANG

We use two methods to estimate the residential and industrial power load $P_{orig}(t)$ in Nanchang: static approximation and dynamic approximation. In static approximation, $P_{orig}(t)$ is assigned as a constant annual mean value. According to [8], the total energy consumption of Nanchang city in 2020 is 25.399 billion KWh, which means the average power load is about 2891.5 MW, and thus $P_{orig}(t) = 2891.5$ MW. Due to the delay in the government's release of detailed power load data, we could only approximate the load in 2022 using the publicly available data for 2020. In dynamic approximation, we utilize the typical load patterns within one day and one year to more precisely approximate the power load of Nanchang. According to [9], the typical load curve in Jiangxi province within one year and one day is shown in Fig. S16. However, the exact values at each time are unknown. We next used the maximum, and minimum power load of Nanchang in 2020 [8] to estimate $P_{orig}(t)$ in every half-hour. Notably, $P_{orig}(t)$ is assumed to be devoid of $P_{BS}(t)$. As depicted in Fig. S16 (a), there are two curves representing the maximum and minimum daily power loads, denoted as $P_{day}^{max}(k)$ and $P_{day}^{min}(k)$ for $k \in \{1, 2, \dots, 366\}$. According to [8], the maximum and minimum power loads of Nanchang city in 2020 are 4650 MW and 1769 MW, respectively, denoted as $P_{year}^{max} = 4650$ MW, $P_{year}^{min} = 1769$ MW. Then, the specific daily values of $P_{day}^{max}(k)$ and $P_{day}^{min}(k)$ are computed as follows,

$$P_{day}^{max}(k) = P_{year}^{min} + r_{year}^{max}(k) * (P_{year}^{max} - P_{year}^{min}), \forall k \in \{1, 2, \dots, 365\}, \quad (S10)$$

$$P_{day}^{min}(k) = P_{year}^{min} + r_{year}^{min}(k) * (P_{year}^{max} - P_{year}^{min}), \forall k \in \{1, 2, \dots, 365\}, \quad (S11)$$

where $r_{year}^{max/min}(k)$ is the ratio of $(P_{day}^{max/min}(k) - P_{year}^{min})$ over $(P_{year}^{max} - P_{year}^{min})$, which can be obtained directly from the curve of Fig. S16 (a) without knowing the exact values. After obtaining P_{day}^{max} and P_{day}^{min} for each day, the detailed half-hourly power load within a day is computed based on the typical load curves for weekdays and weekends, as shown in Fig. S16 (b) and (c). Using the same methods as Eq. (S10) and Eq. (S11), $P_{orig}(t)$ for the k -th day is computed as follows,

$$P_{orig}(t) = P_{day}^{min}(k) + r_{day}(t) * (P_{day}^{max}(k) - P_{day}^{min}(k)), \forall t \in T, \quad (S12)$$

where $r_{day}(t)$ is the ratio of $(P_{orig}(t) - P_{day}^{min})$ over $(P_{day}^{max} - P_{day}^{min})$, which could also be obtained directly from the load curves of weekdays and weekends shown in Fig. S16 (b) and (c).

The above two methods (static approximation and dynamic approximation) to compute $P_{orig}(t)$ may result in different amounts of carbon emissions. To evaluate the difference between the two methods, we first calculated the carbon emissions of base stations using $P_{orig}(t)$ generated by the two methods without considering the PV power generation of base stations. As shown in Fig. S17 (a) and (b), the resultant mobile network carbon emissions using the two methods are the same during some time slots and also show significant differences during others. To determine why the number of carbon emissions using the dynamic approximation method drops sharply during certain time slots, we further show the dynamic load curve of $P_{orig}(t)$ in Fig. S17 (c), and the power generation of XinChang power unit 1 and 2 ($P_{1/2}(t)$) in Fig. S17 (c) and (d). XinChang power unit has a larger capacity with lower c_i^{coal} than the other generation units. As shown in Fig. S17 (c), $P_{1/2}(t)$ essentially maintains maximum power generation (700MW) due to their lower c_i^{coal} ; however, when $P_{orig}(t)$ continues to decrease at about 21:30 each day, $P_{1/2}(t)$ is eventually influenced and begins to decrease. In other words, the decrease in $P_{orig}(t)$ causes $P_{1/2}(t)$ to fall below their maximum capacity after 21:30. From Fig. S17 (d), which shows the additional power generation ($\Delta P_{1/2}(t)$) of XinChang power unit 1 and 2 for mobile network power load, it can be seen that, because $P_{1/2}(t)$ has low values between 21:30 and 7:00 of the following day, the two units with lower carbon emissions factors than the other units are able to provide their rest power capacity to the power load, and thus the carbon emissions amount caused by mobile network power load decreases sharply during that time. The dynamic approximation could demonstrate more realistic carbon emissions caused by mobile networks compared to the static approximation approach. As a result, the dynamic approximation method is applied to obtain $P_{orig}(t)$ in this work.

SUPPLEMENTARY NOTE 4. ENERGY-SAVING METHODS

An Energy-saving method of mobile networks is to switch base stations (BSes) into low-power operational modes by turning off certain RRU components, such as the power amplifier, when the traffic load is extremely low. When a base station goes into sleep mode, its traffic will be handled by nearby active base stations. As illustrated in Fig. S18, when the PRB usage ratio (or traffic load) of base station A is low, base station A enters sleep mode, and the mobile user served is offloaded to adjacent base station B that is referred to as base station A's compensating base station. In particular, a base station is referred to as the compensating base station of another when its maximum communication range is sufficient to cover the normal communication range of another base station. In practice, Energy-saving methods control the working states of cells to determine whether cells enter sleep mode. A cell refers to a carrier on a sector of a base station. A base station generally has multiple cells.

Threshold-based Method

Current mobile networks generally employ a threshold-based method. A cell will enter sleep mode when two conditions are met. The first condition is that it has at least one active compensating cell. The second condition is that its load, as determined by its PRB usage ratio and the number of users, is below a predetermined sleep threshold. Typically, sleep thresholds are established manually based on the knowledge of experts. Table S25 displays the parameter settings of the threshold-based method used in current real-world mobile networks.

Greedy Method

The greedy method [2] is representative of the methods that use combinatorial optimization to optimize the working state of cells, which consists of two steps: grid-based partition and greedy selection of active cells.

Grid-based Partition

We partition the space into small grids based on the compensation relationships between cells, with equivalent cells in each grid. In our case, cells are equivalent if they can communicate with mobile users interchangeably. In other words, two cells are equivalent if they act as compensating cells for one another. When all cells inside are equivalent, a virtual grid is created. Once a cell is not equivalent to every cell in the existing grid, a new grid is created.

Greedy Selection of Active Base Stations

In order to reduce the misalignment of information flow and energy flow in mobile networks, we choose the appropriate set of active cells and put the rest into sleep mode based on the grid-based partition result. The selection must meet coverage and capacity⁵ requirements. For a particular grid, we first identify the time of day with the highest network traffic based on the 24-hour traffic profile and then select the active set of cells for this peak time. Notably, in order to meet the coverage and capacity criteria, the local aggregate capacity of all active cells must be sufficient to handle local traffic. By doing so, the greedy selection algorithm favors cells with greater capacities. Consequently, we arrange each cell in the grid based on decreasing capacity values. The set of active cells is then chosen every half-hour based on the capacity order.

DeepEnergy

Due to that, the total capacity is much larger than the total traffic demand in the system. We consider setting the control status of cells to sleep mode and reallocating the traffic for the active cells to save energy.

Multi-Agent Collaboration Problem

There are three sub-tasks: base station control, cell control, and traffic allocation. Cell control is in the leading role. Once the cell control is obtained, the base station control and traffic allocation can be obtained by simple rules. We consider cell control as a multi-agent collaboration problem: each cell c_n is managed by an agent $agent_n$, and these agents cooperate to minimize the energy consumption of the system. In this problem, agents output actions based on their observations (part of the system state), and these actions act together on the system. The system changes its state based on the joint actions and feeding back rewards to each agent.

⁵The maximum volume of traffic a cell can support is referred to as its capacity.

Observation

The observation of each agent $agent_n$ includes the feature vectors of other cells in the same base station or the same grid. The feature vector of cell c_n consists of time t , the traffic loads of the grid g_m that the cell c_n belongs to in the last four time steps, $(L_{t-4}^m, L_{t-3}^m, L_{t-2}^m, L_{t-1}^m)$, and the device parameters of the cells in $\mathcal{N}_m^g \cup \mathcal{N}_k^b$. \mathcal{N}_m^g denotes the set of cells in the grid g_m and \mathcal{N}_k^b denotes the set of cells of the base station BS_k that the cell c_n belongs to.

Action

The optional action of an agent is setting its corresponding cell to the active or inactive status. The final decision of BSes, cell control, and traffic allocation is obtained based on the agents' decision by the following steps. Firstly, adjust the action output by the agents. If the total capacity of active cells in a grid is less than the traffic demand, the inactive cells would be activated from the largest to the smallest capacity until the total capacity of active cells is higher than the demand. Secondly, allocate predicted traffic on the active cells. The predicted traffic demand in the grid is divided according to the active cells' capacity and then assigned to the corresponding cells. Finally, obtain the control status of BSes and cells. If all cells in a base station were inactive, DeepEnergy would turn off the base station and its cells. Otherwise, the control status of that base station is set to turn on, and the cell's status is set to open (sleep) if its status is active (inactive).

Reward

The decisions aim to save the total energy, including the RRUs, BBUs, and air conditioners. The reward should encourage the agents to cooperate to save energy consumption. When the control states of other cells remain unchanged, the change of the control status of a cell can only affect the energy consumption in the base station it belongs to and the grid it belongs to. Thus, the reward for each agent is set to $r_n = -\sum_{n' \in \mathcal{N}_m^g} P_{n'}^{RRU} - P_k^{BBU} - P_k^{cooling}$. The first term indicates the energy of RRUs in cells that belong to the same grid as cell c_n , so it could encourage the agent to cooperate with agents from these cells $\{c_{n'}\}_{n' \in \mathcal{N}_m^g}$. The second term indicates the energy of BBUs and cooling devices in the base station that cell c_n belongs to, which may encourage the agent to cooperate with the agents from the same base station.

Local Collaboration-based Cell Control

Overview

To solve this multi-agent collaboration problem, we consider training a policy network to output the action based on the current state. A large number of agents is a major challenge. On the one hand, the large-scale agents lead to a massive state space, so when an agent makes the decision, it should efficiently integrate the state of other agents associated with it. For this problem, we construct two graphs based on the intra-grid and intra-BS relationships and then use the graph neural network to integrate the information of the associated nodes in the graphs. On the other hand, large-scale agents also lead to complex interactions between agents, making the expected rewards of different actions difficult to estimate. Thus, we introduce the idea of Mean-Field MARL (MF-MARL [10]) to integrate the effects of other agents' decisions on the target agent and design two masks to decrease the difficulty of action value estimation. In the following, we will build a graph for the relationship among cells, construct a graph neural network-based action value network, and describe how to train the network.

Action-value Network Architecture

Action-value network architecture is as follows: For a cell c_n and its agent, the capacity and device parameters of each cell associated with c_n are embedded in two linear layers. The embeddings of cells from the same grid (or base station) as c_n are integrated by an attention layer. The two integrated embeddings, global values (such as time step and traffic demand in the grid), and masks are concatenated into a single vector, which is then fed into two fully connected layers to produce the final output. The final output is the predicted reward for different actions. The architecture, as mentioned above, can effectively integrate local information from relevant cells with global information.

Action-value Network Update

We design an RL method similar to MF-MAR to train the action-value network. MF-MARL approximates the effect of the actions of all other agents (or neighborhood agents) with one of the averages of these actions. In other words, MF-MARL predicts the action value for an agent

depending on the system state, the agent’s action, and the average action of all other agents (or neighborhood agents). In this problem, we replace the average of the actions with two masks which depend on the action of related agents and directly determine the agent’s reward. The first mask denotes whether the grid’s traffic demand could be met if the agent sets the respective cell to sleep. The second mask denotes whether all other cells under the same base station could sleep if the cell is set to sleep mode.

These masks are derived from the actions of other agents and can only be used as training input. Therefore, each agent has two action-value networks, $q^2(\mathbf{o}_n, a, \mathbf{m}_n; \theta_q^2)$ for training and $q^1(\mathbf{o}_n, a; \theta_q^1)$ for inference, where \mathbf{o} denotes the observation, a denotes the action, \mathbf{m} denotes masks, and θ denotes the parameters of action-value networks. In the execution stage, the action-value network without masks as input, $q^1(\mathbf{o}_n, a; \theta_q^1)$, predicts the rewards associated with different actions, setting the cell to sleep or not, based on the observation. Using ϵ -greedy method, the agent determines the status of the cell by sampling the action based on predicted rewards. After the statuses of all cells determined by the agents are executed, the rewards for all agents are calculated. All agents’ observations, actions, and rewards are appended to the replay buffer. In the training stage, the action-value network with masks as input, $q^2(\mathbf{o}_n, a, \mathbf{m}_n; \theta_q^2)$, is trained with the replay buffer to predict the rewards of different actions based on the observation and masks. The network q^2 is optimized through the following loss function:

$$L_2 = \frac{1}{2} [q^2(\mathbf{o}_n, a, \mathbf{m}_n; \theta_q^2) - r_n]^2, \quad (\text{S13})$$

where the masks \mathbf{m}_n is obtained based on the actions recorded in replay buffer. The action-value network, $q^1(\mathbf{o}_n, a; \theta_q^1)$, is then optimized by imitating the second one, $q^2(\mathbf{o}_n, a, \mathbf{m}_n; \theta_q^2)$,

$$L_1 = \frac{1}{2} \sum_a [q^1(\mathbf{o}_n, a; \theta_q^1) - q^2(\mathbf{o}_n, a, \mathbf{m}_n; \theta_q^2)]^2, \quad (\text{S14})$$

where the mask \mathbf{m}_n are calculated based on the re-sampled actions, which is sampled as the process in the execution stage. The re-sampling process is equivalent to the sampling process for the distribution of the mask vector. Thus, the first network q^1 would learn to predict the rewards of various actions under the sampled distribution of the mask vector. The framework of DeepEnergy is shown in Fig. S19. The algorithm is shown in Algorithm S1.

Algorithm S1. DeepEnergy for Cell and Base Station Status Controlling.

- Require:** The cell IDs belonging to each grid g_m, \mathcal{N}_m^g , the cell IDs belonging to each base station b_k, \mathcal{N}_k^b and the device parameters of the each cells $\{\mathbf{x}_n\}_{n=1}^N$
- 1: Initialization the action-value networks $q^1(\mathbf{o}_n, a; \theta_q^1)$ and $q^2(\mathbf{o}_n, a, \mathbf{m}_n; \theta_q^2)$
 - 2: **while** training not finished **do**
 - 3: **for** $i \leftarrow 1$ to 48 **do**
 - 4: Utilize the action-value network $q^1(\mathbf{o}_n, a; \theta_q^1)$ to predict the value of different actions for each cell
 - 5: Sample the action a^n based on the predicted value
 - 6: Get the traffic demands of all grids at timestep t
 - 7: Use the actions $\{a^n\}_{n=1}^N$ to adjust the control status of cells and base stations
 - 8: Calculate the energy consumption of each cell and each base station
 - 9: Calculate the reward for each agent, $r^n = -\sum_{n' \in \mathcal{N}_m^g} P_{n'}^{RRU} - P_k^{BBU} - P_k^{Air}$
 - 10: Store $\langle \{\mathbf{o}_n\}_{n=1}^N, \{a_n\}_{n=1}^N, \{r_n\}_{n=1}^N \rangle$ to replay buffer
 - 11: **for** $j \leftarrow 1$ to J **do**
 - 12: Sample a batch of samples from replay buffer
 - 13: Randomly select a cell for each sample, and calculate the mask for the cell
 - 14: Update the action-value network q^2 by minimizing the loss of S13
 - 15: Update the action-value network q^1 by minimizing the loss of S14
-

Supplementary Note 5. Estimation of Misalignment Factor Across Provinces

The misalignment factor, denoted by $M = \tilde{E} - \tilde{L}$, measures the discrepancy between the normalized energy consumption (\tilde{E}) and the normalized traffic load \tilde{L} in the mobile network. By analyzing real-world data without energy-saving and simulation results under different energy-saving methods conducted in Nanchang, we find that the misalignment factor of the mobile network varies with the normalized network traffic load and the energy-saving method it uses, as depicted in Fig. S20. Under a specific energy-saving scenario, the misalignment factor (M) linearly decreases as the normalized network traffic load (\tilde{L}) increases, and $M = 0$ when $\tilde{L} = 1$. Thus, we have

$$M = K_\psi(1 - \tilde{L}), \quad (\text{S15})$$

where K_ψ denotes coefficient and depends on the energy-saving scenario ψ . The linear regression model can approximate the misalignment factor with an R-squared of over 0.81 for various energy-saving scenarios (Fig. S21). Table S26 shows the coefficients for different energy-saving scenarios based on the data from Nanchang.

In our case, we assume that all provinces share the same coefficient K_ψ with Nanchang under the energy-saving scenario ψ . Therefore, given the normalized traffic load \tilde{L}_p of province p , we can estimate its misalignment factor $M_{p,\psi}$ under energy-saving scenario ψ as,

$$M_{p,\psi} = K_\psi(1 - \tilde{L}_p). \quad (\text{S16})$$

Notably, the normalized traffic load \tilde{L}_p of province p varies over time, and consequently, so does its misalignment factor $M_{p,\psi}$. Tables S27, S28, S29, and S30 illustrate the estimated misalignment factors for each province under various energy-saving scenarios.

Supplementary Note 6. Generalizability Analysis of DeepEnergy

DeepEnergy is of a high generalizability because it utilizes mean-field MARL to integrate the effects of other agents' decisions on the target agent. To verify the generalizability of DeepEnergy, we partition Nanchang into four regions, according to the city center point. As depicted in Fig. S22, we denote them as Region A, Region B, Region C, and Region D. These four regions have different base station density, network capacities and network traffic loads. We then train DeepEnergy on the data from each of these four regions, and then apply the trained model from each region to the whole Nanchang to test its performance. Table S31 shows that the models trained on data from different regions have similar performance. Further, we use the performance results of the models trained on data from different regions to fit the relation between misalignment factor and the normalized network traffic load (Eq. S15). Different models have similar coefficient K_ψ , reflecting that they have similar energy-saving capabilities (Fig. S23 and Table S32). Consequently, DeepEnergy has high generalizability over different training data.

REFERENCES

1. C.-L. I, S. Han, and S. Bian, "Energy-efficient 5G for a greener future," *Nat. Electron.* **3**, 182–184 (2020).
2. C. Peng, S.-B. Lee, S. Lu, H. Luo, and H. Li, "Traffic-driven power saving in operational 3G cellular networks," in *Proceedings of the 17th annual international conference on Mobile computing and networking*, (2011), pp. 121–132.
3. P.-H. Huang, S.-S. Sun, and W. Liao, "Greencomp: Energy-aware cooperation for green cellular networks," *IEEE Transactions on mobile computing* **16**, 143–157 (2016).
4. Q. Wu, X. Chen, Z. Zhou, L. Chen, and J. Zhang, "Deep reinforcement learning with spatio-temporal traffic forecasting for data-driven base station sleep control," *IEEE/ACM Transactions on Netw.* **29**, 935–948 (2021).
5. S. Rostami, K. Heiska, O. Puchko, K. Leppanen, and M. Valkama, "Pre-grant signaling for energy-efficient 5g and beyond mobile devices: Method and analysis," *IEEE Transactions on Green Commun. Netw.* **3**, 418–432 (2019).
6. D. López-Pérez, A. De Domenico, N. Piovesan, G. Xinli, H. Bao, S. Qitao, and M. Debbah, "A survey on 5G radio access network energy efficiency: Massive mimo, lean carrier design, sleep modes, and machine learning," *IEEE Commun. Surv. & Tutorials* **24**, 653–697 (2022).
7. D. B. Crawley, L. K. Lawrie, F. C. Winkelmann, W. F. Buhl, Y. J. Huang, C. O. Pedersen, R. K. Strand, R. J. Liesen, D. E. Fisher, M. J. Witte *et al.*, "Energyplus: creating a new-generation building energy simulation program," *Energy buildings* **33**, 319–331 (2001).
8. "Notice of the office of the people's government of nanchang city on forwarding the 2021 plan of the municipal development and reform commission and state grid nanchang power supply company for orderly power consumption of nanchang power grid," *Tech. rep., Gazette of Nanchang Municipal People's Government* (2021). http://www.nc.gov.cn/nc_xxgk/jsp/zfgb/ncgb_content.jsp?mid=a731211fe1094abfaea8ab348bd5ba8b.
9. "Notice on signing medium and long term power contracts in 2021," *Tech. rep., National Development and Reform Commission/National Energy Administration* (2021). http://www.gov.cn/zhengce/zhengceku/2020-12/03/content_5566580.htm.
10. Y. Yang, R. Luo, M. Li, M. Zhou, W. Zhang, and J. Wang, "Mean field multi-agent reinforcement learning," in *International conference on machine learning*, (PMLR, 2018), pp. 5571–5580.

LIST OF FIGURES

| | | |
|-----|--|----|
| S1 | Launching 5G Leads to the appearance of energy efficiency trap in Nanchang. (a) The operation of newly launched 5G base stations has led to a sharp increase in energy consumption in Nanchang. (c) Launching 5G Leads to the appearance of an energy efficiency trap and causes extra energy consumption in Nanchang. . . . | 13 |
| S2 | The daily energy consumption vs. the number of base stations. The energy consumption of a mobile network are highly correlated with its number of base stations. | 14 |
| S3 | The spatial distribution of (a) normalized traffic loads of 4G networks, (b) normalized energy consumption of 4G networks, (c) normalized traffic loads of 5G networks, (d) normalized energy consumption of 5G networks. After years of optimization of 4G base station deployments, the energy consumption of 4G, related to the number of base stations, is with a similar spatial distribution of the traffic loads. In contrast, due to the lack of traffic profiles of 5G applications, the deployment of 5G base stations is not optimized. The spatial distribution of 5G network traffic load and energy consumption shows big differences. | 15 |
| S4 | Performance of DeepEnergy on 4G and 5G networks. (a). Temporal distribution of misalignment factors of the 4G networks in Nanchang. (b). Spatial distribution of misalignment factor of the 4G networks in Nanchang. (c). Temporal distribution of misalignment factors of the 5G networks in Nanchang. (d). Spatial distribution of misalignment factors of the 5G networks in Nanchang. DeepEnergy significantly reduces the misalignment between energy consumption and cellular traffic in both 4G and 5G networks. | 16 |
| S5 | The distribution of the grid emission factors derived from the proposed simulation-based model based on Nanchang's data. There is no significant difference in grid emission factors before and after launching the 5G network. | 17 |
| S6 | The energy-traffic curve for mobile networks in Nanchang. Network energy is not proportional to the amount of network traffic it carries (see red dots). The green dashed line represents the desired energy, which is proportional to the volume of traffic. The green star point denotes the (C, E_{Max}) point, where C represents network capacity, which is the maximum amount of traffic that the mobile network can support, and E_{Max} represents the corresponding amount of energy consumed. | 18 |
| S7 | A typical base station in mobile networks. A base station consists of a communication subsystem and a supporting subsystem. The communication subsystem includes the Remote Radio Unit (RRU) and Base Band Unit (BBU), while the supporting subsystem includes the cooling and other auxiliary devices. | 19 |
| S8 | BBU power of a base station is related to the number of cells it has. Generally, base stations with more cells have more BBUs. The BBU power of a particular BS type is mainly distributed in a small interval. | 20 |
| S9 | In 5G networks, RRU power (P_{RRU}) and transmit power (P_{trans}) show a strong linear relationship. Different base station types have specific settings of maximum transmit power. '32TR' and '64TR' denote the number of base station antennas. 'NSA' and 'SA' refer to non-standalone architecture and standalone architecture, respectively. | 21 |
| S10 | Linear models can approximate the relationships between RRU power (P_{RRU}) and transmit power (P_{trans}) for a variety of 5G base stations with high accuracy. | 22 |
| S11 | Scatter plot of RRU power and transmit power for 4G base stations. Linear models can approximate the relationships between RRU power (P_{RRU}) and transmit power (P_{trans}) for a variety of 4G base stations with a high accuracy. | 23 |
| S12 | Scatter plot of transmit power and PRB usage ratio in 5G networks. Transmit power and PRB usage ratio have a significant linear relationship. | 24 |
| S13 | Linear models can approximate the relationships between transmit power (P_{trans}) and PRB usage ratio r_{PRB} for a variety of 5G base stations with a high accuracy. | 25 |
| S14 | (a) Scatter plot of transmit power and PRB usage ratio in 4G networks. Significant linear correlation exists between transmit power and PRB usage ratio. (b)-(d) Linear models can accurately approximate the relationships between transmit power and traffic load (i.e., PRB usage ratio) for various 4G base stations. The slopes and offsets of the regression model vary depending on the base station settings. | 26 |
| S15 | The cumulative distribution function (CDF) of RRU power in sleep mode. a) 4G base stations. b) 5G base stations. | 27 |

| | | |
|-----|--|----|
| S16 | Typical load curve in Jiangxi province: (a) load curve of a year; (b) load curve in a working day; (c) load curve in a weekend day. | 28 |
| S17 | Comparison of the static approximation and dynamic approximation method to compute $P_{orig}(t)$: (a) carbon emissions caused by 4G BS power load from 20 May to 26 May; (b) carbon emissions caused by 5G base station power load from 20 May to 26 May; (c) $P_{orig}(t)$ computed by the dynamic approximation method from 20 May to 26 May, and the resulted power generation of XinChang unit 1 and 2 during 23 May and 24 May; (d) extra power generation of XinChang unit 1 and 2 specifically for 4G and 5G base station load during 23 May and 24 May. | 29 |
| S18 | When the PRB usage ratio (or traffic load) of base station A is low, base station A enters sleep mode and the mobile user served is offloaded to adjacent base station B. In this case, base station B is the compensating base station of base station A. . . | 30 |
| S19 | The neural network architecture of the action-value network. The information of the cells from the same grid or the same base station are integrate to predict the rewards for different actions. | 31 |
| S20 | Misalignment factor vs. the normalized network traffic load for various Energy-saving scenarios. Under a specific Energy-saving scenario, the misalignment factor (M) linearly decreases as the normalized network traffic load (\tilde{L}) increases. | 32 |
| S21 | Linear models can approximate the relationships between the normalized network traffic load (\tilde{L}) and the misalignment factor (M) with high accuracy. | 33 |
| S22 | We partition Nanchang into four regions, according to the city center point, and denote them as Region A, Region B, Region C, and Region D. These four regions have different base station densities, network capacities, and network traffic loads. | 34 |
| S23 | For DeepEnergy models trained on different regions, Linear models can approximate the relationships between the normalized network traffic load (\tilde{L}) and the misalignment factor (M) with high accuracy. | 35 |

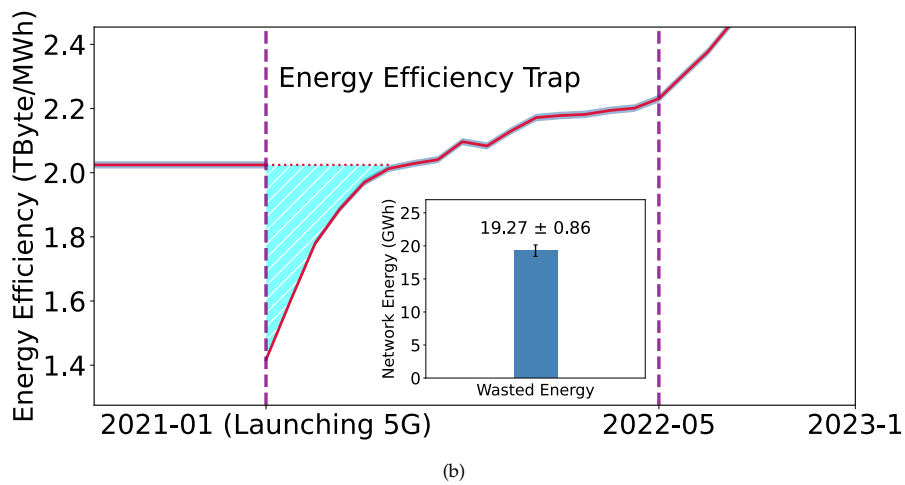
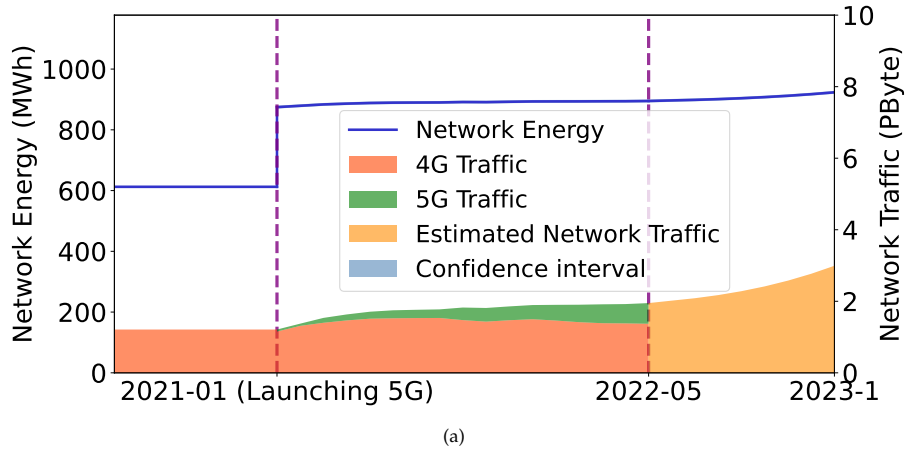


Fig. S1. Launching 5G Leads to the appearance of energy efficiency trap in Nanchang. (a) The operation of newly launched 5G base stations has led to a sharp increase in energy consumption in Nanchang. (c) Launching 5G Leads to the appearance of an energy efficiency trap and causes extra energy consumption in Nanchang.

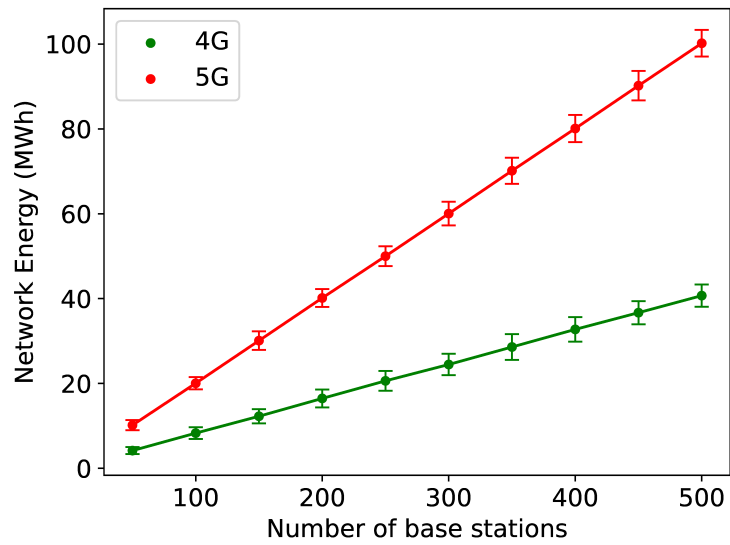


Fig. S2. The daily energy consumption vs. the number of base stations. The energy consumption of a mobile network are highly correlated with its number of base stations.

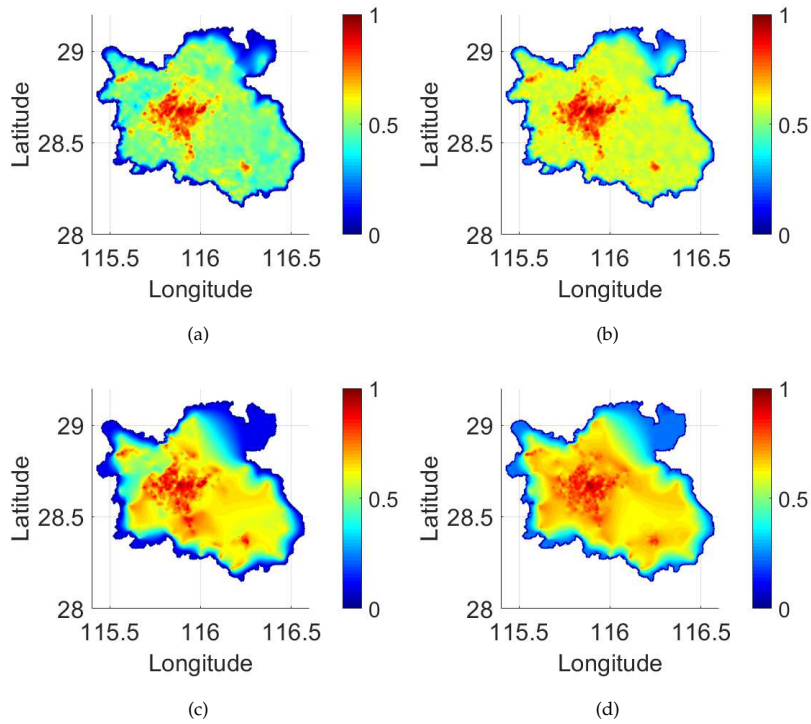


Fig. S3. The spatial distribution of (a) normalized traffic loads of 4G networks, (b) normalized energy consumption of 4G networks, (c) normalized traffic loads of 5G networks, (d) normalized energy consumption of 5G networks. After years of optimization of 4G base station deployments, the energy consumption of 4G, related to the number of base stations, is with a similar spatial distribution of the traffic loads. In contrast, due to the lack of traffic profiles of 5G applications, the deployment of 5G base stations is not optimized. The spatial distribution of 5G network traffic load and energy consumption shows big differences.

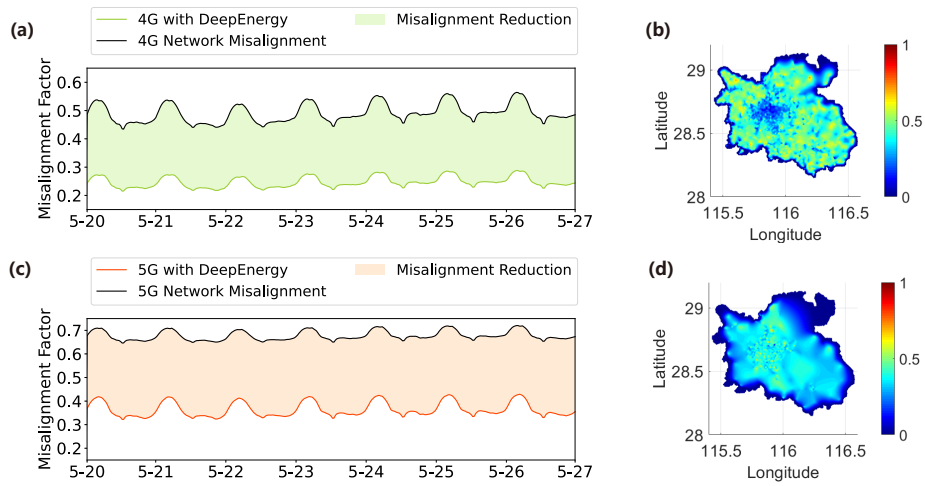


Fig. S4. Performance of DeepEnergy on 4G and 5G networks. (a). Temporal distribution of misalignment factors of the 4G networks in Nanchang. (b). Spatial distribution of misalignment factor of the 4G networks in Nanchang. (c). Temporal distribution of misalignment factors of the 5G networks in Nanchang. (d). Spatial distribution of misalignment factors of the 5G networks in Nanchang. DeepEnergy significantly reduces the misalignment between energy consumption and cellular traffic in both 4G and 5G networks.

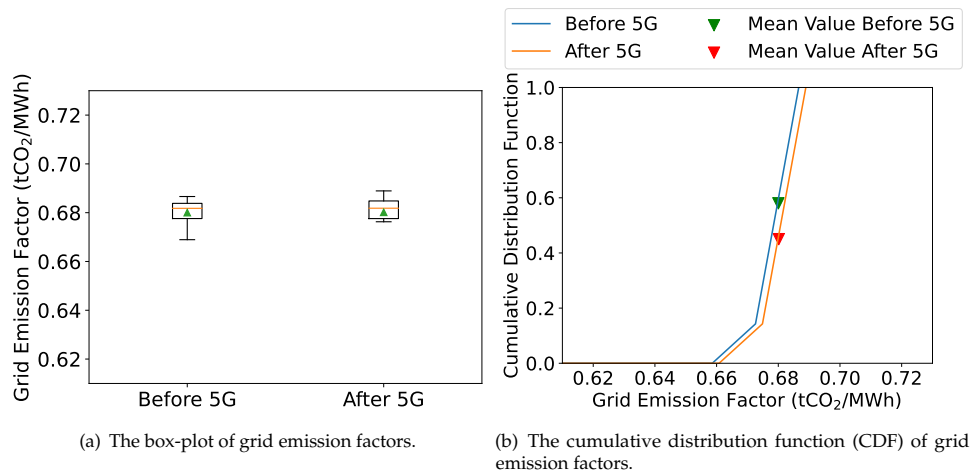


Fig. S5. The distribution of the grid emission factors derived from the proposed simulation-based model based on Nanchang's data. There is no significant difference in grid emission factors before and after launching the 5G network.

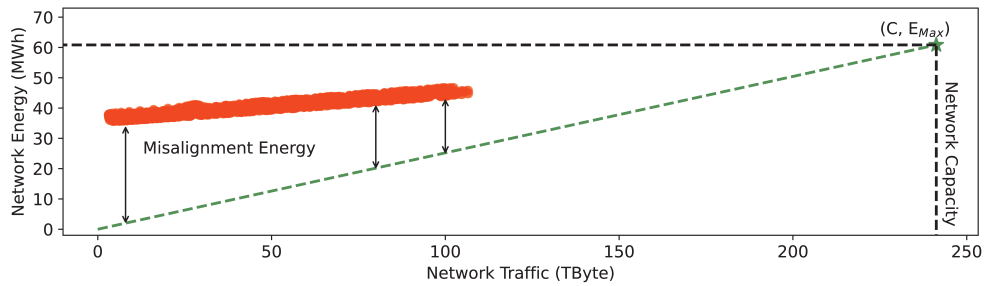


Fig. S6. The energy-traffic curve for mobile networks in Nanchang. Network energy is not proportional to the amount of network traffic it carries (see red dots). The green dashed line represents the desired energy, which is proportional to the volume of traffic. The green star point denotes the (C, E_{Max}) point, where C represents network capacity, which is the maximum amount of traffic that the mobile network can support, and E_{Max} represents the corresponding amount of energy consumed.

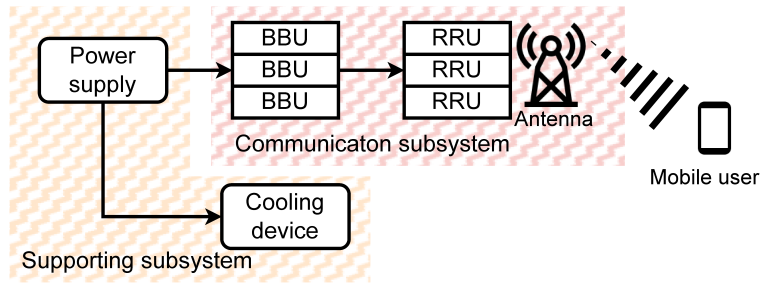


Fig. S7. A typical base station in mobile networks. A base station consists of a communication subsystem and a supporting subsystem. The communication subsystem includes the Remote Radio Unit (RRU) and Base Band Unit (BBU), while the supporting subsystem includes the cooling and other auxiliary devices.

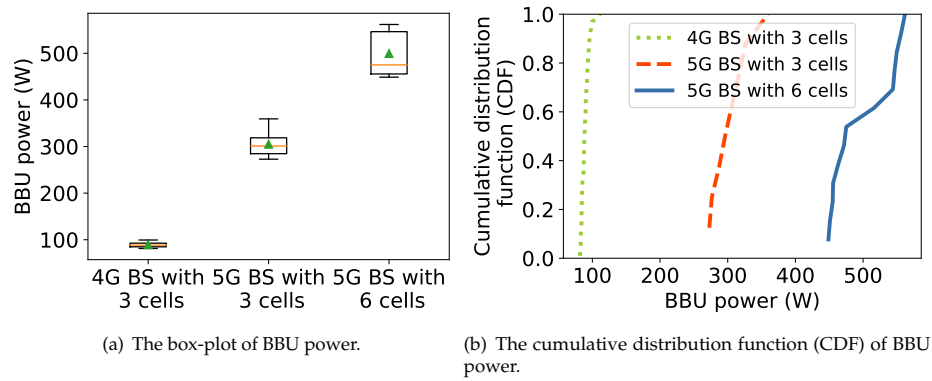
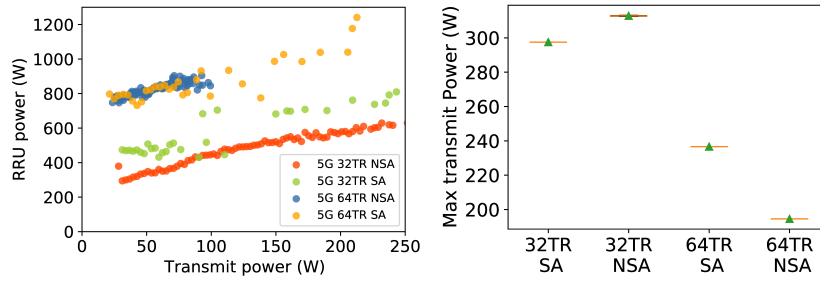


Fig. S8. BBU power of a base station is related to the number of cells it has. Generally, base stations with more cells have more BBUs. The BBU power of a particular BS type is mainly distributed in a small interval.



(a) Scatter plot of RRU power and transmit power (b) Maximum transmit power distribution of different 5G base station types.

Fig. S9. In 5G networks, RRU power (P_{RRU}) and transmit power (P_{trans}) show a strong linear relationship. Different base station types have specific settings of maximum transmit power. '32TR' and '64TR' denote the number of base station antennas. 'NSA' and 'SA' refer to non-standalone architecture and standalone architecture, respectively.

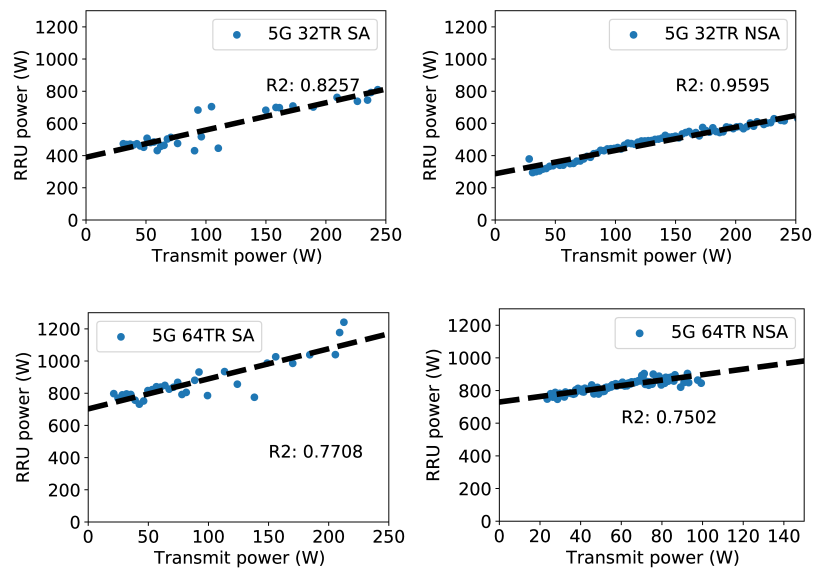


Fig. S10. Linear models can approximate the relationships between RRU power (P_{RRU}) and transmit power (P_{trans}) for a variety of 5G base stations with high accuracy.

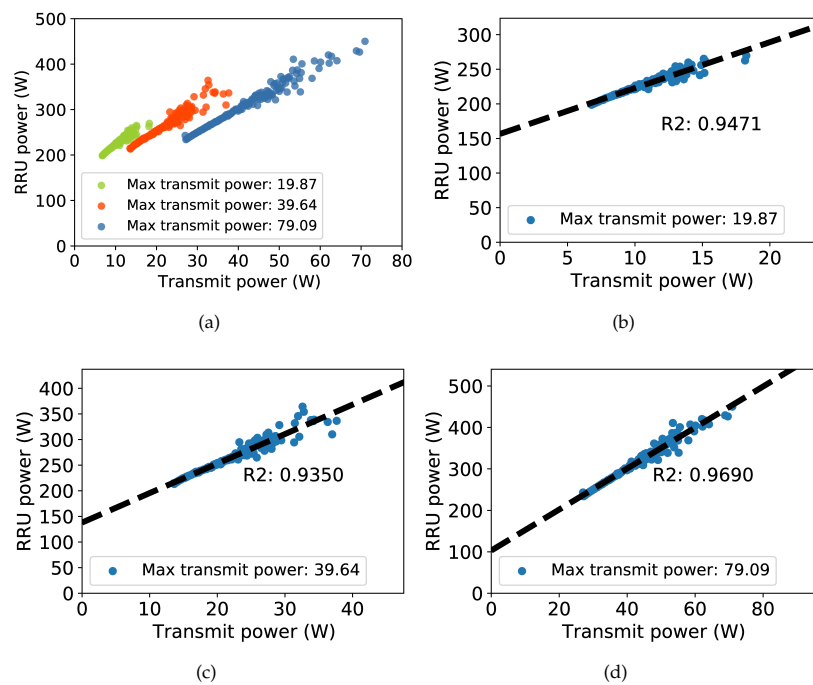


Fig. S11. Scatter plot of RRU power and transmit power for 4G base stations. Linear models can approximate the relationships between RRU power (P_{RRU}) and transmit power (P_{trans}) for a variety of 4G base stations with a high accuracy.

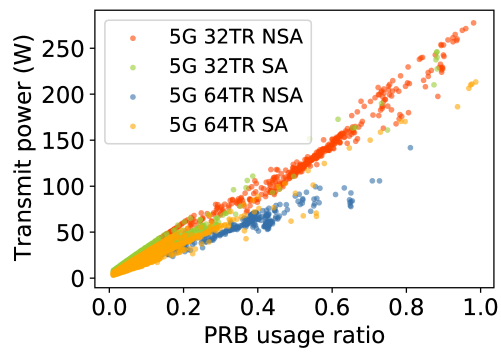


Fig. S12. Scatter plot of transmit power and PRB usage ratio in 5G networks. Transmit power and PRB usage ratio have a significant linear relationship.

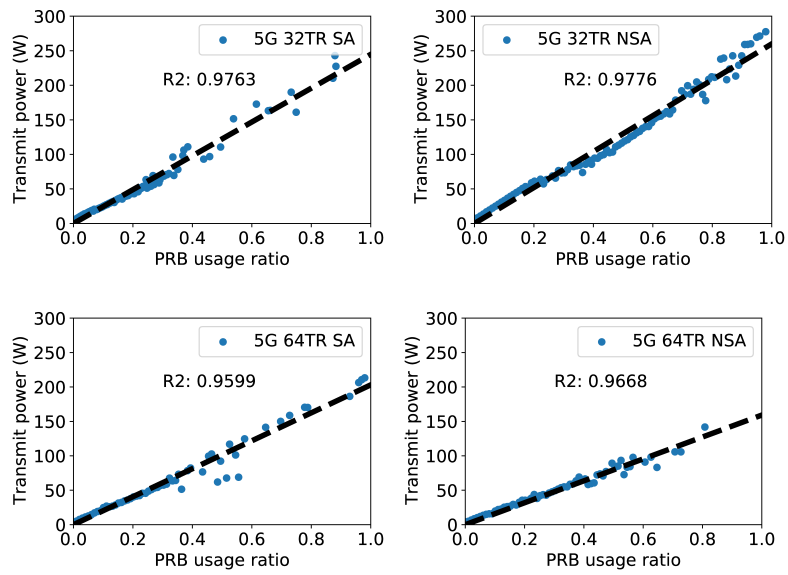


Fig. S13. Linear models can approximate the relationships between transmit power (P_{trans}) and PRB usage ratio r_{PRB} for a variety of 5G base stations with a high accuracy.

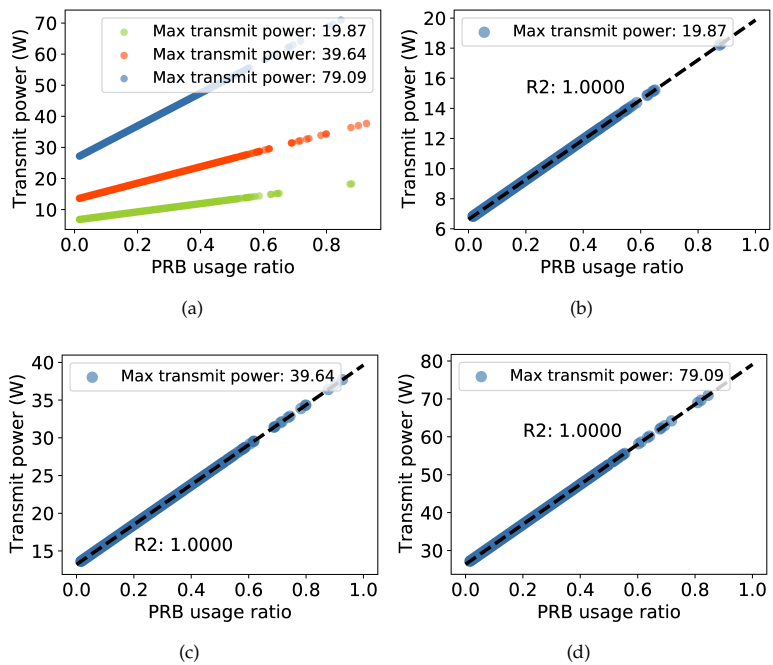


Fig. S14. (a) Scatter plot of transmit power and PRB usage ratio in 4G networks. Significant linear correlation exists between transmit power and PRB usage ratio. (b)-(d) Linear models can accurately approximate the relationships between transmit power and traffic load (i.e., PRB usage ratio) for various 4G base stations. The slopes and offsets of the regression model vary depending on the base station settings.

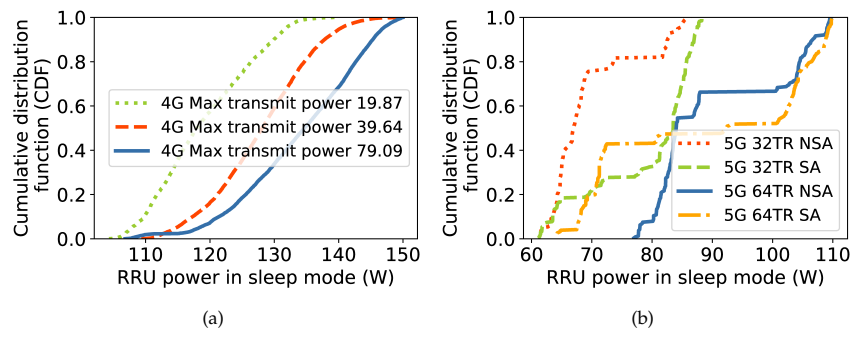


Fig. S15. The cumulative distribution function (CDF) of RRU power in sleep mode. a) 4G base stations. b) 5G base stations.

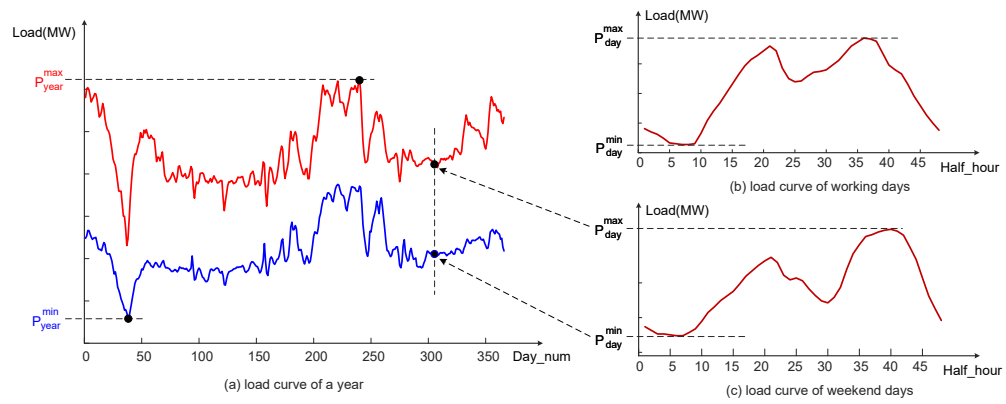


Fig. S16. Typical load curve in Jiangxi province: (a) load curve of a year; (b) load curve in a working day; (c) load curve in a weekend day.

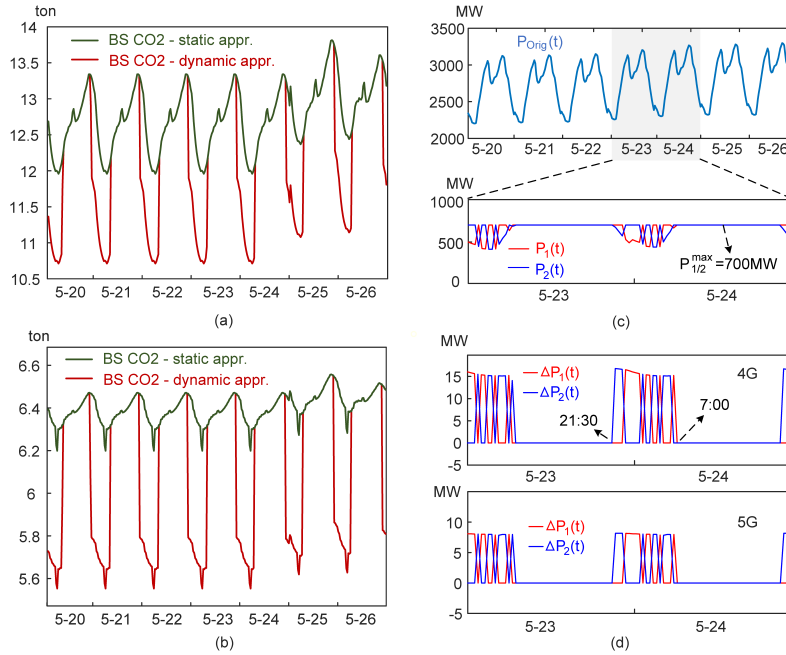


Fig. S17. Comparison of the static approximation and dynamic approximation method to compute $P_{orig}(t)$: (a) carbon emissions caused by 4G BS power load from 20 May to 26 May; (b) carbon emissions caused by 5G base station power load from 20 May to 26 May; (c) $P_{orig}(t)$ computed by the dynamic approximation method from 20 May to 26 May, and the resulted power generation of XinChang unit 1 and 2 during 23 May and 24 May; (d) extra power generation of XinChang unit 1 and 2 specifically for 4G and 5G base station load during 23 May and 24 May.

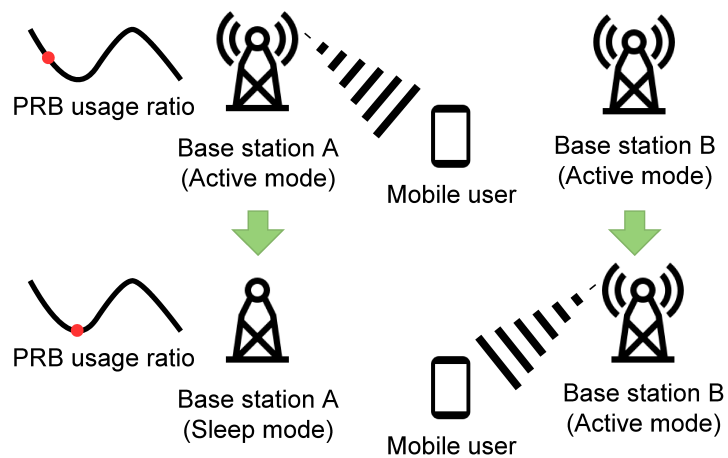


Fig. S18. When the PRB usage ratio (or traffic load) of base station A is low, base station A enters sleep mode and the mobile user served is offloaded to adjacent base station B. In this case, base station B is the compensating base station of base station A.

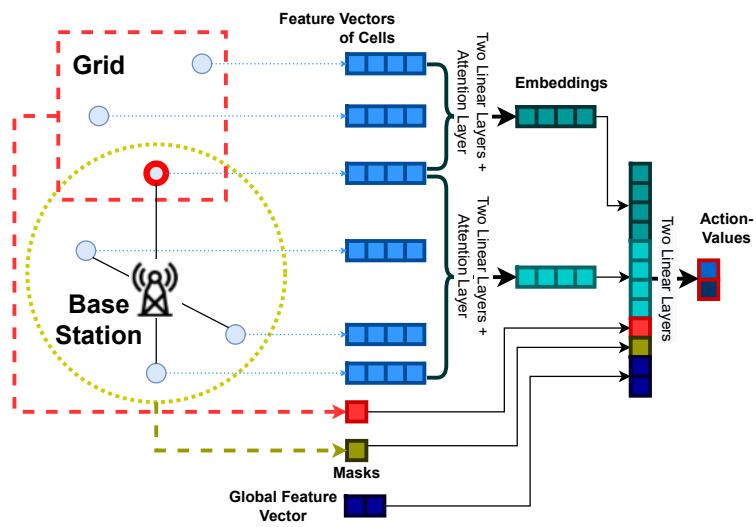


Fig. S19. The neural network architecture of the action-value network. The information of the cells from the same grid or the same base station are integrate to predict the rewards for different actions.

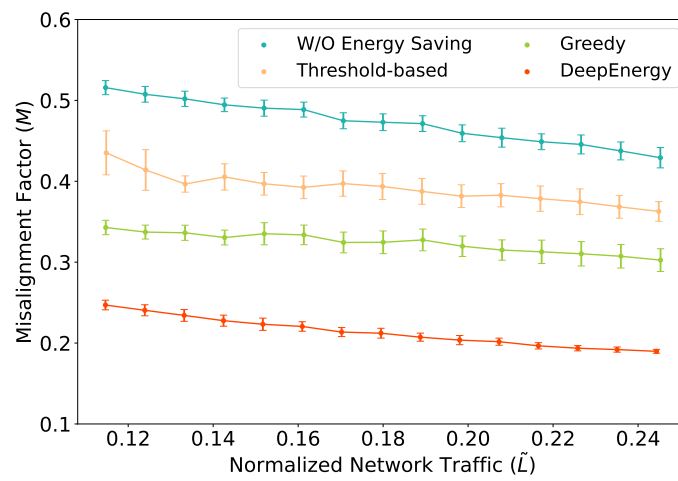


Fig. S20. Misalignment factor vs. the normalized network traffic load for various Energy-saving scenarios. Under a specific Energy-saving scenario, the misalignment factor (M) linearly decreases as the normalized network traffic load (\tilde{L}) increases.

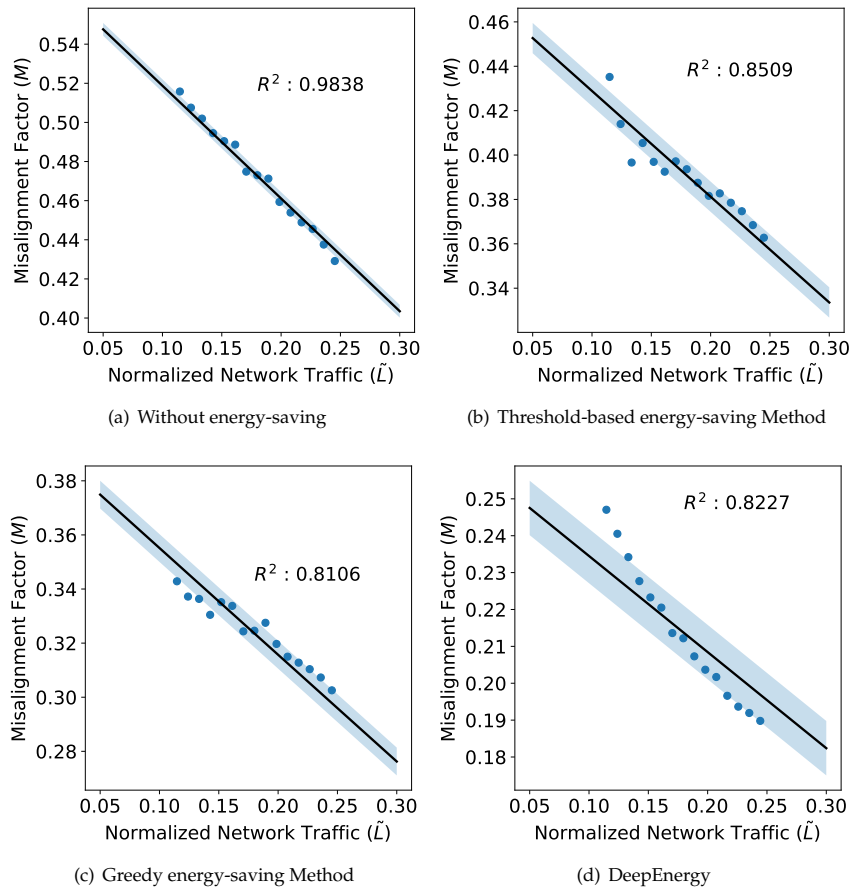


Fig. S21. Linear models can approximate the relationships between the normalized network traffic load (\tilde{L}) and the misalignment factor (M) with high accuracy.

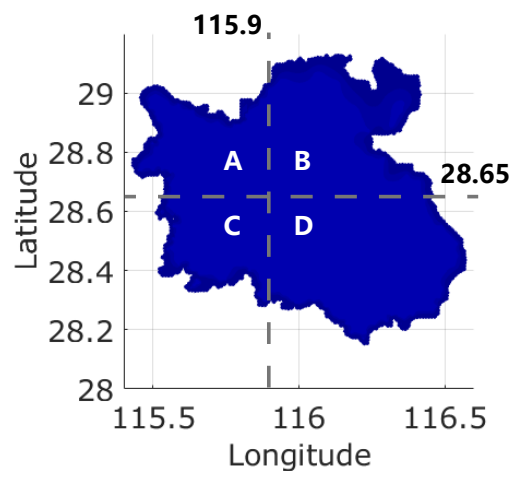


Fig. S22. We partition Nanchang into four regions, according to the city center point, and denote them as Region A, Region B, Region C, and Region D. These four regions have different base station densities, network capacities, and network traffic loads.

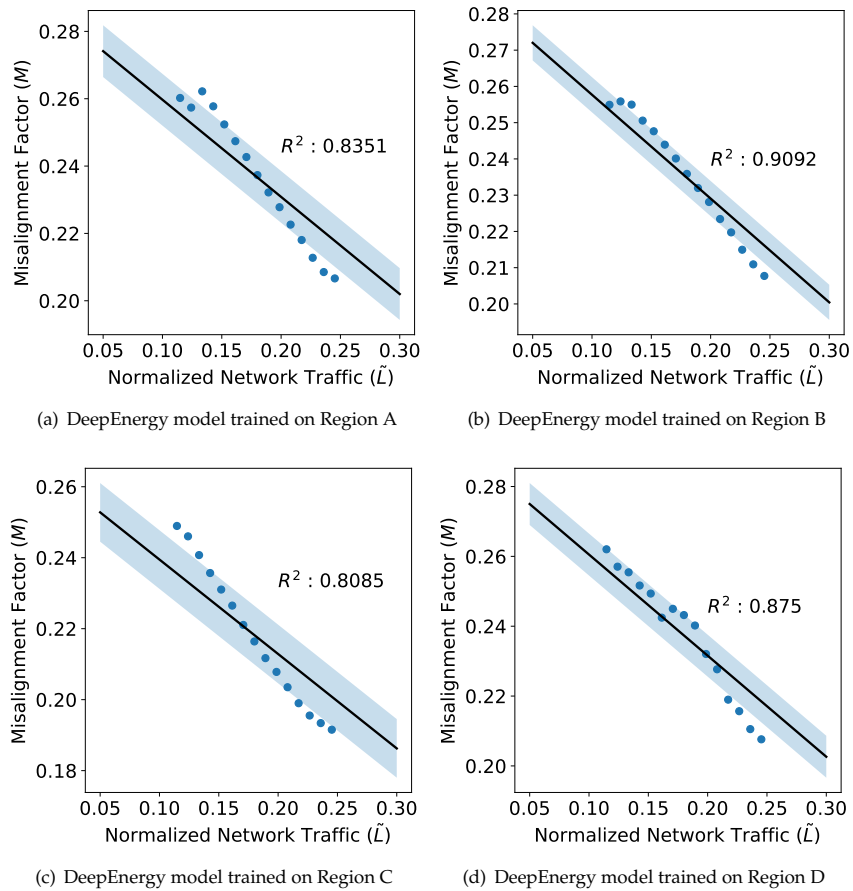


Fig. S23. For DeepEnergy models trained on different regions, Linear models can approximate the relationships between the normalized network traffic load (\tilde{L}) and the misalignment factor (M) with high accuracy.

LIST OF TABLES

| | | |
|-----|---|----|
| S1 | The collected data items of energy consumption data and network traffic data. (NA refers to 'not available'). | 37 |
| S2 | Monthly network traffic statistics in Nanchang, measured in PBytes. And, the number of mobile users in Nanchang, expressed as a million. | 38 |
| S3 | The number of 4G and 5G base stations across different provinces in China as of January 2021. | 39 |
| S4 | The number of mobile users across China's various provinces, expressed as a million. | 40 |
| S5 | Parameter setting of PV system simulation | 41 |
| S6 | Generation unit configuration in Nanchang. | 42 |
| S7 | Additional carbon emissions across different provinces in China, the unit is KtCO ₂ . | 43 |
| S8 | Wasted energy consumption across different provinces in China, the unit is GWh. | 44 |
| S9 | Reduction in carbon emissions using different energy-saving methods across different provinces in China in 2021 compared to the case without energy-saving, the unit is KtCO ₂ . | 45 |
| S10 | Reduction in carbon emissions using different energy-saving methods across different provinces in China in 2022 compared to the case without energy-saving, the unit is KtCO ₂ . | 46 |
| S11 | Reduction in carbon emissions using different energy-saving methods across different provinces in China in 2023 compared to the case without energy-saving, the unit is KtCO ₂ . | 47 |
| S12 | Reduction in energy consumption using different energy-saving methods across different provinces in China in 2021 compared to the case without energy-saving, the unit is GWh. | 48 |
| S13 | Reduction in energy consumption using different energy-saving methods across different provinces in China in 2022 compared to the case without energy-saving, the unit is MWh. | 49 |
| S14 | Reduction in energy consumption using different energy-saving methods across different provinces in China in 2023 compared to the case without energy-saving, the unit is GWh. | 50 |
| S15 | Energy consumption of mobile networks across different province in China over years, the unit is GWh. | 51 |
| S16 | Carbon emissions of mobile networks across different province in China over years, the unit is KtCO ₂ . | 52 |
| S17 | Data used for investment, operation and maintenance costs of photovoltaic system. | 53 |
| S18 | Number of base stations and R^2 score of estimated M and ground truth in four regions. | 54 |
| S19 | The R^2 score of estimated M and ground truth of different traffic load. | 55 |
| S20 | Average and standard deviation of BBU power for different types of base stations. | 56 |
| S21 | Linear regression analysis for RRU power consumption in 5G networks. | 57 |
| S22 | Linear regression analysis for RRU power consumption in 4G networks. | 58 |
| S23 | Average and standard deviation of RRU power in sleep mode for different types of base stations. | 59 |
| S24 | Parameter settings of EnergyPlus to simulation the power consumption of base stations' cooling subsystem. | 60 |
| S25 | Parameter settings of the threshold-based method used in current real-world mobile networks. (NA refers to 'not available') | 61 |
| S26 | Linear regression analysis for misalignment factor. | 62 |
| S27 | The estimated misalignment factors across provinces without energy-saving. | 63 |
| S28 | The estimated misalignment factors across provinces with threshold-based energy-saving method. | 64 |
| S29 | The estimated misalignment factors across provinces with greedy energy-saving method. | 65 |
| S30 | The estimated misalignment factors across provinces with DeepEnergy. | 66 |
| S31 | The performance of the models trained on data from different regions in Nanchang. | 67 |
| S32 | Linear regression analysis for misalignment factor of DeepEnergy models trained on different regions. | 68 |

Table S1. The collected data items of energy consumption data and network traffic data. (NA refers to 'not available'.)

| Items collected | Description | Power consumption data | Network performance data |
|-----------------|---|------------------------|--------------------------|
| Base station ID | An unique identification for the base station where the data is collected | ✓ | ✓ |
| Timestamp | The time the record was gathered | ✓ | ✓ |
| PRB usage ratio | The percentage of the base station's total available physical resource blocks (PRB) that are currently being utilized | ✓ | ✓ |
| Traffic volume | Average volume of downlink traffic, measured in KBytes | ✓ | ✓ |
| # of users | Average number of users served | ✓ | ✓ |
| Data rate | Average downlink data rate of users served, measured in Mbps | ✓ | ✓ |
| Transmit power | Average transmit power of the base station, measured in Watts | ✓ | NA |
| BBU power | Average power consumption of the base station's base band units (BBU), measured in Watts | ✓ | NA |
| RRU power | Average power consumption of the base station's remote radio units (RRU), measured in Watts | ✓ | NA |
| Element power | Average power consumption of the base station, measured in Watts | ✓ | NA |
| Sleep time | Average time of the base station is in sleep mode | ✓ | NA |

Table S2. Monthly network traffic statistics in Nanchang, measured in PBytes. And, the number of mobile users in Nanchang, expressed as a million.

| Month | Traffic volume of 4G networks | Traffic volume of 5G networks | Traffic volume of mobile networks | Number of mobile users |
|---------|-------------------------------|-------------------------------|-----------------------------------|------------------------|
| 2021-01 | 1.1536 | 0.0569 | 1.2105 | 7.241 |
| 2021-02 | 1.3128 | 0.0622 | 1.375 | 7.218 |
| 2021-03 | 1.3991 | 0.1364 | 1.5355 | 7.344 |
| 2021-04 | 1.4649 | 0.1673 | 1.6322 | 7.386 |
| 2021-05 | 1.5131 | 0.1953 | 1.7084 | 7.433 |
| 2021-06 | 1.5246 | 0.2237 | 1.7483 | 7.524 |
| 2021-07 | 1.5306 | 0.2319 | 1.7625 | 7.575 |
| 2021-08 | 1.5333 | 0.2405 | 1.7738 | 7.626 |
| 2021-09 | 1.4736 | 0.3518 | 1.8254 | 7.797 |
| 2021-10 | 1.4311 | 0.3821 | 1.8132 | 7.816 |
| 2021-11 | 1.4701 | 0.3870 | 1.8571 | 7.827 |
| 2021-12 | 1.4985 | 0.3963 | 1.8948 | 7.838 |
| 2022-01 | 1.4614 | 0.4394 | 1.9008 | 7.981 |
| 2022-02 | 1.4159 | 0.4881 | 1.9040 | 8.048 |
| 2022-03 | 1.3873 | 0.5280 | 1.9153 | 8.084 |
| 2022-04 | 1.3820 | 0.5400 | 1.9220 | 7.960 |
| 2022-05 | 1.3719 | 0.5777 | 1.9496 | 7.874 |

Table S3. The number of 4G and 5G base stations across different provinces in China as of January 2021.

| Province | # of 4G Base Stations | # of 5G Base Stations |
|----------------|-----------------------|-----------------------|
| Beijing | 24305 | 15293 |
| Tianjing | 15009 | 9451 |
| Hebei | 107949 | 38758 |
| Shanxi | 64850 | 26122 |
| Inner Mongolia | 36502 | 15993 |
| Liaoning | 63647 | 19745 |
| Jilin | 32089 | 9590 |
| Heilongjiang | 46940 | 21158 |
| Shanghai | 25672 | 24881 |
| Jiangsu | 93128 | 69458 |
| Zhejiang | 92217 | 58079 |
| Anhui | 71780 | 35477 |
| Fujian | 96086 | 29828 |
| Jiangxi | 71101 | 37764 |
| Shandong | 117311 | 58687 |
| Henan | 97658 | 34639 |
| Hubei | 82828 | 37536 |
| Hunan | 84584 | 31804 |
| Guangdong | 124663 | 90689 |
| Guangxi | 72839 | 20929 |
| Hainan | 14808 | 6690 |
| Chongqing | 60704 | 23969 |
| Sichuan | 149584 | 35068 |
| Guizhou | 79910 | 33592 |
| Yunnan | 106092 | 42795 |
| Tibet | 16502 | 2880 |
| Shaanxi | 61301 | 24552 |
| Gansu | 48530 | 10034 |
| Qinghai | 12547 | 3246 |
| Ningxia | 11556 | 5588 |
| Xinjiang | 48386 | 10964 |

Table S4. The number of mobile users across China's various provinces, expressed as a million.

| Province | 2021-01 | 2021-02 | 2021-03 | 2021-04 | 2021-05 | 2021-06 | 2021-07 | 2021-08 | 2021-09 | 2021-10 | 2021-11 | 2021-12 | 2022-01 | 2022-02 | 2022-03 | 2022-04 | 2022-05 |
|----------------|---------|---------|---------|---------|---------|---------|---------|---------|---------|---------|---------|---------|----------|---------|---------|---------|---------|
| Beijing | 39,064 | 38,704 | 38,643 | 38,51 | 38,461 | 38,661 | 38,835 | 39,178 | 39,458 | 39,32 | 39,464 | 39,72 | 39,5035 | 39,287 | 39,338 | 39,398 | 39,407 |
| Tianjing | 17,11 | 17,064 | 17,136 | 17,187 | 17,194 | 17,363 | 17,361 | 17,244 | 17,29 | 17,421 | 17,448 | 17,451 | 17,439 | 17,427 | 17,484 | 17,531 | 17,415 |
| Hebei | 83,36 | 83,477 | 83,912 | 84,032 | 84,061 | 84,304 | 84,699 | 85,064 | 85,718 | 86,015 | 86,106 | 86,435 | 86,5345 | 86,634 | 86,613 | 86,512 | 86,479 |
| Shanxi | 40,228 | 40,182 | 40,45 | 40,402 | 40,394 | 40,67 | 40,681 | 40,822 | 41,141 | 41,154 | 41,137 | 41,26 | 41,308 | 41,356 | 41,677 | 41,626 | 41,725 |
| Inner Mongolia | 29,622 | 29,457 | 29,567 | 29,505 | 29,489 | 29,482 | 29,537 | 29,663 | 29,76 | 29,802 | 29,972 | 30,169 | 30,1345 | 30,10 | 30,245 | 30,274 | 30,335 |
| Liaoning | 48,738 | 48,579 | 48,848 | 48,864 | 48,884 | 48,965 | 49,061 | 49,191 | 49,681 | 49,719 | 49,720 | 49,752 | 49,73 | 49,708 | 50,068 | 49,941 | 50,102 |
| Jilin | 28,701 | 28,571 | 28,765 | 28,77 | 28,884 | 29,01 | 29,104 | 29,153 | 29,324 | 29,376 | 29,563 | 29,665 | 29,6765 | 29,688 | 29,597 | 29,415 | 29,674 |
| Heilongjiang | 38,444 | 37,258 | 37,397 | 37,314 | 37,423 | 37,455 | 37,395 | 37,437 | 37,827 | 38,007 | 38,129 | 37,595 | 37,7335 | 37,872 | 37,926 | 37,995 | 38,078 |
| Shanghai | 42,776 | 42,729 | 42,938 | 43,389 | 43,78 | 43,969 | 44,159 | 44,314 | 44,459 | 44,591 | 44,714 | 43,988 | 44,016 | 44,044 | 44,019 | 43,592 | 42,854 |
| Jiangsu | 98,971 | 99,075 | 99,671 | 99,586 | 99,767 | 100,184 | 100,412 | 100,508 | 100,814 | 101,449 | 101,579 | 101,795 | 102,254 | 102,713 | 103,358 | 103,302 | 103,628 |
| Zhejiang | 85,852 | 85,102 | 85,643 | 86,473 | 86,796 | 87,018 | 87,432 | 87,978 | 88,425 | 88,628 | 88,625 | 88,596 | 88,833 | 89,07 | 89,93 | 90,098 | 90,45 |
| Anhui | 60,256 | 60,558 | 60,762 | 60,932 | 61,312 | 61,532 | 61,648 | 61,835 | 62,028 | 62,069 | 62,027 | 61,926 | 62,2785 | 62,631 | 62,856 | 62,846 | 62,911 |
| Fujian | 47,393 | 47,275 | 47,603 | 47,708 | 47,813 | 47,912 | 47,859 | 48,204 | 48,395 | 48,475 | 48,485 | 48,243 | 48,3355 | 48,428 | 48,633 | 48,614 | 48,604 |
| Jiangxi | 42,494 | 43,007 | 43,323 | 43,399 | 43,617 | 44,007 | 44,187 | 44,574 | 44,978 | 45,139 | 44,769 | 44,968 | 45,6215 | 46,275 | 46,421 | 45,896 | 44,94 |
| Shandong | 109,071 | 108,654 | 109,231 | 109,601 | 109,944 | 110,074 | 110,492 | 110,994 | 111,506 | 112,203 | 112,214 | 112,485 | 112,931 | 113,377 | 114,236 | 114,586 | 115,179 |
| Henan | 100,514 | 101,16 | 101,813 | 101,833 | 101,949 | 102,311 | 102,50 | 102,459 | 102,783 | 103,426 | 103,421 | 103,526 | 103,7915 | 104,057 | 104,478 | 104,558 | 104,641 |
| Hubei | 56,811 | 57,061 | 57,48 | 57,45 | 57,514 | 57,661 | 57,726 | 58,264 | 58,637 | 58,868 | 58,935 | 58,711 | 58,862 | 59,013 | 59,254 | 59,381 | 59,411 |
| Hunan | 67,194 | 67,612 | 67,859 | 68,002 | 68,367 | 68,538 | 68,894 | 68,954 | 69,519 | 69,521 | 69,387 | 69,423 | 69,347 | 69,271 | 69,43 | 69,405 | 69,521 |
| Guangdong | 155,369 | 153,943 | 154,715 | 156,70 | 157,088 | 157,586 | 158,84 | 159,857 | 161,224 | 162,058 | 162,541 | 162,678 | 162,8955 | 163,113 | 165,621 | 166,343 | 166,69 |
| Guangxi | 53,329 | 53,796 | 54,061 | 54,012 | 54,018 | 54,008 | 54,288 | 54,716 | 54,971 | 55,125 | 55,077 | 55,114 | 55,233 | 55,352 | 56,063 | 56,231 | 56,616 |
| Hainan | 11,352 | 11,195 | 11,374 | 11,366 | 11,368 | 11,324 | 11,298 | 11,285 | 11,502 | 11,566 | 11,573 | 11,589 | 11,564 | 11,539 | 11,734 | 11,633 | 11,571 |
| Chongqing | 36,401 | 36,691 | 36,92 | 36,849 | 36,906 | 36,928 | 37,031 | 37,284 | 37,571 | 37,663 | 37,612 | 37,511 | 37,8435 | 38,176 | 38,356 | 38,408 | 38,509 |
| Sichuan | 91,246 | 91,53 | 91,995 | 91,473 | 91,695 | 92,587 | 92,677 | 92,692 | 92,894 | 93,117 | 93,154 | 93,389 | 93,7805 | 94,172 | 94,835 | 95,082 | 95,168 |
| Guizhou | 40,935 | 41,162 | 41,483 | 41,363 | 41,382 | 41,409 | 41,448 | 42,026 | 42,228 | 42,404 | 42,436 | 42,699 | 42,871 | 43,043 | 43,292 | 43,27 | 43,312 |
| Yunnan | 49,534 | 49,706 | 50,103 | 49,95 | 49,623 | 49,715 | 50,02 | 50,271 | 50,473 | 50,321 | 50,359 | 50,457 | 50,4385 | 50,42 | 50,63 | 50,583 | 50,478 |
| Tibet | 3,219 | 3,155 | 3,138 | 3,197 | 3,195 | 3,212 | 3,245 | 3,258 | 3,305 | 3,322 | 3,316 | 3,334 | 3,3235 | 3,313 | 3,344 | 3,355 | 3,349 |
| Shaanxi | 45,897 | 45,534 | 45,405 | 46,095 | 46,222 | 46,735 | 47,069 | 47,242 | 47,496 | 47,681 | 47,720 | 47,778 | 47,728 | 47,678 | 48,373 | 47,964 | 48,045 |
| Gansu | 26,738 | 26,69 | 26,912 | 26,937 | 27,069 | 27,178 | 27,221 | 27,308 | 27,466 | 27,482 | 27,402 | 27,447 | 27,463 | 27,479 | 27,597 | 27,589 | 27,60 |
| Qinghai | 6,594 | 6,506 | 6,528 | 6,541 | 6,588 | 6,63 | 6,661 | 6,689 | 6,755 | 6,77 | 6,789 | 6,805 | 6,804 | 6,803 | 6,846 | 6,857 | 6,93 |
| Ningxia | 8,392 | 8,383 | 8,413 | 8,41 | 8,416 | 8,429 | 8,453 | 8,536 | 8,617 | 8,644 | 8,669 | 8,661 | 8,7115 | 8,762 | 8,858 | 8,844 | 8,866 |
| Xinjiang | 28,466 | 28,558 | 28,945 | 29,062 | 29,024 | 29,067 | 29,053 | 29,123 | 29,679 | 29,675 | 29,644 | 29,654 | 29,73 | 29,806 | 29,911 | 29,962 | 30,002 |

Table S5. Parameter setting of PV system simulation

| Parameter Name | Description | Value in Simulation |
|-----------------|---|-----------------------------|
| Lon | Longitude of the Base station | Dependent on BSes |
| Lat | Latitude of the Base station | Dependent on BSes |
| System Capacity | Nameplate capacity (kW), converted from PV panel area | PV panel area \times 0.16 |
| Azimuth | Azimuth angle (degrees) | 180 |
| Tile | Tile angle (degrees) | 16 |
| Losses | Total conversion loss of the system | 14.08 |

Table S6. Generation unit configuration in Nanchang.

| Power Plant | N_{unit} | P_i^{max} | c_i^{power} | $c_i^{up/down}$ | $T_i^{up/down}$ |
|-------------|------------|-------------|----------------|-----------------|------------------|
| XinChang | 2 | 700 MW | 264.62 RMB/MWh | 700,000 RMB | 8 (i.e., 4 hour) |
| NanChang | 2 | 150 MW | 295.39 RMB/MWh | 150,000 RMB | 8 (i.e., 4 hour) |
| HongPing | 4 | 300 MW | 295.39 RMB/MWh | 300,000 RMB | 8 (i.e., 4 hour) |

Table S7. Additional carbon emissions across different provinces in China, the unit is KtCO₂.

| Province | Without Energy-saving | Threshold-based method | Greedy | DeepEnergy |
|-----------------------|---------------------------|--------------------------|-------------------------|----------------------|
| Beijing | 522.607±21.703 | 305.581±11.299 | 143.671±4.287 | 4.592±0.357 |
| Tianjing | 319.228±14.464 | 185.326±7.511 | 85.617±2.208 | 2.581±0.126 |
| Hebei | 836.627±35.177 | 248.501±7.675 | 46.549±1.146 | 0.0±0.0 |
| Shanxi | 649.464±29.644 | 252.944±9.349 | 43.173±0.963 | 0.0±0.0 |
| Inner Mongolia | 434.953±17.666 | 194.915±7.172 | 37.493±0.475 | 0.0±0.0 |
| Liaoning | 368.728±14.193 | 75.564±1.668 | 16.662±2.113 | 0.0±0.0 |
| Jilin | 161.809±5.94 | 30.039±1.022 | 7.268±0.774 | 0.0±0.0 |
| Heilongjiang | 634.722±27.492 | 307.026±12.343 | 76.28±1.414 | 0.0±0.0 |
| Shanghai | 1062.309±47.839 | 710.352±29.49 | 440.367±18.228 | 56.374±0.563 |
| Jiangsu | 2536.13±116.663 | 1569.896±67.25 | 843.571±33.058 | 40.628±1.012 |
| Zhejiang | 1928.413±90.51 | 1109.701±49.74 | 502.994±22.5 | 16.555±1.273 |
| Anhui | 1004.825±47.978 | 491.846±19.35 | 128.773±3.424 | 0.781±0.413 |
| Fujian | 576.596±24.672 | 115.012±3.804 | 25.064±3.209 | 0.0±0.0 |
| Jiangxi | 1128.359±53.311 | 559.295±22.982 | 159.996±5.408 | 3.248±1.645 |
| Shandong | 1658.913±79.541 | 823.681±33.062 | 233.366±6.608 | 2.106±1.069 |
| Henan | 697.864±26.921 | 199.715±6.548 | 38.319±1.428 | 0.0±0.0 |
| Hubei | 1009.093±43.985 | 449.994±19.428 | 87.054±3.153 | 0.0±0.0 |
| Hunan | 714.896±28.868 | 236.243±7.347 | 42.25±1.844 | 0.0±0.0 |
| Guangdong | 3164.488±151.681 | 1929.178±88.293 | 1002.169±44.563 | 51.056±1.233 |
| Guangxi | 318.733±13.288 | 57.184±1.824 | 12.709±0.513 | 0.0±0.0 |
| Hainan | 188.059±7.477 | 86.129±2.185 | 17.991±0.124 | 0.0±0.0 |
| Chongqing | 563.769±23.978 | 207.374±6.858 | 35.903±1.347 | 0.0±0.0 |
| Sichuan | 386.484±14.094 | 67.572±2.084 | 11.397±5.951 | 0.0±0.0 |
| Guizhou | 848.09±39.111 | 340.227±13.72 | 60.413±1.794 | 0.0±0.0 |
| Yunnan | 1115.895±49.994 | 442.586±16.232 | 70.043±1.835 | 0.0±0.0 |
| Tibet | 18.545±0.618 | 3.877±0.512 | 0.0±0.0 | 0.0±0.0 |
| Shaanxi | 588.265±26.86 | 218.129±8.946 | 41.424±1.244 | 0.0±0.0 |
| Gansu | 76.092±2.448 | 15.973±2.469 | 1.664±0.849 | 0.0±0.0 |
| Qinghai | 44.888±1.383 | 8.16±0.169 | 1.401±0.723 | 0.0±0.0 |
| Ningxia | 157.105±6.819 | 75.137±2.41 | 18.599±0.212 | 0.0±0.0 |
| Xinjiang | 99.964±3.338 | 19.448±0.756 | 3.152±1.626 | 0.0±0.0 |
| All over China | 23815.926±1067.671 | 11336.618±463.515 | 4235.346±173.034 | 177.925±7.695 |

Table S8. Wasted energy consumption across different provinces in China, the unit is GWh.

| Province | Without Energy-saving | Threshold-based method | Greedy | DeepEnergy |
|-----------------------|--------------------------|--------------------------|------------------------|-----------------------|
| Beijing | 768.541±9.86 | 449.383±7.888 | 211.281±5.371 | 6.754±0.826 |
| Tianjing | 469.453±4.317 | 272.539±3.869 | 125.908±3.688 | 3.796±0.394 |
| Hebei | 1230.334±14.89 | 365.443±8.676 | 68.454±2.389 | 0.0±0.0 |
| Shanxi | 955.095±8.291 | 371.977±6.621 | 63.489±2.011 | 0.0±0.0 |
| Inner Mongolia | 639.636±8.635 | 286.639±5.134 | 55.136±2.38 | 0.0±0.0 |
| Liaoning | 542.248±8.615 | 111.124±3.661 | 24.502±3.331 | 0.0±0.0 |
| Jilin | 237.954±4.282 | 44.175±0.928 | 10.688±1.298 | 0.0±0.0 |
| Heilongjiang | 933.414±10.095 | 451.508±6.473 | 112.176±4.212 | 0.0±0.0 |
| Shanghai | 1562.22±14.403 | 1044.635±13.285 | 647.599±8.571 | 82.903±5.536 |
| Jiangsu | 3729.604±30.173 | 2308.671±25.996 | 1240.545±18.747 | 59.747±2.755 |
| Zhejiang | 2835.902±20.146 | 1631.913±15.092 | 739.698±7.209 | 24.346±2.173 |
| Anhui | 1477.685±9.606 | 723.303±10.687 | 189.373±5.373 | 1.148±0.651 |
| Fujian | 847.936±9.499 | 169.135±3.574 | 36.859±4.742 | 0.0±0.0 |
| Jiangxi | 1659.351±11.434 | 822.493±10.727 | 235.288±5.016 | 4.776±2.478 |
| Shandong | 2439.578±15.449 | 1211.296±16.994 | 343.185±9.116 | 3.097±1.677 |
| Henan | 1026.27±15.899 | 293.699±6.519 | 56.352±0.96 | 0.0±0.0 |
| Hubei | 1483.96±15.383 | 661.757±7.403 | 128.02±2.37 | 0.0±0.0 |
| Hunan | 1051.317±14.455 | 347.416±8.229 | 62.132±3.356 | 0.0±0.0 |
| Guangdong | 4653.659±29.007 | 2837.027±23.849 | 1473.779±14.654 | 75.083±2.827 |
| Guangxi | 468.725±6.034 | 84.094±3.368 | 18.69±1.041 | 0.0±0.0 |
| Hainan | 276.558±4.093 | 126.661±3.758 | 26.457±1.691 | 0.0±0.0 |
| Chongqing | 829.072±9.628 | 304.962±6.567 | 52.798±0.917 | 0.0±0.0 |
| Sichuan | 568.358±10.106 | 99.371±3.609 | 16.761±8.455 | 0.0±0.0 |
| Guizhou | 1247.191±10.033 | 500.335±7.086 | 88.843±3.488 | 0.0±0.0 |
| Yunnan | 1641.022±15.189 | 650.862±11.457 | 103.005±2.847 | 0.0±0.0 |
| Tibet | 27.272±0.581 | 5.701±0.803 | 0.0±0.0 | 0.0±0.0 |
| Shaanxi | 865.096±7.42 | 320.778±4.39 | 60.918±1.449 | 0.0±0.0 |
| Gansu | 111.9±2.482 | 23.49±3.613 | 2.447±1.261 | 0.0±0.0 |
| Qinghai | 66.011±1.578 | 12.0±0.4 | 2.061±1.052 | 0.0±0.0 |
| Ningxia | 231.037±2.565 | 110.495±2.508 | 27.352±1.222 | 0.0±0.0 |
| Xinjiang | 147.006±3.19 | 28.6±0.446 | 4.635±2.365 | 0.0±0.0 |
| All over China | 35023.421±327.353 | 16671.497±233.626 | 6228.45±130.595 | 261.654±19.321 |

Table S9. Reduction in carbon emissions using different energy-saving methods across different provinces in China in 2021 compared to the case without energy-saving, the unit is KtCO₂.

| Province | Threshold-based method | Greedy | DeepEnergy |
|-----------------------|-------------------------|--------------------------|---------------------------|
| Beijing | 113.212±6.012 | 206.025±10.941 | 357.881±19.005 |
| Tianjing | 71.688±3.91 | 130.46±7.115 | 226.619±12.36 |
| Hebei | 381.211±20.326 | 693.736±36.989 | 1205.07±64.253 |
| Shanxi | 246.157±13.439 | 447.961±24.456 | 778.14±42.482 |
| Inner Mongolia | 143.018±7.775 | 260.267±14.15 | 452.103±24.58 |
| Liaoning | 209.421±11.318 | 381.109±20.597 | 662.014±35.779 |
| Jilin | 102.375±5.491 | 186.303±9.992 | 323.623±17.358 |
| Heilongjiang | 187.061±10.171 | 340.417±18.509 | 591.329±32.152 |
| Shanghai | 162.226±8.679 | 295.222±15.795 | 512.822±27.437 |
| Jiangsu | 500.884±26.949 | 911.519±49.042 | 1583.376±85.189 |
| Zhejiang | 446.032±23.734 | 811.698±43.192 | 1409.98±75.028 |
| Anhui | 300.536±16.031 | 546.921±29.173 | 950.043±50.675 |
| Fujian | 324.297±17.424 | 590.162±31.708 | 1025.154±55.079 |
| Jiangxi | 315.382±17.073 | 573.938±31.069 | 996.973±53.97 |
| Shandong | 491.851±26.215 | 895.08±47.706 | 1554.82±82.869 |
| Henan | 334.855±17.514 | 609.375±31.873 | 1058.529±55.365 |
| Hubei | 333.443±17.888 | 606.806±32.553 | 1054.068±56.548 |
| Hunan | 305.15±16.34 | 555.318±29.736 | 964.627±51.653 |
| Guangdong | 652.722±34.571 | 1187.837±62.913 | 2063.36±109.284 |
| Guangxi | 231.728±12.433 | 421.703±22.625 | 732.529±39.302 |
| Hainan | 59.229±3.351 | 107.787±6.098 | 187.234±10.594 |
| Chongqing | 228.378±12.447 | 415.607±22.652 | 721.94±39.348 |
| Sichuan | 441.848±23.469 | 804.083±42.709 | 1396.752±74.189 |
| Guizhou | 312.687±17.019 | 569.035±30.972 | 988.455±53.8 |
| Yunnan | 407.881±22.292 | 742.269±40.568 | 1289.377±70.47 |
| Tibet | 46.126±2.686 | 83.942±4.889 | 145.813±8.492 |
| Shaanxi | 229.54±12.256 | 417.722±22.304 | 725.613±38.744 |
| Gansu | 137.524±7.434 | 250.269±13.528 | 434.735±23.499 |
| Qinghai | 38.898±2.176 | 70.788±3.959 | 122.964±6.877 |
| Ningxia | 48.223±2.692 | 87.756±4.898 | 152.439±8.509 |
| Xinjiang | 141.318±7.684 | 257.173±13.984 | 446.729±24.29 |
| All over China | 7944.901±426.799 | 14458.289±776.697 | 25115.113±1349.179 |

Table S10. Reduction in carbon emissions using different energy-saving methods across different provinces in China in 2022 compared to the case without energy-saving, the unit is KtCO₂.

| Province | Threshold-based method | Greedy | DeepEnergy |
|-----------------------|-------------------------|--------------------------|---------------------------|
| Beijing | 110.464±5.769 | 201.024±10.498 | 349.193±18.236 |
| Tianjing | 70.318±3.786 | 127.967±6.89 | 222.288±11.969 |
| Hebei | 373.951±19.694 | 680.523±35.839 | 1182.118±62.255 |
| Shanxi | 242.432±13.11 | 441.182±23.859 | 766.365±41.444 |
| Inner Mongolia | 140.434±7.546 | 255.564±13.732 | 443.933±23.854 |
| Liaoning | 204.927±10.92 | 372.931±19.872 | 647.809±34.519 |
| Jilin | 99.845±5.265 | 181.7±9.581 | 315.627±16.643 |
| Heilongjiang | 184.057±9.907 | 334.95±18.03 | 581.834±31.319 |
| Shanghai | 159.727±8.459 | 290.675±15.393 | 504.924±26.739 |
| Jiangsu | 492.119±26.188 | 895.567±47.657 | 1555.666±82.784 |
| Zhejiang | 438.147±23.052 | 797.349±41.95 | 1385.054±72.87 |
| Anhui | 294.916±15.544 | 536.694±28.288 | 932.277±49.138 |
| Fujian | 319.909±17.039 | 582.176±31.009 | 1011.283±53.864 |
| Jiangxi | 311.811±16.761 | 567.44±30.503 | 985.684±52.986 |
| Shandong | 481.253±25.299 | 875.794±46.04 | 1521.32±79.975 |
| Henan | 325.137±16.669 | 591.691±30.335 | 1027.812±52.694 |
| Hubei | 328.318±17.441 | 597.479±31.74 | 1037.865±55.135 |
| Hunan | 299.22±15.816 | 544.527±28.782 | 945.883±49.997 |
| Guangdong | 638.209±33.325 | 1161.425±60.646 | 2017.482±105.346 |
| Guangxi | 225.841±11.913 | 410.991±21.68 | 713.921±37.66 |
| Hainan | 58.292±3.264 | 106.081±5.94 | 184.271±10.318 |
| Chongqing | 224.669±12.12 | 408.858±22.056 | 710.216±38.313 |
| Sichuan | 431.935±22.606 | 786.044±41.139 | 1365.416±71.461 |
| Guizhou | 308.795±16.678 | 561.952±30.352 | 976.152±52.723 |
| Yunnan | 403.642±21.921 | 734.556±39.893 | 1275.979±69.296 |
| Tibet | 45.811±2.656 | 83.368±4.834 | 144.817±8.397 |
| Shaanxi | 225.492±11.903 | 410.355±21.662 | 712.816±37.629 |
| Gansu | 134.826±7.193 | 245.359±13.089 | 426.207±22.737 |
| Qinghai | 38.235±2.113 | 69.581±3.845 | 120.867±6.679 |
| Ningxia | 47.426±2.618 | 86.307±4.765 | 149.921±8.277 |
| Xinjiang | 138.334±7.418 | 251.742±13.5 | 437.295±23.451 |
| All over China | 7798.493±413.996 | 14191.853±753.398 | 24652.295±1308.707 |

Table S11. Reduction in carbon emissions using different energy-saving methods across different provinces in China in 2023 compared to the case without energy-saving, the unit is KtCO₂.

| Province | Threshold-based method | Greedy | DeepEnergy |
|-----------------------|-------------------------|--------------------------|--------------------------|
| Beijing | 87.902±3.771 | 159.966±6.862 | 277.873±11.92 |
| Tianjing | 58.519±2.723 | 106.495±4.955 | 184.989±8.607 |
| Hebei | 315.702±14.624 | 574.521±26.613 | 997.986±46.228 |
| Shanxi | 211.837±10.413 | 385.505±18.95 | 669.65±32.918 |
| Inner Mongolia | 119.537±5.691 | 217.535±10.356 | 377.874±17.989 |
| Liaoning | 167.387±7.59 | 304.615±13.812 | 529.138±23.993 |
| Jilin | 79.275±3.427 | 144.267±6.237 | 250.602±10.834 |
| Heilongjiang | 158.901±7.699 | 289.17±14.011 | 502.31±24.338 |
| Shanghai | 136.175±6.378 | 247.813±11.606 | 430.47±20.16 |
| Jiangsu | 422.044±20.106 | 768.044±36.589 | 1334.149±63.558 |
| Zhejiang | 374.717±17.56 | 681.918±31.956 | 1184.542±55.51 |
| Anhui | 247.851±11.473 | 451.045±20.878 | 783.498±36.267 |
| Fujian | 282.145±13.732 | 513.453±24.99 | 891.906±43.41 |
| Jiangxi | 285.787±14.493 | 520.081±26.375 | 903.419±45.815 |
| Shandong | 398.144±18.119 | 724.551±32.974 | 1258.598±57.278 |
| Henan | 244.038±9.617 | 444.106±17.501 | 771.445±30.401 |
| Hubei | 286.491±13.795 | 521.362±25.104 | 905.645±43.608 |
| Hunan | 247.78±11.271 | 450.915±20.51 | 783.273±35.628 |
| Guangdong | 528.743±23.928 | 962.217±43.546 | 1671.442±75.642 |
| Guangxi | 178.257±7.714 | 324.397±14.039 | 563.501±24.386 |
| Hainan | 50.779±2.564 | 92.408±4.666 | 160.52±8.106 |
| Chongqing | 195.239±9.521 | 355.299±17.327 | 617.181±30.099 |
| Sichuan | 350.97±15.556 | 638.701±28.31 | 1109.471±49.176 |
| Guizhou | 279.188±14.088 | 508.071±25.638 | 882.557±44.534 |
| Yunnan | 367.085±18.719 | 668.029±34.065 | 1160.416±59.174 |
| Tibet | 43.458±2.431 | 79.086±4.425 | 137.378±7.686 |
| Shaanxi | 193.432±9.109 | 352.012±16.576 | 611.47±28.794 |
| Gansu | 111.752±5.131 | 203.369±9.337 | 353.267±16.219 |
| Qinghai | 33.082±1.626 | 60.203±2.96 | 104.578±5.142 |
| Ningxia | 41.444±2.066 | 75.42±3.76 | 131.01±6.532 |
| Xinjiang | 114.093±5.26 | 207.629±9.573 | 360.666±16.629 |
| All over China | 6611.755±310.196 | 12032.202±564.502 | 20900.822±980.581 |

Table S12. Reduction in energy consumption using different energy-saving methods across different provinces in China in 2021 compared to the case without energy-saving, the unit is GWh.

| Province | Threshold-based method | Greedy | DeepEnergy |
|-----------------------|------------------------|-------------------------|------------------------|
| Beijing | 166.488±0.144 | 302.978±0.262 | 526.296±0.456 |
| Tianjing | 105.424±0.06 | 191.853±0.109 | 333.263±0.19 |
| Hebei | 560.605±0.365 | 1020.2±0.664 | 1772.162±1.154 |
| Shanxi | 361.995±0.226 | 658.765±0.411 | 1144.324±0.715 |
| Inner Mongolia | 210.321±0.084 | 382.746±0.152 | 664.857±0.264 |
| Liaoning | 307.972±0.023 | 560.454±0.043 | 973.55±0.074 |
| Jilin | 150.551±0.05 | 273.976±0.092 | 475.916±0.159 |
| Heilongjiang | 275.089±0.111 | 500.613±0.202 | 869.602±0.35 |
| Shanghai | 238.568±0.112 | 434.15±0.203 | 754.151±0.353 |
| Jiangsu | 736.595±0.124 | 1340.47±0.225 | 2328.494±0.391 |
| Zhejiang | 655.93±0.498 | 1193.674±0.905 | 2073.499±1.573 |
| Anhui | 441.965±0.279 | 804.296±0.507 | 1397.121±0.881 |
| Fujian | 476.907±0.116 | 867.885±0.211 | 1507.58±0.366 |
| Jiangxi | 463.797±0.076 | 844.027±0.138 | 1466.137±0.239 |
| Shandong | 723.31±0.486 | 1316.294±0.885 | 2286.5±1.537 |
| Henan | 492.433±0.821 | 896.14±1.493 | 1556.661±2.594 |
| Hubei | 490.358±0.158 | 892.362±0.288 | 1550.099±0.501 |
| Hunan | 448.75±0.19 | 816.643±0.345 | 1418.57±0.6 |
| Guangdong | 959.886±0.966 | 1746.819±1.758 | 3034.353±3.053 |
| Guangxi | 340.776±0.108 | 620.151±0.197 | 1077.248±0.342 |
| Hainan | 87.102±0.227 | 158.51±0.414 | 275.343±0.719 |
| Chongqing | 335.85±0.179 | 611.187±0.326 | 1061.677±0.566 |
| Sichuan | 649.776±0.555 | 1182.475±1.011 | 2054.047±1.756 |
| Guizhou | 459.834±0.211 | 836.816±0.383 | 1453.611±0.666 |
| Yunnan | 599.825±0.41 | 1091.573±0.747 | 1896.142±1.297 |
| Tibet | 67.833±0.29 | 123.443±0.527 | 214.43±0.916 |
| Shaanxi | 337.559±0.194 | 614.296±0.353 | 1067.078±0.613 |
| Gansu | 202.241±0.017 | 368.042±0.031 | 639.316±0.053 |
| Qinghai | 57.204±0.112 | 104.1±0.204 | 180.83±0.354 |
| Ningxia | 70.916±0.131 | 129.053±0.239 | 224.175±0.415 |
| Xinjiang | 207.82±0.084 | 378.196±0.153 | 656.954±0.265 |
| All over China | 11683.678±7.406 | 21262.189±13.478 | 36933.99±23.412 |

Table S13. Reduction in energy consumption using different energy-saving methods across different provinces in China in 2022 compared to the case without energy-saving, the unit is MWh.

| Province | Threshold-based method | Greedy | DeepEnergy |
|-----------------------|-------------------------|-------------------------|-------------------------|
| Beijing | 162.447±0.284 | 295.624±0.517 | 513.52±0.898 |
| Tianjing | 103.41±0.013 | 188.187±0.023 | 326.894±0.041 |
| Hebei | 549.927±0.718 | 1000.769±1.307 | 1738.409±2.27 |
| Shanxi | 356.517±0.039 | 648.797±0.071 | 1127.008±0.123 |
| Inner Mongolia | 206.52±0.049 | 375.829±0.089 | 652.843±0.154 |
| Liaoning | 301.364±0.206 | 548.428±0.375 | 952.66±0.651 |
| Jilin | 146.831±0.182 | 267.206±0.331 | 464.157±0.575 |
| Heilongjiang | 270.672±0.039 | 492.574±0.07 | 855.638±0.122 |
| Shanghai | 234.893±0.238 | 427.463±0.433 | 742.535±0.752 |
| Jiangsu | 723.704±0.547 | 1317.01±0.995 | 2287.744±1.729 |
| Zhejiang | 644.334±0.876 | 1172.572±1.593 | 2036.844±2.768 |
| Anhui | 433.7±0.548 | 789.256±0.996 | 1370.995±1.731 |
| Fujian | 470.454±0.333 | 856.142±0.605 | 1487.181±1.051 |
| Jiangxi | 458.545±0.099 | 834.47±0.18 | 1449.536±0.312 |
| Shandong | 707.726±0.991 | 1287.933±1.804 | 2237.235±3.134 |
| Henan | 478.143±1.292 | 870.134±2.351 | 1511.488±4.084 |
| Hubei | 482.82±0.409 | 878.646±0.744 | 1526.273±1.292 |
| Hunan | 440.03±0.49 | 800.775±0.891 | 1391.005±1.548 |
| Guangdong | 938.543±1.646 | 1707.979±2.995 | 2966.885±5.203 |
| Guangxi | 332.12±0.405 | 604.398±0.737 | 1049.884±1.28 |
| Hainan | 85.724±0.173 | 156.002±0.315 | 270.987±0.548 |
| Chongqing | 330.396±0.008 | 601.261±0.015 | 1044.435±0.026 |
| Sichuan | 635.198±1.038 | 1155.947±1.889 | 2007.965±3.281 |
| Guizhou | 454.111±0.019 | 826.4±0.034 | 1435.517±0.059 |
| Yunnan | 593.592±0.201 | 1080.23±0.365 | 1876.439±0.635 |
| Tibet | 67.369±0.27 | 122.6±0.492 | 212.966±0.855 |
| Shaanxi | 331.606±0.392 | 603.463±0.713 | 1048.259±1.238 |
| Gansu | 198.274±0.123 | 360.823±0.225 | 626.776±0.39 |
| Qinghai | 56.228±0.073 | 102.325±0.132 | 177.746±0.23 |
| Ningxia | 69.744±0.086 | 126.922±0.157 | 220.473±0.273 |
| Xinjiang | 203.432±0.07 | 370.21±0.127 | 643.081±0.221 |
| All over China | 11468.373±11.854 | 20870.372±21.573 | 36253.375±37.473 |

Table S14. Reduction in energy consumption using different energy-saving methods across different provinces in China in 2023 compared to the case without energy-saving, the unit is GWh.

| Province | Threshold-based method | Greedy | DeepEnergy |
|-----------------------|------------------------|-------------------------|--------------------------|
| Beijing | 129.268±1.431 | 235.244±2.604 | 408.636±4.523 |
| Tianjing | 86.058±0.64 | 156.61±1.166 | 272.043±2.025 |
| Hebei | 464.268±3.551 | 844.884±6.461 | 1467.626±11.224 |
| Shanxi | 311.525±1.499 | 566.919±2.728 | 984.78±4.738 |
| Inner Mongolia | 175.789±1.118 | 319.904±2.035 | 555.698±3.535 |
| Liaoning | 246.158±2.123 | 447.963±3.863 | 778.144±6.711 |
| Jilin | 116.581±1.252 | 212.157±2.278 | 368.532±3.957 |
| Heilongjiang | 233.677±1.289 | 425.251±2.346 | 738.692±4.076 |
| Shanghai | 200.257±1.429 | 364.431±2.6 | 633.044±4.517 |
| Jiangsu | 620.653±3.929 | 1129.476±7.149 | 1961.984±12.419 |
| Zhejiang | 551.055±3.917 | 1002.82±7.128 | 1741.973±12.381 |
| Anhui | 364.487±2.8 | 663.301±5.095 | 1152.203±8.85 |
| Fujian | 414.919±2.198 | 755.078±4.001 | 1311.626±6.95 |
| Jiangxi | 420.275±1.369 | 764.825±2.491 | 1328.557±4.326 |
| Shandong | 585.506±4.953 | 1065.516±9.014 | 1850.879±15.658 |
| Henan | 358.88±5.225 | 653.097±9.509 | 1134.477±16.519 |
| Hubei | 421.311±2.451 | 766.709±4.461 | 1331.831±7.749 |
| Hunan | 364.382±3.091 | 663.11±5.625 | 1151.872±9.77 |
| Guangdong | 777.563±6.776 | 1415.025±12.331 | 2458.003±21.419 |
| Guangxi | 262.143±2.803 | 477.054±5.1 | 828.677±8.86 |
| Hainan | 74.675±0.259 | 135.894±0.471 | 236.058±0.819 |
| Chongqing | 287.116±1.493 | 522.499±2.717 | 907.619±4.72 |
| Sichuan | 516.132±4.978 | 939.267±9.059 | 1631.576±15.736 |
| Guizhou | 410.57±1.441 | 747.164±2.622 | 1297.879±4.554 |
| Yunnan | 539.832±1.607 | 982.396±2.924 | 1706.495±5.079 |
| Tibet | 63.909±0.127 | 116.302±0.23 | 202.026±0.4 |
| Shaanxi | 284.459±1.957 | 517.664±3.561 | 899.221±6.187 |
| Gansu | 164.342±1.324 | 299.072±2.409 | 519.51±4.185 |
| Qinghai | 48.65±0.234 | 88.535±0.425 | 153.791±0.738 |
| Ningxia | 60.946±0.25 | 110.911±0.456 | 192.661±0.792 |
| Xinjiang | 167.784±1.319 | 305.336±2.401 | 530.391±4.17 |
| All over China | 9723.169±68.831 | 17694.415±125.26 | 30736.503±217.586 |

Table S15. Energy consumption of mobile networks across different province in China over years, the unit is GWh.

| Province | 2021 | 2022 | 2023 |
|-----------------------|------------------------|------------------------|------------------------|
| Beijing | 1116.67±4.57 | 1130.76±5.06 | 1253.08±9.31 |
| Tianjing | 677.3±2.85 | 684.21±3.1 | 748.28±5.43 |
| Hebei | 3606.84±10.22 | 3644.1±11.45 | 3960.27±21.94 |
| Shanxi | 2263.84±7.3 | 2282.79±7.95 | 2449.12±13.66 |
| Inner Mongolia | 1339.32±4.87 | 1352.51±5.33 | 1466.14±9.3 |
| Liaoning | 1998.27±7.83 | 2021.1±8.63 | 2225.03±15.74 |
| Jilin | 1000.49±4.38 | 1013.47±4.84 | 1125.06±8.81 |
| Heilongjiang | 1746.02±6.02 | 1761.28±6.53 | 1897.93±11.17 |
| Shanghai | 1541.67±5.05 | 1554.21±5.48 | 1681.25±9.86 |
| Jiangsu | 4641.51±12.15 | 4686.25±13.62 | 5067.6±26.17 |
| Zhejiang | 4133.64±8.52 | 4173.9±9.84 | 4518.92±21.12 |
| Anhui | 2805.45±6.71 | 2833.9±7.64 | 3089.76±15.98 |
| Fujian | 2967.5±6.59 | 2989.65±7.34 | 3194.71±14.26 |
| Jiangxi | 2857.09±6.45 | 2875.7±7.07 | 3016.96±11.77 |
| Shandong | 4632.22±12.08 | 4686.5±13.85 | 5139.0±28.55 |
| Henan | 3290.93±10.12 | 3340.16±11.74 | 3781.06±26.33 |
| Hubei | 3073.59±7.21 | 3099.73±8.08 | 3327.01±15.65 |
| Hunan | 2887.99±9.2 | 2917.95±10.23 | 3197.02±19.87 |
| Guangdong | 6159.93±14.25 | 6234.9±16.64 | 6830.88±35.67 |
| Guangxi | 2214.26±7.89 | 2244.21±8.92 | 2503.33±17.83 |
| Hainan | 550.64±3.2 | 555.44±3.39 | 596.26±5.0 |
| Chongqing | 2098.21±6.55 | 2117.15±7.2 | 2277.38±12.72 |
| Sichuan | 4185.95±11.27 | 4236.27±12.94 | 4676.94±27.57 |
| Guizhou | 2831.47±7.2 | 2851.54±7.88 | 3012.65±13.29 |
| Yunnan | 3675.93±9.61 | 3697.31±10.33 | 3895.8±17.03 |
| Tibet | 407.55±2.35 | 409.2±2.42 | 421.97±2.95 |
| Shaanxi | 2149.09±5.58 | 2169.94±6.27 | 2343.94±12.07 |
| Gansu | 1298.18±4.75 | 1311.81±5.24 | 1437.1±9.69 |
| Qinghai | 360.95±1.9 | 364.38±2.04 | 392.39±3.18 |
| Ningxia | 444.71±2.12 | 448.82±2.28 | 481.4±3.54 |
| Xinjiang | 1337.87±5.36 | 1353.1±5.89 | 1484.85±10.53 |
| All over China | 74295.13±214.15 | 75042.23±239.24 | 81493.12±455.99 |

Table S16. Carbon emissions of mobile networks across different province in China over years, the unit is KtCO₂.

| Province | 2021 | 2022 | 2023 |
|-----------------------|-------------------------|-------------------------|-------------------------|
| Beijing | 759.34±44.26 | 768.92±45.13 | 852.1±52.66 |
| Tianjing | 460.57±26.9 | 465.26±27.33 | 508.83±31.35 |
| Hebei | 2452.65±139.69 | 2477.99±141.95 | 2692.99±161.07 |
| Shanxi | 1539.41±88.32 | 1552.3±89.48 | 1665.4±99.67 |
| Inner Mongolia | 910.74±52.64 | 919.71±53.46 | 996.98±60.47 |
| Liaoning | 1358.83±78.95 | 1374.35±80.36 | 1513.02±92.94 |
| Jilin | 680.33±39.86 | 689.16±40.67 | 765.04±47.6 |
| Heilongjiang | 1187.3±68.39 | 1197.67±69.32 | 1290.59±77.66 |
| Shanghai | 1048.34±60.2 | 1056.86±60.97 | 1143.25±68.77 |
| Jiangsu | 3156.23±179.05 | 3186.65±181.75 | 3445.97±204.74 |
| Zhejiang | 2810.88±157.81 | 2838.25±160.23 | 3072.87±180.98 |
| Anhui | 1907.71±107.77 | 1927.05±109.48 | 2101.04±124.85 |
| Fujian | 2017.9±113.63 | 2032.96±114.98 | 2172.41±127.46 |
| Jiangxi | 1942.82±109.48 | 1955.48±110.61 | 2051.53±119.16 |
| Shandong | 3149.91±178.66 | 3186.82±181.92 | 3494.52±209.06 |
| Henan | 2237.83±128.03 | 2271.31±131.0 | 2571.12±157.63 |
| Hubei | 2090.04±117.97 | 2107.82±119.55 | 2262.37±133.32 |
| Hunan | 1963.84±112.58 | 1984.2±114.42 | 2173.98±131.57 |
| Guangdong | 4188.75±236.28 | 4239.73±240.75 | 4645.0±276.26 |
| Guangxi | 1505.7±86.92 | 1526.06±88.76 | 1702.26±104.65 |
| Hainan | 374.44±22.5 | 377.7±22.81 | 405.46±25.47 |
| Chongqing | 1426.79±81.7 | 1439.66±82.86 | 1548.62±92.7 |
| Sichuan | 2846.44±161.7 | 2880.67±164.75 | 3180.32±191.4 |
| Guizhou | 1925.4±109.08 | 1939.05±110.3 | 2048.6±120.09 |
| Yunnan | 2499.63±141.79 | 2514.17±143.09 | 2649.15±155.18 |
| Tibet | 277.14±16.64 | 278.25±16.75 | 286.94±17.6 |
| Shaanxi | 1461.38±82.87 | 1475.56±84.13 | 1593.88±94.67 |
| Gansu | 882.76±51.05 | 892.03±51.9 | 977.23±59.69 |
| Qinghai | 245.45±14.61 | 247.78±14.83 | 266.83±16.68 |
| Ningxia | 302.4±17.84 | 305.2±18.11 | 327.35±20.2 |
| Xinjiang | 909.75±52.94 | 920.1±53.88 | 1009.69±62.04 |
| All over China | 50520.69±2880.11 | 51028.72±2925.51 | 55415.32±3317.61 |

Table S17. Data used for investment, operation and maintenance costs of photovoltaic system.

| | Component | Value | Unit |
|-------------------------|--|--------------|-------------|
| Initial investment cost | PV Modules | 3 | CNY/W |
| | Supporting structures | 0.3 | CNY/W |
| | Inverter | 0.3 | CNY/W |
| | Wirings | 0.2 | CNY/W |
| | Insurance | 0.035 | CNY/W |
| | Engineering (design, transport and assembly, installation) | 0.6 | CNY/W |
| | Junction boxes | 0.1 | CNY/W |
| Annual cost | Operation and maintenance cost | 0.03 | CNY/W |
| | Inverter replacement cost (every ten years) | 0.3 | CNY/W |
| Other details | PV panels' conversion efficiency | 16 | % |
| | Inflation rate | 3.5 | % |
| | Discount rate | 0.3 | % |
| | Lifetime of the inverter | 10 | Year |
| | Lifetime of PV System | 20 | Year |

Table S18. Number of base stations and R^2 score of estimated M and ground truth in four regions.

| | Region A | Region B | Region C | Region D |
|-------------|----------|----------|----------|----------|
| Num of BSes | 5344 | 3439 | 2457 | 3003 |
| R^2 of | 0.9544 | 0.9654 | 0.9628 | 0.9537 |

Table S19. The R^2 score of estimated M and ground truth of different traffic load.

| Simulated Future Network | R^2 |
|---------------------------------|--------|
| 40% of Capacity | 0.7800 |
| 50% of Capacity | 0.8284 |
| 60% of Capacity | 0.8701 |
| 70% of Capacity | 0.8977 |
| 80% of Capacity | 0.9211 |
| 90% of Capacity | 0.9384 |

Table S20. Average and standard deviation of BBU power for different types of base stations.

| Base station types | Average (W) | Standard deviation |
|---------------------------|--------------------|---------------------------|
| 4G BS with 3 cells | 89.3771 | 5.5947 |
| 5G BS with 3 cells | 305.0409 | 26.8226 |
| 5G BS with 6 cells | 499.6484 | 44.3751 |

Table S21. Linear regression analysis for RRU power consumption in 5G networks.

(a) RRU power vs. transmit power in 5G networks

Linear regression model: $P_{RRU} = \alpha \cdot P_{trans} + \gamma$

Dependent variable
Transmit power (P_{trans})

| Base station types | Slope (α) | Offset (γ) | R^2 |
|--------------------|--------------------|---------------------|--------|
| 5G 32TR SA | 1.6928 | 389.7695 | 0.8257 |
| 5G 32TR NSA | 1.4474 | 287.3546 | 0.9595 |
| 5G 64TR SA | 1.8684 | 702.5641 | 0.7708 |
| 5G 64TR NSA | 1.6761 | 729.7315 | 0.7502 |

(b) Transmit power vs. PRB usage ratio in 5G networks

Linear regression model: $P_{trans} = \beta \cdot r_{PRB} + \sigma$

Dependent variable
PRB usage ratio (r_{PRB})

| Base station types | Slope (β) | Offset (σ) | R^2 |
|--------------------|-------------------|---------------------|--------|
| 5G 32TR SA | 244.7592 | 0 | 0.9763 |
| 5G 32TR NSA | 259.9553 | 0 | 0.9776 |
| 5G 64TR SA | 203.0841 | 0 | 0.9599 |
| 5G 64TR NSA | 159.1848 | 0 | 0.9668 |

Table S22. Linear regression analysis for RRU power consumption in 4G networks.

(a) RRU power vs. transmit power in 4G networks

Linear regression model: $P_{RRU} = \alpha \cdot P_{trans} + \gamma$

Dependent variable
Transmit power (P_{trans})

| Base station settings | Slope (α) | Offset (γ) | R^2 |
|----------------------------------|--------------------|---------------------|--------|
| 4G Max transmit power: 19.87 (W) | 6.6283 | 156.6234 | 0.9471 |
| 4G Max transmit power: 39.64 (W) | 5.7572 | 138.0120 | 0.9350 |
| 4G Max transmit power: 79.09 (W) | 4.9461 | 103.0757 | 0.9690 |

(b) Transmit power vs. PRB usage ratio in 4G networks

Linear regression model: $P_{trans} = \beta \cdot r_{PRB} + \sigma$

Dependent variable
PRB usage ratio (r_{PRB})

| Base station settings | Slope (α) | Offset (γ) | R^2 |
|----------------------------------|--------------------|---------------------|--------|
| 4G Max transmit power: 19.87 (W) | 13.2436 | 6.6208 | 1.0000 |
| 4G Max transmit power: 39.64 (W) | 26.4262 | 13.2127 | 1.0000 |
| 4G Max transmit power: 79.09 (W) | 52.7272 | 26.3637 | 1.0000 |

Table S23. Average and standard deviation of RRU power in sleep mode for different types of base stations.

| Base station types | Average (W) | Standard deviation |
|----------------------------------|-------------|--------------------|
| 5G 32TR SA | 78.9992 | 8.7932 |
| 5G 32TR NSA | 69.4302 | 7.0611 |
| 5G 64TR SA | 88.4698 | 17.4029 |
| 5G 64TR NSA | 90.5637 | 11.0712 |
| 4G Max transmit power: 19.87 (W) | 119.0310 | 7.5044 |
| 4G Max transmit power: 39.64 (W) | 127.9319 | 7.6571 |
| 4G Max transmit power: 79.09 (W) | 133.9013 | 9.2278 |

Table S24. Parameter settings of EnergyPlus to simulation the power consumption of base stations' cooling subsystem.

| Parameters | Settings |
|-------------------------------------|--|
| Room size | 5·4·3 m^3 |
| Electric equipment | Communication subsystem of base stations |
| Indoor proper operating temperature | 20°C |
| Outdoor air temperature | Meteorological weather |

Table S25. Parameter settings of the threshold-based method used in current real-world mobile networks. (NA refers to ‘not available’)

| Device type | Time of a day | Metric | Sleep mode | Turn off |
|-------------|-----------------------------|-----------------|------------|----------|
| 5G cells | Nighttime (0.00am - 6.00am) | # of users | 5 | 2 |
| | | PRB usage ratio | 0.05 | 0.05 |
| | Daytime (6.00am - 11.59pm) | # of users | NA | NA |
| | | PRB usage ratio | NA | NA |
| 4G cells | Nighttime (0.00am - 6.00am) | # of users | 10 | NA |
| | | PRB usage ratio | 0.2 | NA |
| | Daytime (6.00am - 11.59pm) | # of users | 10 | NA |
| | | PRB usage ratio | 0.2 | NA |

Table S26. Linear regression analysis for misalignment factor.

Linear regression model: $M = K_\psi(1 - \tilde{L})$

Dependent variable
Normalized network traffic load \tilde{L}

| Energy-saving scenarios | K_ψ | R^2 |
|--------------------------------------|----------|--------|
| Without energy-saving | 0.5764 | 0.9838 |
| Threshold-based energy-saving method | 0.4765 | 0.8509 |
| Greedy energy-saving method | 0.3946 | 0.8106 |
| DeepEnergy | 0.2606 | 0.8227 |

Table S31. The performance of the models trained on data from different regions in Nanchang.

| Models | Energy-saving rate of the whole Nanchang |
|-------------------------------|---|
| Trained on Region A | 0.4295 |
| Trained on Region B | 0.4482 |
| Trained on Region C | 0.4492 |
| Trained on Region D | 0.4252 |
| Trained on the whole Nanchang | 0.4373 |

Table S32. Linear regression analysis for misalignment factor of DeepEnergy models trained on different regions.

| Linear regression model: $M = K_\psi(1 - \tilde{L})$ | | |
|---|----------|--------|
| Dependent variable | | |
| Normalized network traffic load \tilde{L} | | |
| DeepEnergy models | K_ψ | R^2 |
| DeepEnergy model trained on Region A | 0.2885 | 0.8351 |
| DeepEnergy model trained on Region B | 0.2863 | 0.9092 |
| DeepEnergy model trained on Region C | 0.2661 | 0.8085 |
| DeepEnergy model trained on Region D | 0.2895 | 0.8750 |
| DeepEnergy model trained on the whole Nanchang | 0.2606 | 0.8227 |